ROCKSLIDES AND ROCK AVALANCHES OF THE KOKOMEREN RIVER BASIN (CENTRAL TIEN SHAN)

ICL SUMMER SCHOOL ON ROCKSLIDES AND RELATED PHENOMENA

GUIDEBOOK

C-106 PROJECT OF THE INTERNATIONAL PROGRAMME ON LANDSLIDES

A.L. Strom & K.E. Abdrakhmatov

Moscow–Bishkek, 2016

CONTENT

I N T R O D U C T I O N

Large-scale catastrophic bedrock slope failures belong to the most hazardous natural phenomena that endanger people living in mountainous regions. Unlike "common" landslides and rockfalls affecting just collapsing slopes themselves and areas directly at their feet, the simultaneous failure of millions and sometimes billions of cubic meters of rock can devastate vast areas, spreading up to 5-10 km and even more from the source zone. Moreover, they often cause river damming with disastrous secondary effects such as valley inundation and subsequent outburst floods. For example, the 1786 earthquake-triggered Dadu rockslide in China formed a dam, which subsequent failure killed about 100,000 people downstream, thus being the most disastrous rockslide catastrophe ever reported [Lee & Dai 2011]. In 1841 and 1858, catastrophic floods occurred due to failure of rockslide dams that had blocked the Indus River and its large tributary, the Hunza River, respectively [Hewitt 2002]. In 1881, a rock avalanche destroyed Elm village in Switzerland; this was the first time a long runout event was described scientifically [Heim 1882, Hsü 1975]. In 1911, the Usoi rockslide dammed the Murgab River in Pamirs and formed the 500-m deep Sarez Lake that still poses a potential threat for a large part of the Amu-Daria River basin [Gaziev 1984, Alford and Schuster 2000, Strom 2014]. In 1949, the Khait rock avalanche caused by a M7.4 earthquake buried Khait town with several thousands of its inhabitants [Leonov 1960, Evans et al. 2009]. It was the most disastrous landslide event in the entire Central Asia region. In 1963, the breach of the Issyk Lake rockslide dam near Almaty City in Kazakhstan produced a debris flow that devastated the entire valley and caused numerous casualties [Litovchenko 1964, Strom 2010b, 2013a]. This tragic list was extended by the 2005 M7.6 Kashmir earthquake in Pakistan and the 2008 M8 Wenchuan earthquake in Sichuan (China) where thousands of people were buried by numerous large-scale rockslides. The Wenchuan earthquake formed numerous river blockages and only enormous efforts undertaken by Chinese authorities prevented catastrophic outburst floods [Yin, et al 2008, Wang, et al. 2009, Cui, et al 2009].

Such phenomena have attracted researchers' attention for many years, beginning with the pioneering study of the Elm rock avalanche by A. Heim [1882]. The main objective of the Summer School on Rockslides and Related Phenomena in Kokomeren River Valley in Kyrgyzstan is to acquaint participants with various morphological types of bedrock landslides, their internal structure and with basic methods used for their identification. Emphasis will be placed on the geological and neotectonic framework in which large rock massifs fail catastrophically, on surface ruptures in particular. The latter are considered as traces of strong past earthquakes, which, as we assume, repeatedly shook the study region and, therefore, can occur here in future. On the other hand, large-scale prehistoric rockslides are often treated as evidence of strong past earthquakes and field evidence that allows such conclusions [Strom 2013b] are demonstrated and analyzed as well.

The choice of this particular area – the Kokomeren River basin (Figure 1) – for the training course is based on the extremely favorable combination of several factors:

- Presence of numerous rockslides and rock avalanches ranging from several millions to more than one billion cubic meters in volume within a limited area (Figure 2).
- Variability of morphological types of the phenomena in question. There are rockslides that originated in igneous (granites), metamorphic (gneiss) and in sedimentary (sandstone, conglomerate, etc.) rocks with well-expressed bedding, those with compact bodies that form high natural dams and those transformed into long runout rock avalanches; confined and unconfined events; rockslides with nearly intact bodies and those deeply incised by erosion, providing excellent opportunity to study their internal structure. Expressive evidence of river valley inundation is visible, as well as traces left by disastrous outburst floods.
- Arid climate of the Tien Shan, favorable to very good exposure of both overall morphology of rockslides and other geomorphic phenomena and of minor topographic features, which are not masked by vegetation.
- Very expressive neotectonic structure, presence of numerous active faults and surface ruptures, allowing better understanding of geological and seismotectonic framework in which rockslides have occurred.

- Accessibility of the study area located near the road at one-day trip distance from Bishkek City – capital of Kyrgyzstan. Bishkek is connected by direct flights with Moscow, Istanbul, Urumchi and other cities. It is also possible to arrive via Almaty – former capital of Kazakhstan.

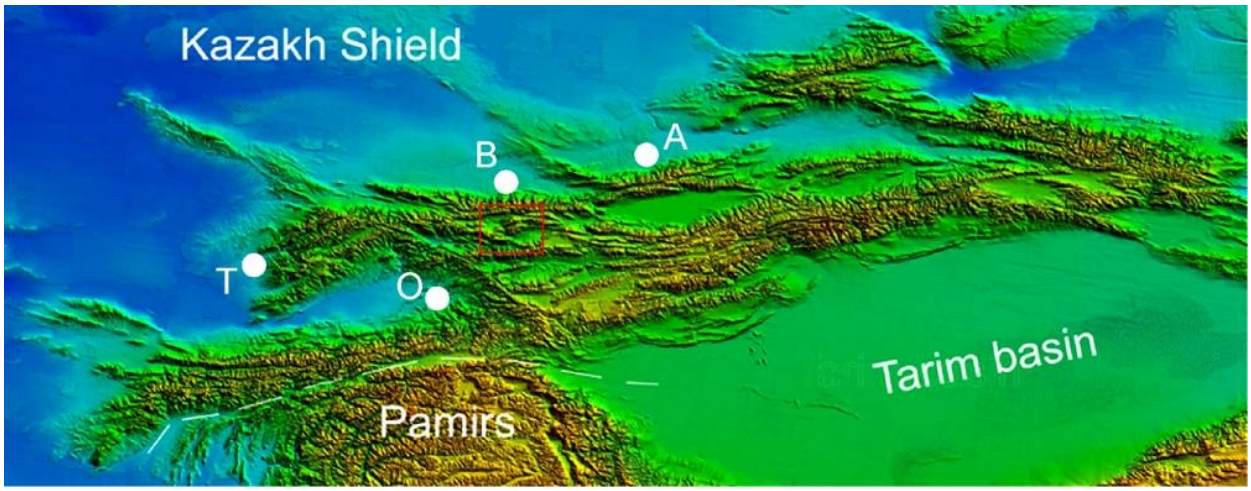

Figure 1. Position of the Kokomeren River basin within the Tien Shan Mountain system
Study region is marked by red rectangle. B – Bishkek, O – Osh, A – Almaty, T – Tashkent

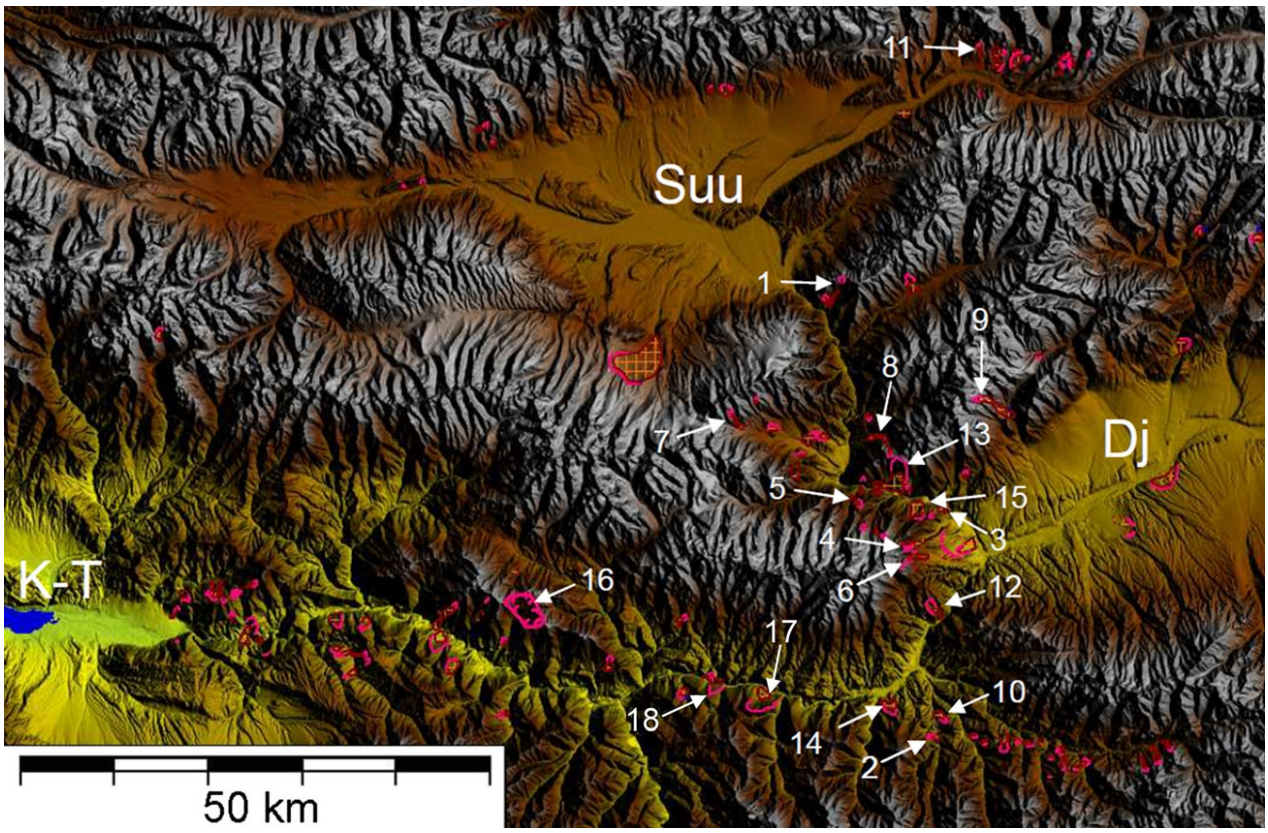

Figure 2. Location of bedrock slope failures in the central part of the Kokomeren River basin
Red lines – headscarps; hatched areas – landslide bodies; numbered features are described in the text in detail. Fragment of the 3" SRTM DEM as the background. Selected features most of which are demonstrated during the training course: 1—Seit, 2—Ak-Kiol, 3—Mini-Köfels, 4—Kashkasu, 5—Northern Karakungey, 6—Southern Karakungey, 7—Chongsu, 8—Sarysu, 9—Ming-Teke, 10—Lower Ak-Kiol, 11—Snake-Head, 12—Lower-Aral, 13—Kokomeren, 14—Ornok, 15—Displaced Peneplain, 16—Kyzylkiol, 17—Karachauli, and 18—Lower Kokomeren.

This Guidebook presents brief descriptions of the most interesting rockslides and rock avalanches, which can be visited during the training course. Case studies are presented in the following order: those describing various morphological types of rockslides and rock avalanches first, then case studies allowing better understanding of rockslide internal structure and grain-size composition, and finally those characterizing outburst floods caused by landslide dam breaches and some other interesting features of the study region at the end. The authors will be grateful for any comments, corrections and suggestions, which will help the improvement of the guidebook.

1 GEOLOGICAL BACKGROUND (FACTORS GOVERNING BEDROCK SLOPE FAILURES)

1.1 Geology

The Tien Shan is a typical basin-and-range mountain system that has been formed mainly in Neogene-Quaternary time (with some evidence of activation in the Paleogene), most likely due to north-south compression. Neotectonic deformations started after a long period of planation, which lasted almost all Mesozoic Era and up to the Eocene [Makarov, 1977, Chedia, 1986]. In the Paleozoic Era this region had been subjected to intensive tectonic deformations of Caledonian and Varissian stages that formed the complex structure of its basement. The region in question, in particular, had been formed mainly during the Caledonian stage. Mountain ranges that rise up to 4000 m a.s.l. comprise rocks representing Caledonian basement. They are divided by intermontane depressions filled by Neogene and Quaternary sediments (Figure 3).

The most widely distributed types of basement rocks within the study area are Paleozoic granites of Ordovician and, locally, Silurian ages. Between the Kysyl-Oi and Djumgal depressions there is a rock massif composed of Late Precambrian metasediments and gneiss intruded by the above-mentioned granites. Devonian sandstone is present at the northeastern part of the study region, north of the Suusamyr depression. The southern part of the study area, south of the East-West trending Minkush-Kokomeren Neogene depression is composed of Ordovician, Devonian and Carboniferous sediments representing the frontal zone of the Varissian thrust belt.

Neogene deposits are widely distributed in the depressions and, locally, remain at high altitudes within the ridges. They are represented by terrigenous red beds (sandstone, conglomerate, siltstone, mudstone) of the Kyrgyz series overlain by whitish sandstones, siltstones and mudstones of the Tien Shan series, which, in turn, are overlain by much coarser deposits (upper molasse) of the Sharpyldak series. The presence of the deposits of the Kyrgyz and, likely, Tien Shan series at high elevation within mountain ranges indicates that they were accumulated in the shallow basins before the neotectonic orogeny started in the Late Pliocene or Pleistocene. In contrast, the Sharpyldak conglomerates can be found in depressions only. At several outcrops outside the study region, however, one can find the inverse sedimentation order, with coarse debris flow deposits at the base overlain by finer Miocene strata, which likely indicate penultimate orogenic movements [Abdrakhmatov, et al., 1994].

Quaternary deposits are represented by glacial moraine and alluvial deposits of Middle and Late Pleistocene and Holocene ages and talus. Locally, rockslide bodies and lacustrine sediments of rockslide dammed lakes are present. It should be pointed out that, unlike in the Alps, Pamirs or Eastern part of the Tien Shan, there are no indications that Quaternary glaciation affected large neotectonic depressions and main river valleys in the region in question. The latter are purely erosional features. Thus, large-scale bedrock slope failures cannot be related to postglacial debuttressing.

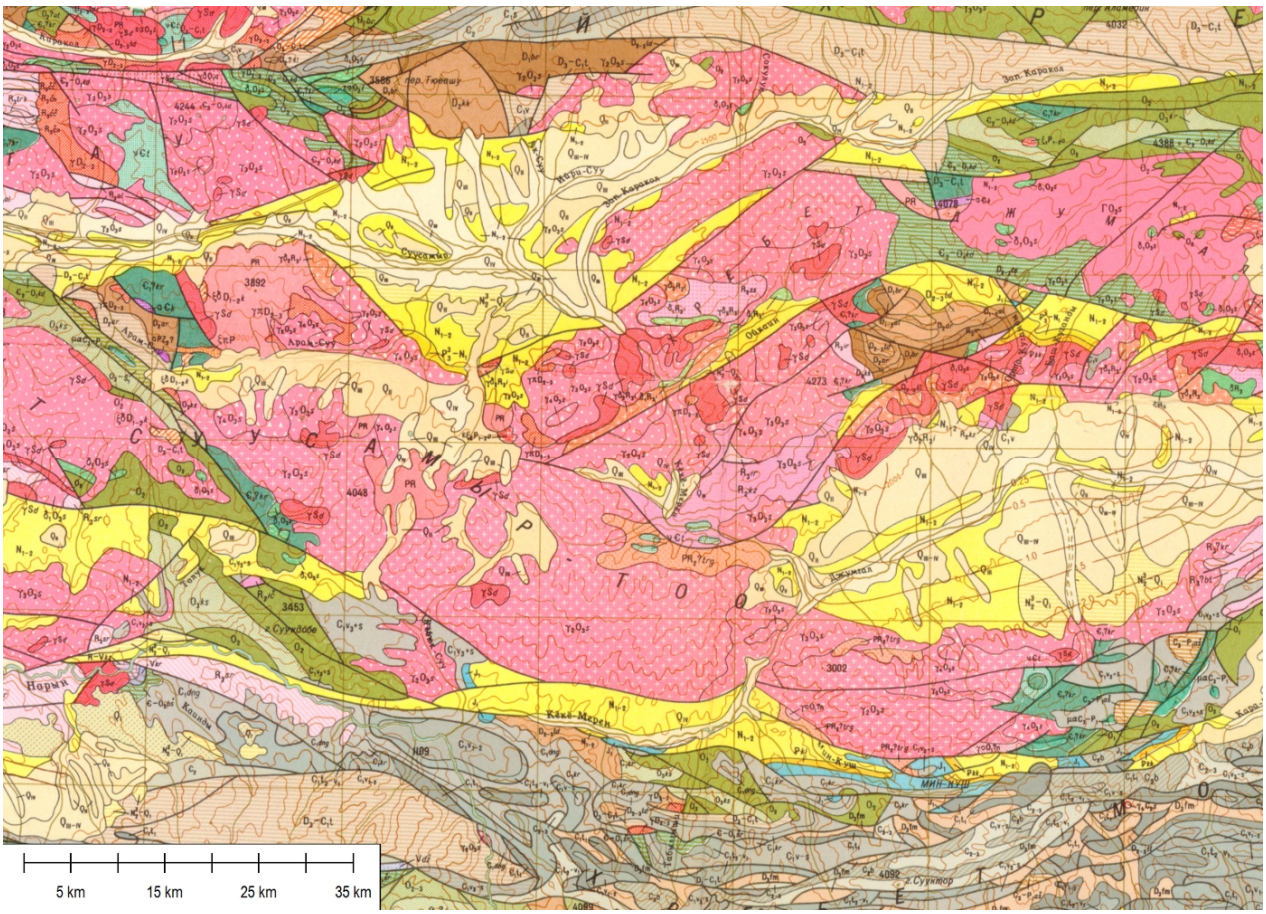

Figure 3. Geological map of the study region
Fragment of the 1:500 000 Geological map of Kyrgyzstan

1.2 Geomorphology and neotectonics

As mentioned above, the Tien Shan is a typical basin-and-range mountain system (Figure 4) that has been formed during the Neogene-Quaternary periods due to north-south compression. It should be noted that the expressiveness of neotectonic structure in the Tien Shan is one of the best in the world. Moreover, the concept of Neotectonics itself was developed by S.S. Shultz [1948] based on his field studies carried out just in this mountain system. Later, V.I. Makarov [1977] and O.K. Chedia [1986] studied and described the Tien Shan neotectonics on a more regular basis.

The extreme expressiveness of neotectonic features in the Tien Shan is stipulated by the presence of the Pre-Neogene planation surface overlain by the sequence of variegated Cenozoic sediments, whose deformation reflects post-Neogene tectonic movements. In general one can see fragments of this surface that were tilted and ruptured (Figure 5), though sometimes both Paleozoic basement and overlaying Cenozoic sediments had been subjected to intensive folding (Figure 6). Intensive neotectonic deformations resulted in the presence of Neogene deposits both in neotectonic depressions and, locally, on the planar surfaces inside high ridges raised sometimes about 1 km above present-day river valleys, as can be observed when comparing the position of the Neogene red beds in the intermontane Kyzyl-Oi depression and on the adjacent connection between the Djumgal and Suusamyr Ranges (Figure 8).

Large basement folds feature distinct asymmetry and series of them form systems characterized by either northward or southward vergence [Sadybakasov 1972, 1990]. Steeper fold limbs are usually associated with neotectonic reverse faults, some of which also have a significant strike-slip component indicating a transpression style of deformation [Delvaux, et al. 2000]. Many of the large faults that divide neotectonic uplifts and depressions show evidence of Late Pleistocene – Holocene surface rupturing.

Expressive faults displacing minor topographic features and/or recent sediments can be found at the northern boundary of the Suusamyr depression (Figure 9), along northern (Figure 10) and south-eastern (Figure 11 – Figure 13) boundaries of the small Kyzyl-Oi depression, at the boundary between the Djumgal Range and the depression of the same name (Figure 14). Some of them, such as the fault shown in Figure 12, demonstrate clear evidence of strike-slip movements (Figure 13), while others are predominantly reverse faults, though these, rather often, are represented by up-slope facing scarps (see Figure 9 and Figure 14). Several recent faults that pass near rockslide sites will be described hereafter.

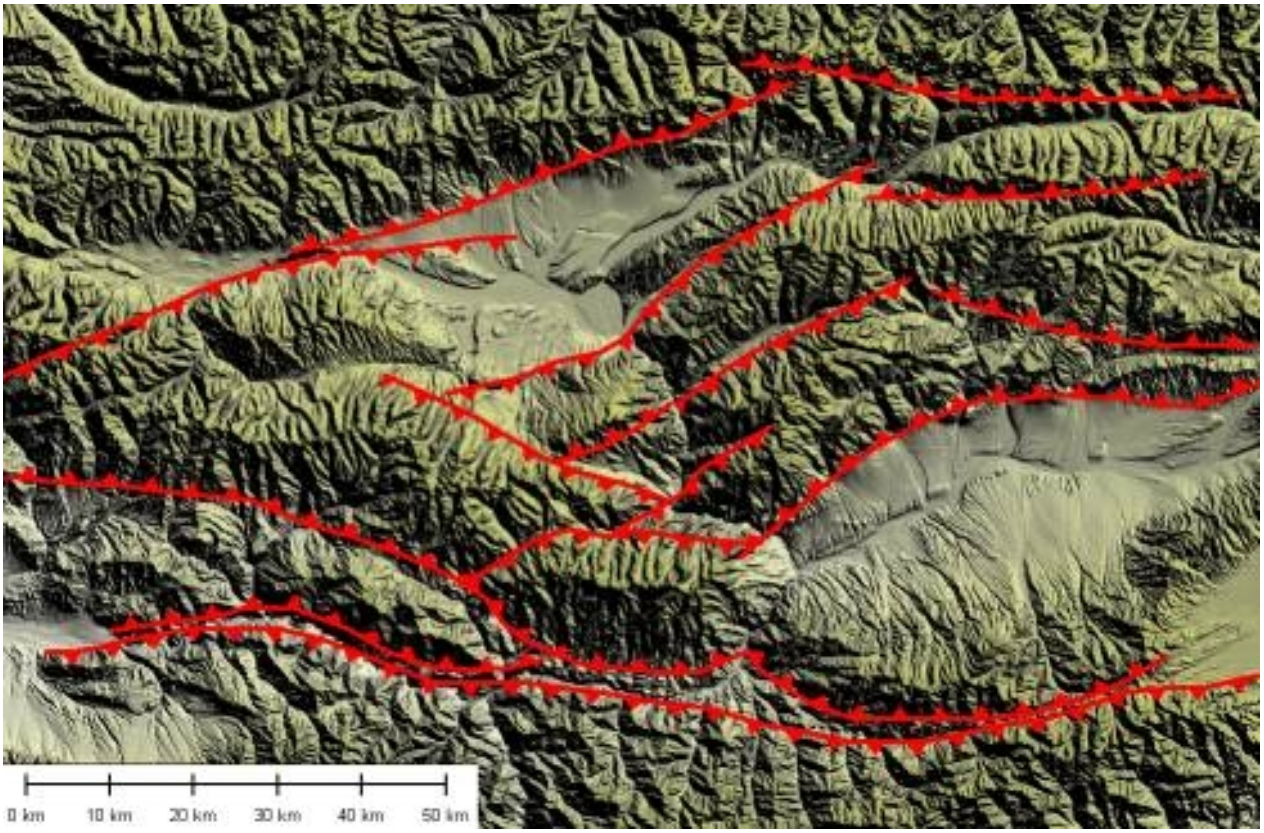

Figure 4. Simplified scheme of neotectonic faults of the study area
Red lines – main active faults. Triangles are on the upthrown sides

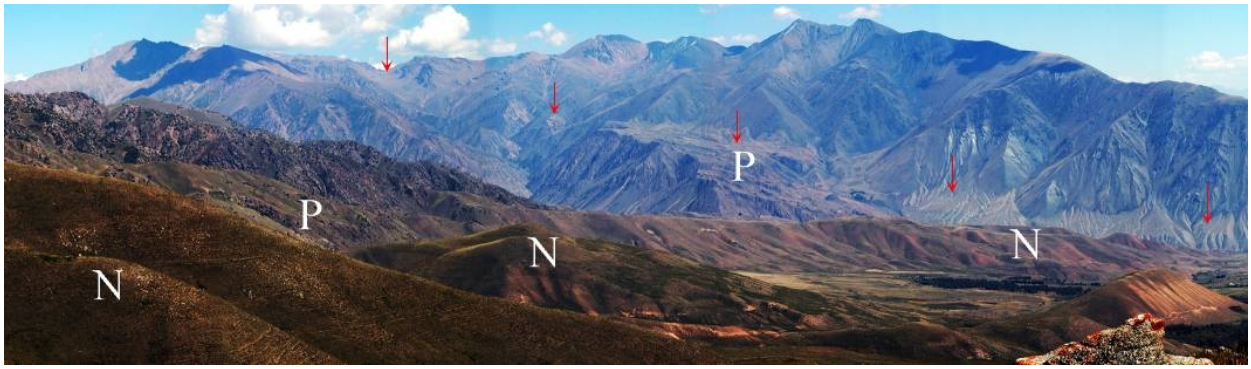

Figure 5. Tilted and warped planation surface (P) - bottom of the Kyzyl-Oi neotectonic depression
Fault bounding the depression is marked by red arrows. Planation surface inclination increases at the left part of the panorama foreground where it is overlain by Neogene red beds (N)

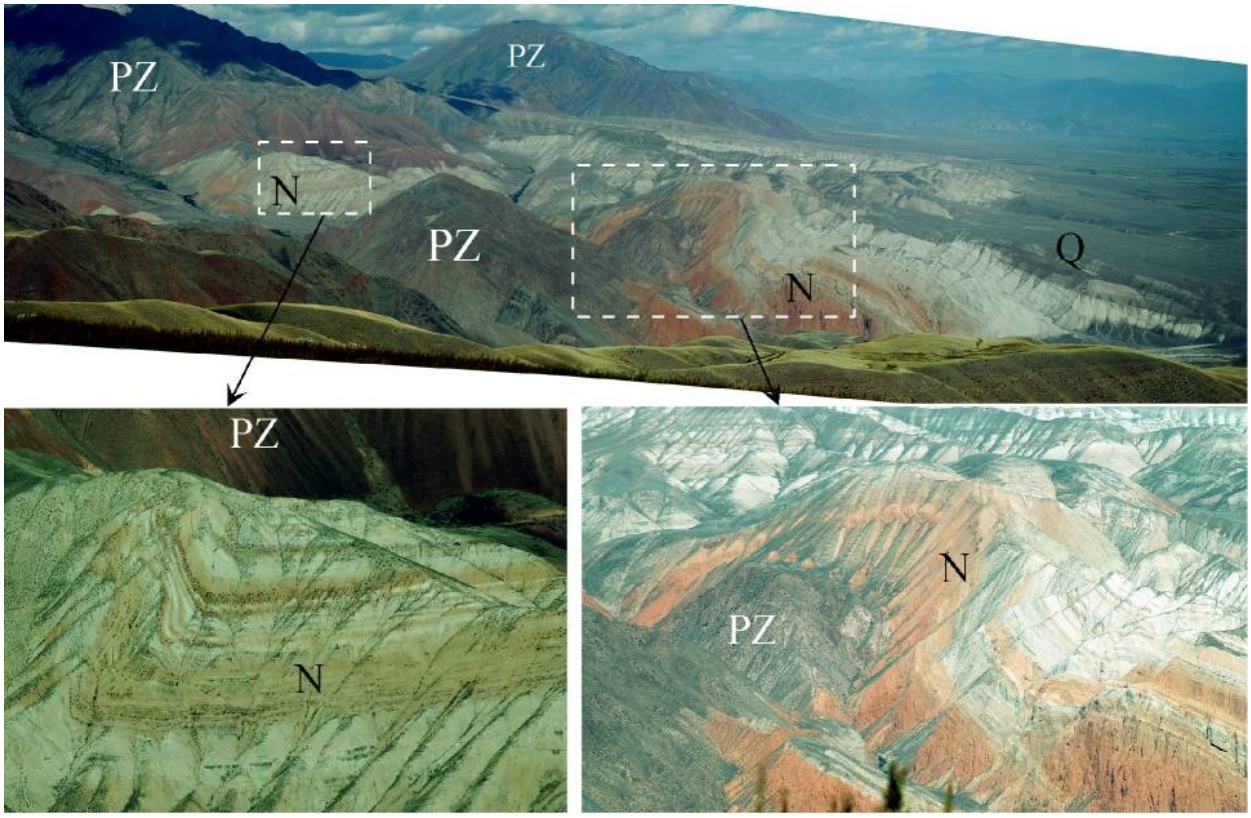

Figure 6. Folding of pre-Neogene planation surface and overlying N-Q sediments at the north-western part of the Djumgal intermontane depression.

Figure 7. Angular unconformity between folded Neogene deposits and overlying Pleistocene sediments at the right part of the panorama shown on Figure 6

The light brownish Pleistocene strata at the right side are tilted at a smaller angle than whitish Neogene below

Figure 8. Uplifted pre-Neogene planation surface south from the Kyzul-Oi depression

Arrows mark the reverse fault that divides the Suusamyr (Suu) and Djumgal (Dj) neotectonic anticlines (ridges).

Several active faults can be traced inside intermontane depressions. One of them, in particular, can be considered as an eastern extension of an active fault that was ruptured during the 1992 Suusamyr earthquake. It displaces recent sediments and forms a north-facing scarp that stretches along the central part of the Suusamyr valley (Figure 15).

It is likely that the above-mentioned surface ruptures are associated with strong past earthquakes. The outcrop shown on Figure 11, in particular, demonstrates direct and indirect evidence of multiple Quaternary seismotectonic events. The first one can be revealed from the presence of angular boulders (2 on Figure 11) that could only originate from the opposite slope of the Kokomeren River.

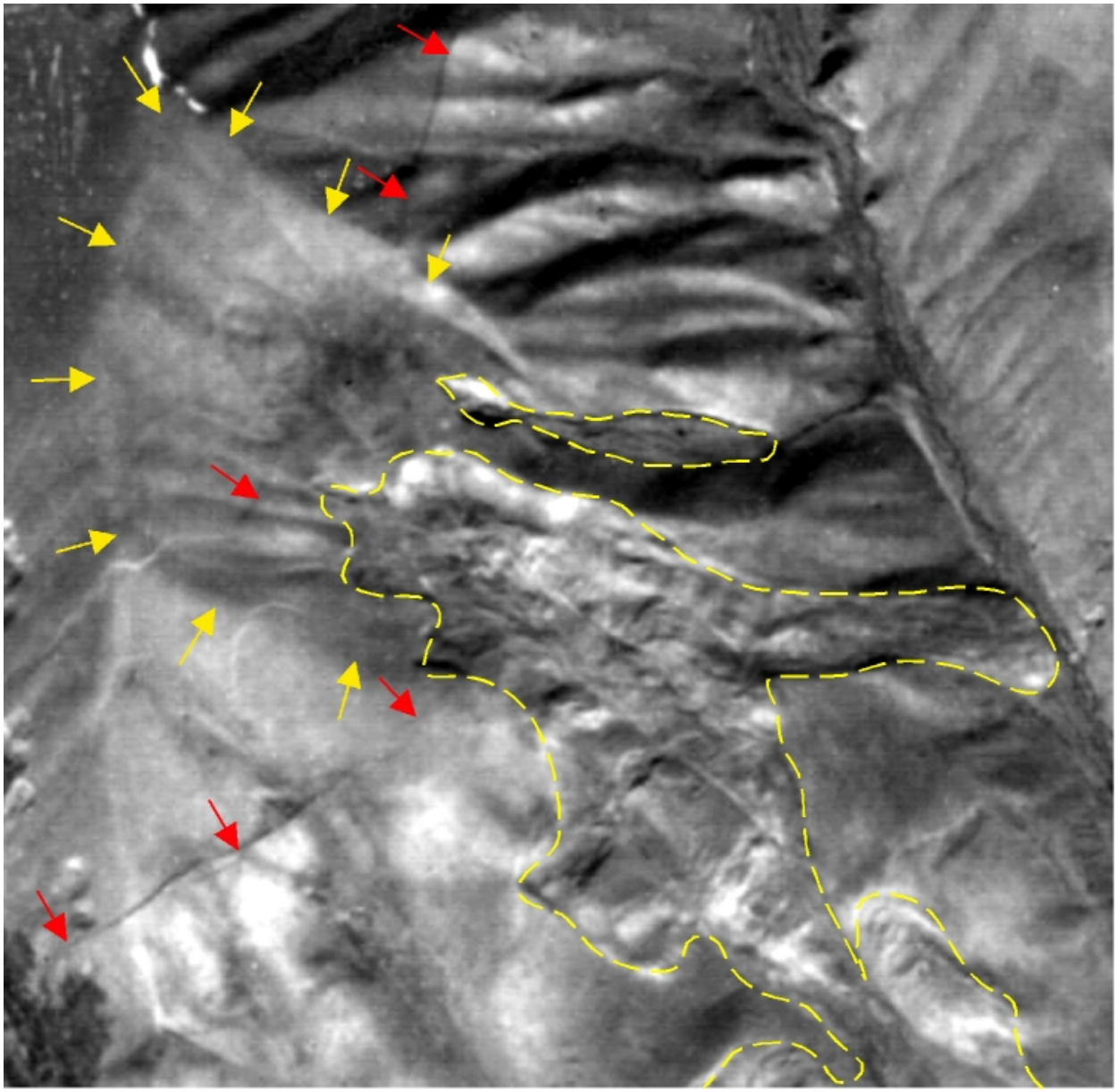

Figure 9. Surface ruptures associated with landslides at the northern boundary of the Suusamyr intermontane depression

Red arrows mark surface ruptures, orange arrows – assumed scar of old bedrock landslide; dashed yellow lines – boundaries of the more recent (modern) landslides. Fragment of high-resolution space photograph

The large distance from the source zone that is atypical of such deposits allows the assumption that slope failure was associated with a strong earthquake. It is supported by the following observations:

1 – Quaternary sediments rest on bedrock represented by crushed and mylonitized Paleozoic metasediments (1 on Figure 11), indicating the presence of a long-lived large fault zone. 2 – Scree material is mixed partially with alluvial boulders and this unit is overlain by fine lacustrine sediments

with gravel-pebble interbeds (3 on Figure 11) accumulated in the lake dammed several kilometers downstream by the giant Pleistocene Kokomeren rockslide (see section 3.1). Thus, rockfalls at the site in question occurred simultaneously with large rockslide formation [Strom, Stepanchikova 2008, Strom 2013b].

The significant tilting of the above succession, including fine well-bedded silt sediments that could accumulate initially as horizontal layers only, indicates the next tectonic event. 20-30º tilting could result from the predominantly vertical displacement along the active fault.

Since the recent fault shown on Figure 12 is characterized by predominantly strike-slip kinematics (see Figure 13), this offset should occur during the third, most recent tectonic event.

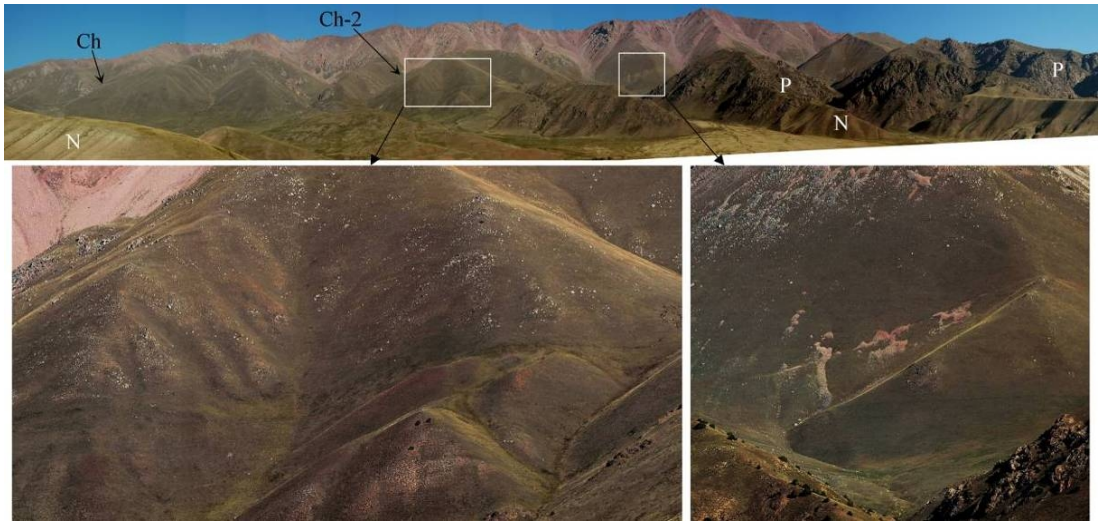

Figure 10. Surface ruptures along the North-Kyzyl-Oi fault zone.
Ch and Ch-2 – the Chongsu and Chongsu-2 rockslides. Rocky hills in the panorama foreground represent the steeply tilted and intensively eroded Pre-Neogene planation surface (P) overlain by Neogene red beds (N)

Figure 11. Outcrop downstream from the Kyzyl-Oi village between Chongsuu and Kobiuksuu River mouths (41.93º N, 74.15º E) with evidence of multiple recent tectonic movements.
1 – crushed and mylonitized Paleozoic bedrock – fault zone material; 2 – angular boulders of Paleozoic metasediments – ancient scree that could fell from the opposite slope of the Kokomeren River valley only; 3 – tilted and ruptured succession of the lacustrine and fluvial sediments accumulated in the lake, which had been formed by the Kokomeren rockslide (see section 3.1.4); outlined fragment with the most recent rupture is shown on Figure 12; 4 - younger alluvium overlying this succession.

Figure 12. Surface rupture displacing the succession of lacustrine and fluvial sediments
Vertical separation of layers visible in the outcrop resulted from the significant left-lateral offset of tilted layers that is proved by the presence of nearly horizontal striae of the rupture surface (Figure 13).

One of the most promising ways to verify the assumption of simultaneous tectonic and rock slope deformations is to date surface ruptures and rock slope failures located nearby [Bull, 1996]. Their ages' coincidence should be a strong argument in favor of the seismic origin of both features.

Some other peculiarities of the dammed lake sediments will be described later in section 3.1.4, focused on the evidence of valley inundation and subsequent dam's breach.

Figure 13. Slickenlines on the sliding surface of a recent fault shown on Figure 12 indicating strike-slip sense of motion

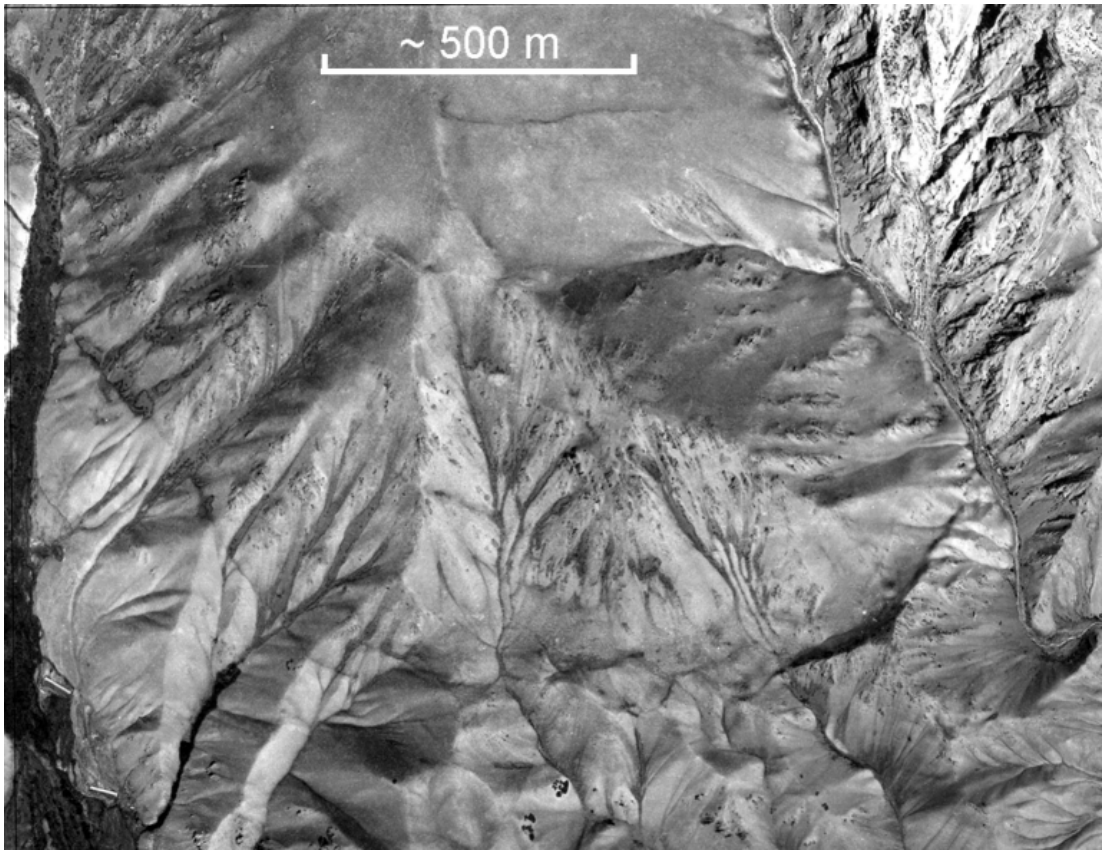

Figure 14. Bow-shaped surface rupture at the fault zone dividing the Djumgal Range and the Djumgal depression west of the Mingteke rock avalanche.
Take notice of up-slope facing escarpments, most expressive at the eastern part of the area

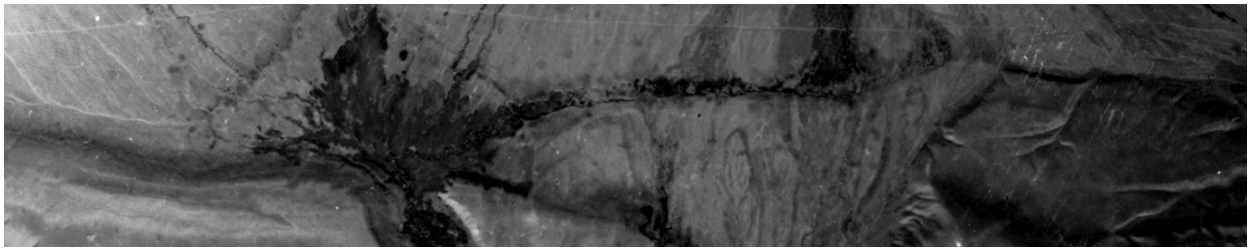

Figure 15. 2.5-km long fragment of the north-facing escarpment of prehistoric surface rupture in the central part of Suusamyr neotectonic depression
This active fault extends westward where it almost merges with the surface rupture of the 1992 Suusamyr earthquake shown on Figure 23 and 24

An interesting manifestation of Quaternary tectonics can be found in the central part of the Djumgal depression just north of the town of Chaek. The depression is an asymmetric syncline about 70 km long and up to 30-35 km wide (see Figure 4) with a rather gentle southern limb and a complexly faulted and folded northern boundary (see Figure 6, Figure 7). An system of plateau-like hills up to 2.5-3.0 km wide stretches along the syncline axis for more than 25 km. Its most impressive part is located in the central part of the depression just north of Chaek (Figure 16).

An uplifted block is formed by an anticline in Neogene deposits, whose crest has been eroded and overlain by Quaternary fluvial and/or debris flow deposits (Figure 17) of the alluvial fans that originated northward, in the Djumgal Range. The style of deformation of this Quaternary material differs significantly from that of the Neogene sediments. While the latter was folded quite intensively so that layers in the anticline limbs dip up to approximately 30º, the Quaternary cover is almost horizontal with more or less uniform thickness (see Figure 17). At the same time, this layer on top of the plateau-like surface was separated from its source area, and larger offset of the older terrace surfaces in comparison

with younger terraces indicates recurrent displacements along the fault that bound the Chaek uplift from the north (Figure 18).

This means that folding that took place in the Neogene (N_2-Q_1?) was replaced by pure block movements in the Late Quaternary – Holocene.

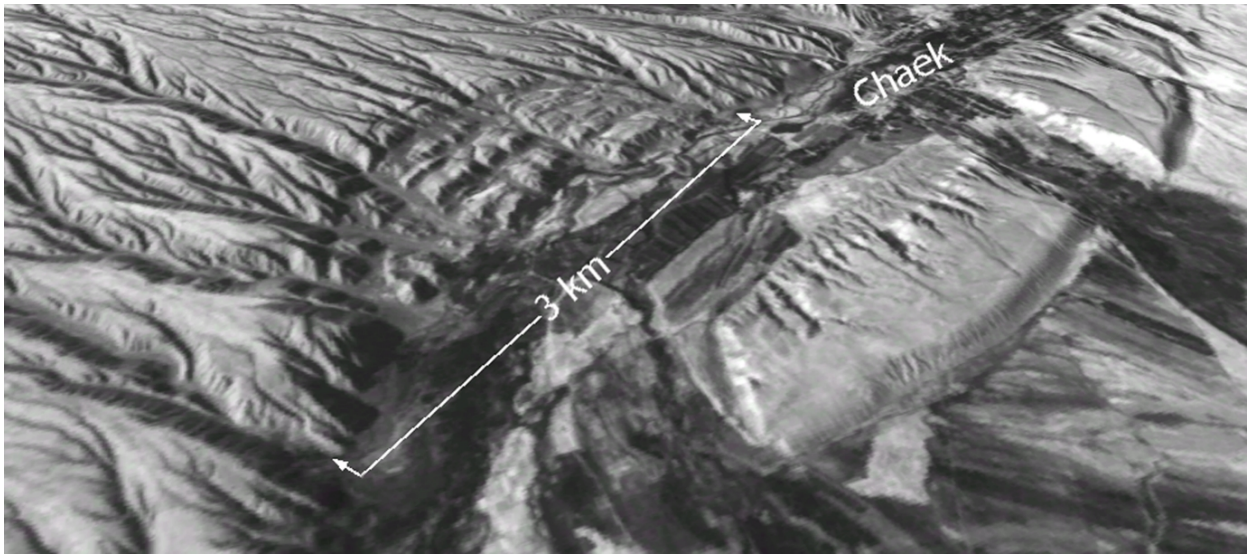

Figure 16. Quaternary uplift at the right bank of the Djumgal River valley north of Chaek.
The rotational Chaek landslide is on the left bank of the river (see section 5.2)

Figure 17. The plateau-like uplift north of Chaek

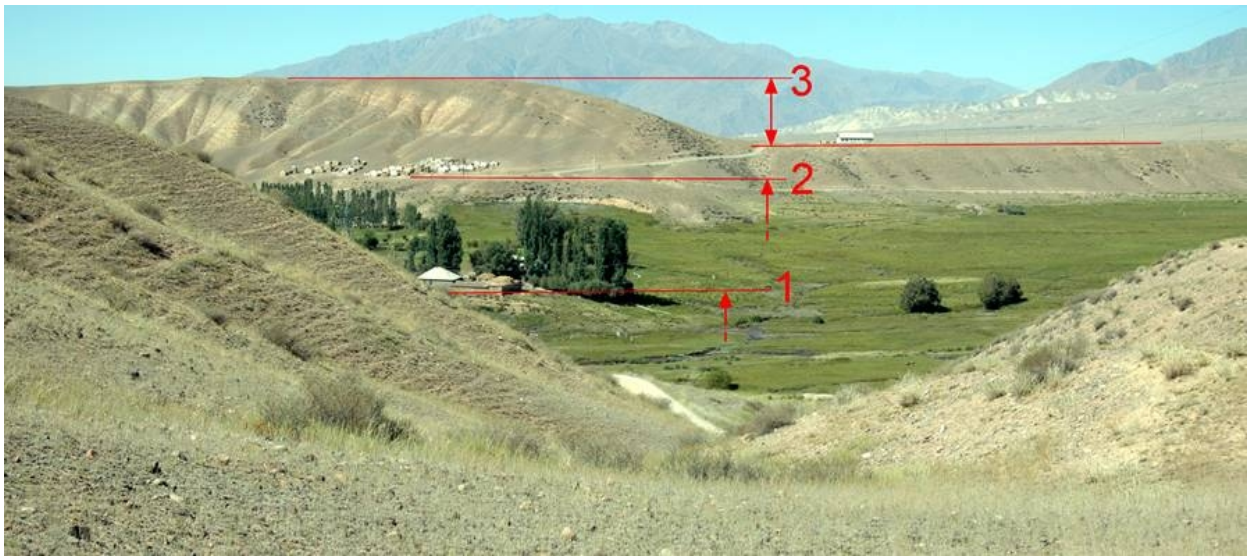

Figure 18. River terraces at the northern boundary of the Chaek uplift displaced by the fault.
The increasing difference between terrace levels (1, 2, 3) indicates recurrent displacement along this surface rupture

The structural peculiarities of this recent fault can be observed and studied in a small clay quarry about 500 m east of the cross-cutting stream. Despite the lack of distinct geomorphic evidence outside the cross-cutting river valley, it was found that this fault dips southward at a very low angle, presumably with large (up to ~7 m) single-event displacements. Recent offsets occurred along several rupture planes. Ruptures shown in Figure 20 in fact consist of at least two fault planes (Figure 19, Figure 20). The lower one, in turn, also consists of two planes (Figure 21). This site is a good place to perform detailed paleoseismological investigations.

Figure 19. Surface ruptures in the western wall of the quarry (arrows)

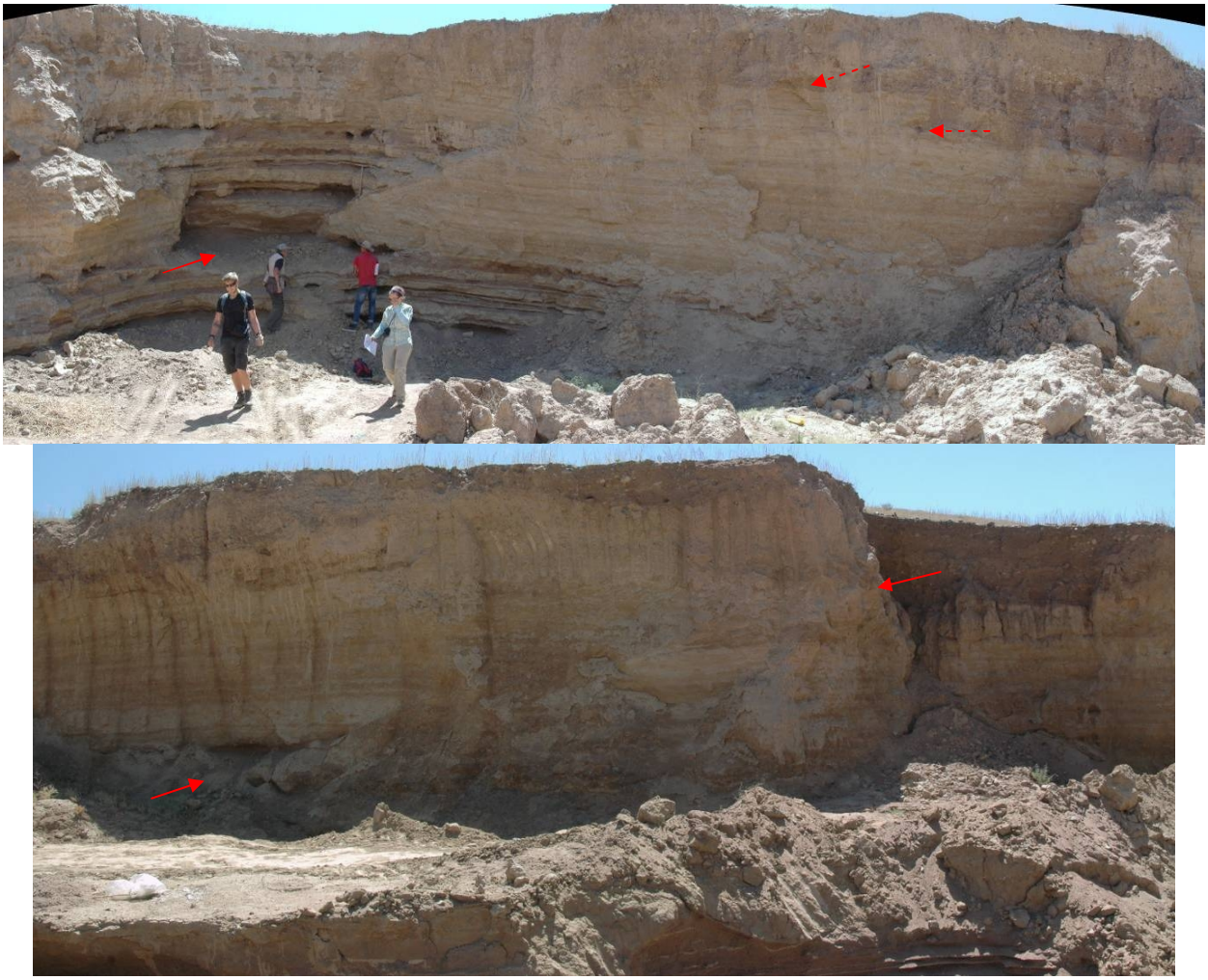

Figure 20. Above – upper (southern) rupture plane; below – lower (northern) rupture plane
Dashed arrows mark possibly bifurcated rupture surfaces

Figure 21. Doubled fault planes of the surface rupture at the bottom of the quarry wall

1.3 Seismicity

Tien Shan is a seismically active zone where numerous strong earthquakes have occurred in the XIX-XX Centuries (Figure 22). Most of them have happened along the northern and southern limits of this mountain system and west of the diagonal Talas-Fergana fault. In the past, most of the Tien Shan mountainous areas were inhabited by nomads, who did not have written history, so historical data on past earthquakes are rare – regular written records started from the middle of the XIX Century only [Mushketov & Orlov 1893].

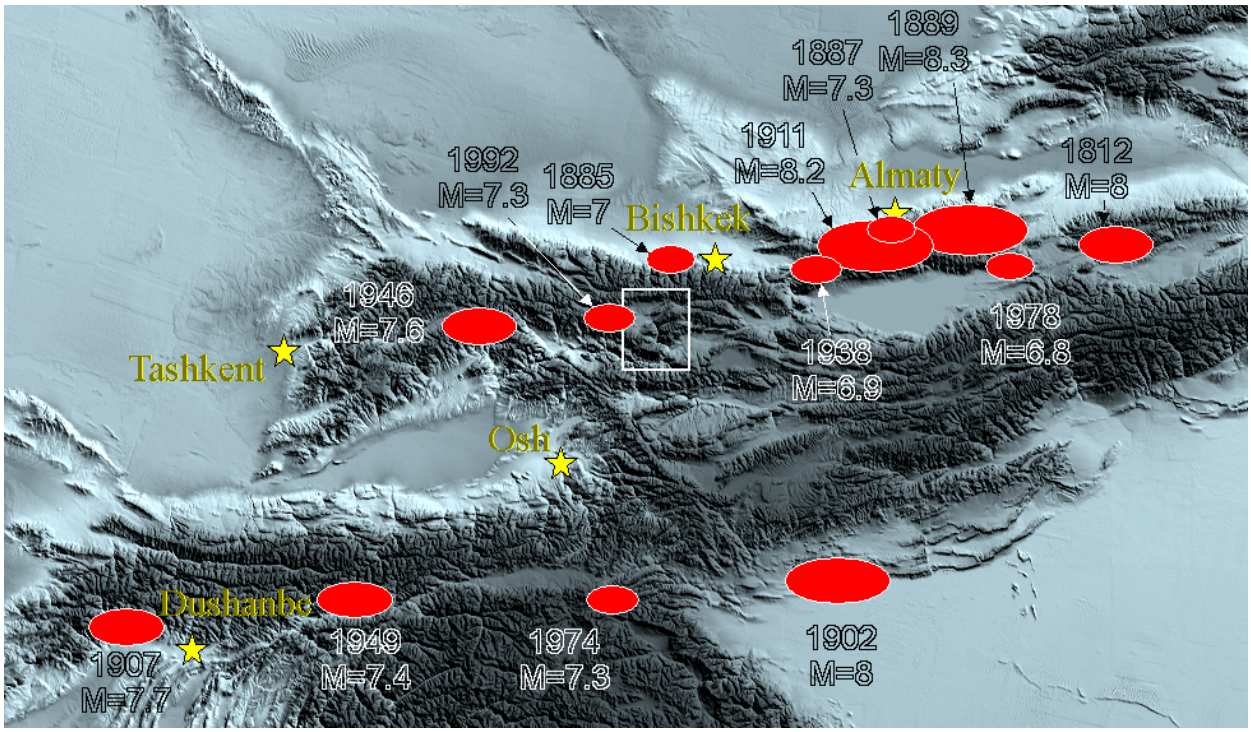

Figure 22. Largest earthquakes of the Tien Shan region
Study area is outlined by the rectangle

The first recorded strong earthquake, the geological effects of which have been described in a special publication, was the 1885 Belovodsk one (M~7.0) that severely affected the northern foothills of the Kyrgyz Range west of the present-day Bishkek City [Ignatiev 1886]. Nothing was reported, however, about its effects in the Suusamyr Valley and further to the south. Other strong events occurred about 100 km to the north-east of the Kokomeren River basin, where one of the strongest intra-continental seismic events – the M8.2 Kemin earthquake – caused extensive surface faulting and slope failure north of Issyk-Kul Lake [Bogdanovich et. al. 1914, Kuchai 1969, Delvaux 2001]. In 1946 the M7.6 Chatkal earthquake occurred at almost the same distance to the west from our region and affected mainly the western side of the Talas-Ferghana fault [Leonov 1970, Kuchai 1971].

No strong seismic events occurred in the historical period in the Kokomeren River basin until August 19, 1992, when the M7.3 Suusamyr earthquake shook the area. The earthquake was accompanied by surface rupture [Ghose, et al., 1997]. Surface faulting associated with this event was very expressive at the eastern part of the epicentral zone (42.21º N, 73.64º E) where three sub-parallel reverse faults ruptured the Suusamyr River floodplain and channel, which resulted in the river's diversion (Figure 23).

These fault scarps are still very expressive, especially the northern one (Figure 24). Another 6-km long source fault fragment ruptured the surface about 25 km to the west; no evidence of surface faulting was found between these two faults [Bogachkin, et al., 1997].

Figure 23. Surface rupture (reverse fault) of the M 7.3 Suusamyr earthquake
Above, photo made in August 25, 1992, few days after the earthquake. Below – left part of the same scarp in 2006, 14 years later

Fortunately this earthquake affected a sparsely populated area and, thus, caused only about 50 casualties. Most of the victims were killed due to landslides in Neogene and Quaternary deposits in the Toluk intermontane depression at the southern foot of the Suusamyr Range (Figure 25), 15-20 km south of the epicenter.

Several other landslides occurred at the Chet-Korumdy Ridge in the western part of the Suusamyr depression [Havenith et al. 2006] (Figure 26) (No 18 on Figure 2). Due to the construction of the new Bishkek-Osh highway most of them were reworked significantly. It is interesting that these landslides occurred strictly at locations of pre-existing slope instabilities (indicated by morphological features such as tension cracks), which are clearly visible at some parts of the Chet-Kurumdy Ridge, above or near the 1992 landslide headscarps (Figure 27). They are well visible on the aerial and space photographs made

before the earthquake (Figure 28-A). Some of them were activated, while much larger, potentially unstable sections of the same slope remained intact (see right side of Figure 28-A and B).

Figure 24. 1992 fault scarp about 2.5 m high on the Suusamyr first river terrace
Boy staying at the footwall is about 1.7 m high. Photo made in 2006

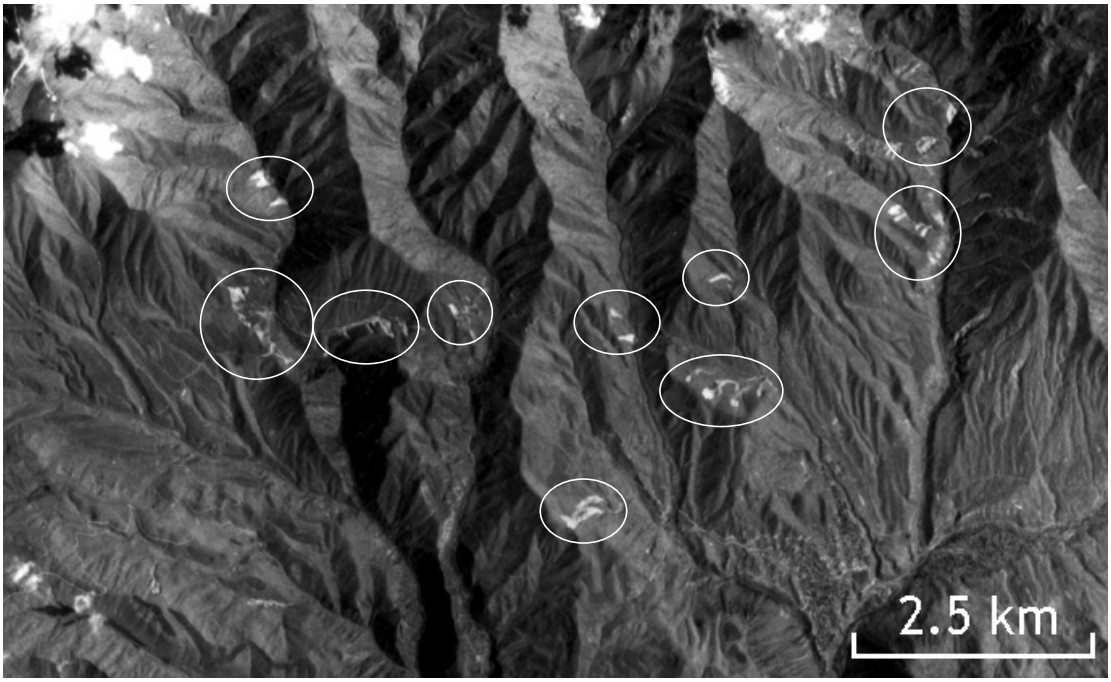

Figure 25. Landslides triggered by the Suusamyr earthquake at the southern foot of the Suusamyr Range (outlined). Fragment of the KFA-1000 space image of obtained about 1 year after the earthquake

Figure 26. Landslide on the southern slope of the Chet-Korumdy Ridge triggered by the Suusamyr earthquake
Photographed on August 25, 1992

Figure 27. Toppling at the central part of the Chet-Korumdu Ridge above the 1992 landslide scar
Photographed in 2006

Only one really large rockslide (about 40 million cubic meters in volume) occurred during this event about 40 km west-south-west of the epicenter in the upper reaches of the Belaldy River valley, north of the Toktogul reservoir at 42.06º N, 73.15º E (Figure 29). It dammed the stream and the dam's breach 10 months later (in June, 1993) caused a devastating debris flow that affected Belaldy and Torkent villages located 17 and 30 km downstream, respectively [Ghose, et al. 1997].

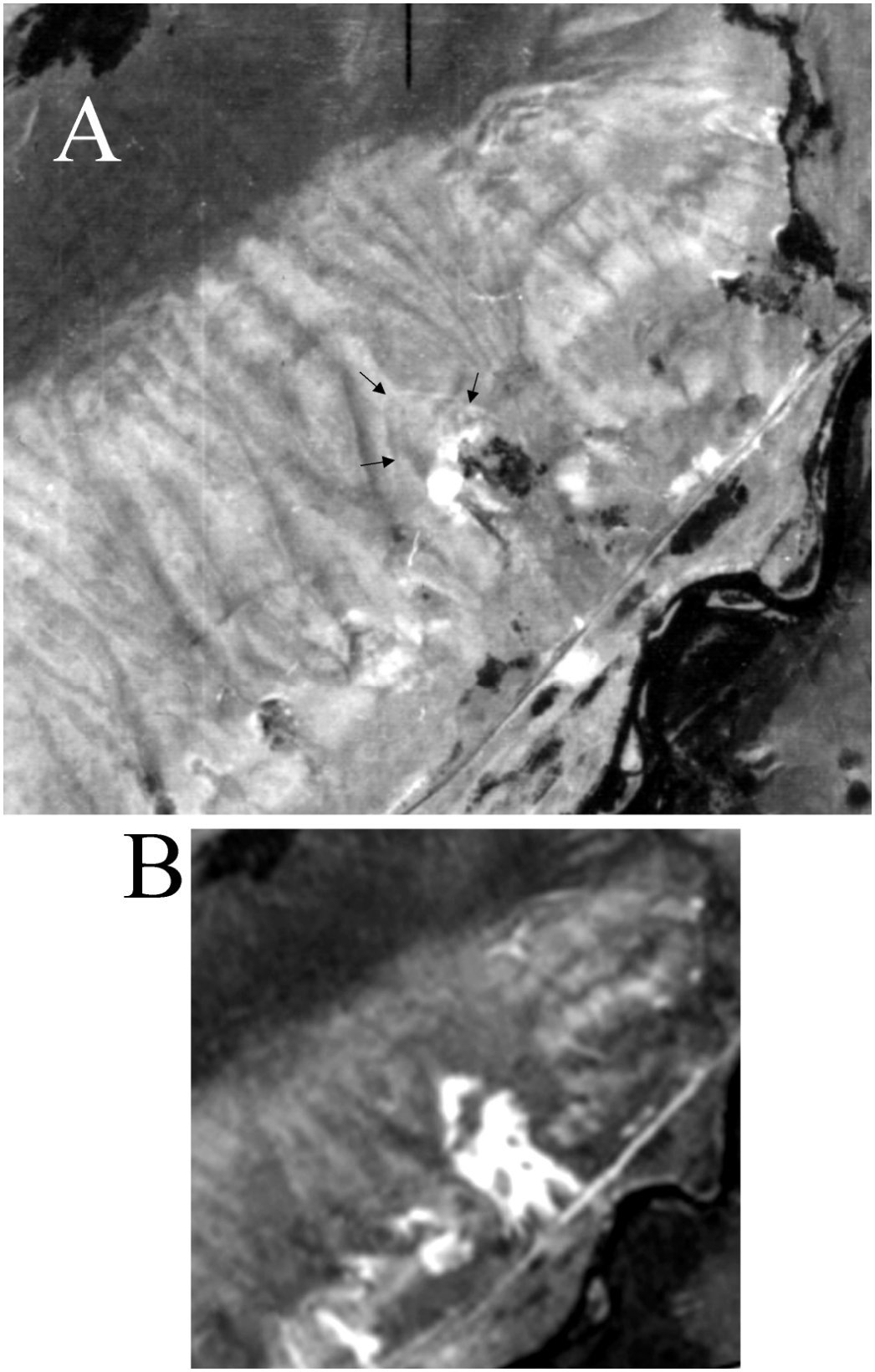

Figure 28. Comparison of zoomed space images of the same section of the Chet-Korumdy Ridge
A – obtained before the Suusamyr earthquake (2-m resolution), B – one year later (8-m resolution). Note presence of the arcuate fracture that formed the scar before the event (arrows on Figure A)

Figure 29. Rockslide in the upper reaches of the Belaldy creek caused by the 1992 Suusamyr earthquake River valley downstream was affected by the debris flow that occurred about one year later. Zoomed fragment of the KFA-1000 space image

In the deep Kokomeren River valley the Suusamyr earthquake caused only minor rockfalls (Figure 30), most of which can be hardly identified now, 15 years after the event.

Figure 30. 1992 Earthquake induced rockfall on the right bank of the Kokomeren River valley
Photo was made about a week after the event

1.4 Hydrogeological conditions

It is well known that groundwater is one of the main factors governing slope stability. However, in most of the case studies that will be described hereafter, its role seems to be less important than in the formation of landslides in nonlithified soils. Deep valleys with high slopes composed of fractured bedrock provide good drainage conditions. Poor rock masses saturation is facilitated by an arid climate with an average precipitation rate of about 450-800 mm/year (of course in the past, when most of rockslides occurred, climate could have differed from the modern one). We should also take into consideration that most of the study area is located below snow-line, which, at present, is at the elevation of about 3800 m a.s.l. in this part of the Tien Shan. Practically there are few, if any, springs directly inside rockslide scars. However, such springs are typical at the distal parts of rockslide deposits. It seems that the source of this water, apart from rain and snowmelt water that infiltrates into huge granular mass of rockslide debris and releases gradually, is condensation in the porous upper parts of rockslide bodies composed of large angular boulders with free air circulation between them.

2 MORPHOLOGICAL TYPES OF ROCKSLIDES AND ROCK AVALANCHES

Morphological types of large-scale rock slope failures are presented according to classification proposed in [Strom 1996, 2006, 2010a], which is based on debris distribution along the runout path (Figure 31). Three main types are selected: 1 – the Primary type with two subtypes (1a – in unconfined or in laterally confined conditions where debris moves down-valley without significant obstacles in its path, and 1b – when debris has to climb over the opposite slope of a valley); 2 – the Jumping type characterized by a sliding surface that daylights much above the foot of a steep slope; and 3 – the Secondary type characterized by bipartite morphology with a compact body at its proximal end, and a long-runout 'secondary' avalanche. The Secondary rock avalanches also can be ascribed to two subtypes – the "Classical" and the "Bottleneck".

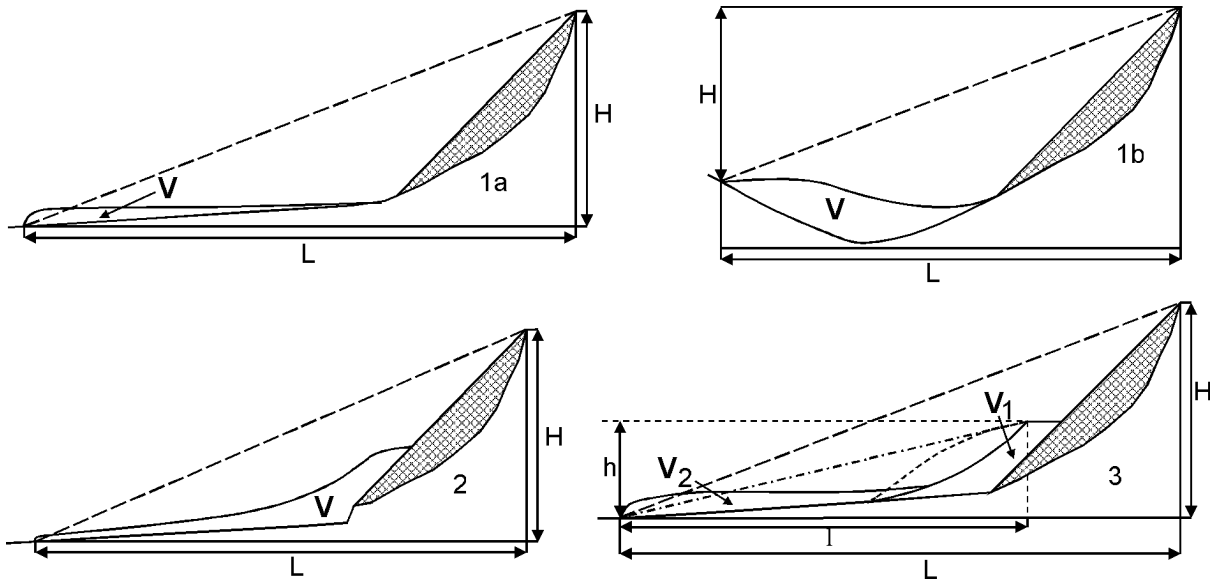

Figure 31. Rock avalanche types [after Strom, 1996, modified].

1 – Primary rock avalanche. The entire rock mass is involved in the avalanche-like motion; 1a – in unconfined or laterally confined conditions, 1b – in a narrow valley. 2 – Jumping rock avalanche with compact proximal and gradually thinning avalanche-like parts. 3 – Secondary rock avalanche ("classical" subtype) characterized by compact proximal accumulation with the prominent secondary scar above the avalanche-like part. H – height drop (vertical distance between the headscarp crown and the deposits tip); h – that of the secondary rock avalanche; L – runout; l - secondary rock avalanche runout; V – entire volume, V_1 – volume of the compact part of the secondary rock avalanche, V_2 – that of its avalanche-like part.

Figure 31-3 represents what could be classified as a "classical" subtype, whose characteristic feature is a concave shape of the compact proximal part – the so-called 'secondary scar' that marks the boundary between the compact and highly mobile avalanche-like portions of the debris [Strom 1996, 2006]. The "bottleneck" subtype of secondary rock avalanches is also characterized by bipartite mass distribution, but without a pronounced secondary scar. This type originates when rapidly moving debris passes through a sharp valley constriction. A portion of the debris that passes through such a 'bottleneck' has an abnormally long runout that sometimes exceeds the runout of similar-sized rock avalanches that moved over unconfined areas without barriers restricting their motion.

It was hypothesized [Strom, 2010a] that secondary rock avalanches of both subtypes originate due to momentum transfer from the rapidly decelerating portion of debris that accumulates at the proximal part of the deposition zone to the portion retaining possibility of further motion. This is reasoned to provide the latter's acceleration resulting in extra-mobility.

2.1 Primary rock avalanches

2.1.1 The Seit rock avalanche

This impressive rock avalanche (No 1 on Figure 2) is located 5-6 km downstream of the Kojamkul village named after a local very strong man who lived here in the beginning of the XX century and who brought a 690 kg boulder to the grave of his friend that can be seen at the side of the highway, though it was partially destroyed by the 1992 Suusamyr earthquake.

An enormous deposit of angular granite boulders fills the small gully at the eastern flank of the Kokomeren River valley at 42.11° N, 74.14° E, whereas the rock avalanche scar is seen far away on the ridge slope (Figure 32).

This is a classical example of the "Primary" rock avalanche type [Strom 1996, 2006], where practically all debris accumulates at the avalanche's distal part (Figure 33, Figure 34). The rock avalanche seems to be rather recent – we assume that it occurred about several hundred to a few thousand years ago. This assumption is based on the fact that the deposit's distal tip fills the stream

incised into a low terrace (Figure 35). The thickest Archa (Central Asian juniper) trees growing on its surface are up to 320 years old according to tree ring dating (Figure 36) (Olga Maksimova, personal communication), which gives us the upper limit of the slope failure age.

Figure 32. Overview of the Seit primary rock avalanche

The rock avalanche was formed by the collapse of about 20 million cubic meters of granite and granodiorite in the upper reaches of a deep, dry valley (Figure 37). Though the upper part of the transitional zone is almost debris-free now, the thickness of debris that travelled through this zone can be reconstructed from the trimlines that remain on the slopes more than 100 meters above the resultant deposit's surface (Figure 38, Figure 39). We should note that similar phenomena indicating changes in debris thickness during rock avalanche motion can be observed at several other rock avalanches, which will be described hereafter.

Such a rapid decrease in the thickness of moving rock avalanche debris indicates an abrupt change in debris properties. It can be hypothesized that the rockslide had moved as a more or less rigid body characterized by a relatively high angle of internal friction at the time of initiation, but later on, while the level of material crushing in rock avalanche interiors increased, the rock avalanche debris started behaving more as a liquid and really "flowed out" towards the distal end of the depositional zone. Possible causes of fragmentation have been described in McSaveney and Davies 2006, Davies and McSaveney, 2011, Strom 1994, 2006, Dubovskoi et al, 2008, Strom and Prernik, 2013.

Rapid rock avalanche motion halted when the mass struck the sharp bend in the slope composed partially of granite and partially of boulders in sandy-gravel fill, which represent either the reworked glacial deposits or much older rock avalanche deposits whose source zone cannot be identified with confidence now (Figure 40). The frontal part of the rock avalanche has an expressive wavy surface with longitudinal levees and furrows (Figure 41), whose orientation reflects the direction of debris motion. It seems that motion halted abruptly. This is indicated by the presence of angular boulders with X-like fractures (Figure 42) caused, most likely, by the collision of nearby boulders during debris motion. However, they did not separate into several "independent" blocks afterward.

The uppermost part of the rock avalanche deposits is composed of huge angular boulders (see Figure 42), while debris below this carapace seems to be crushed to a much greater extent (see Figure 35).

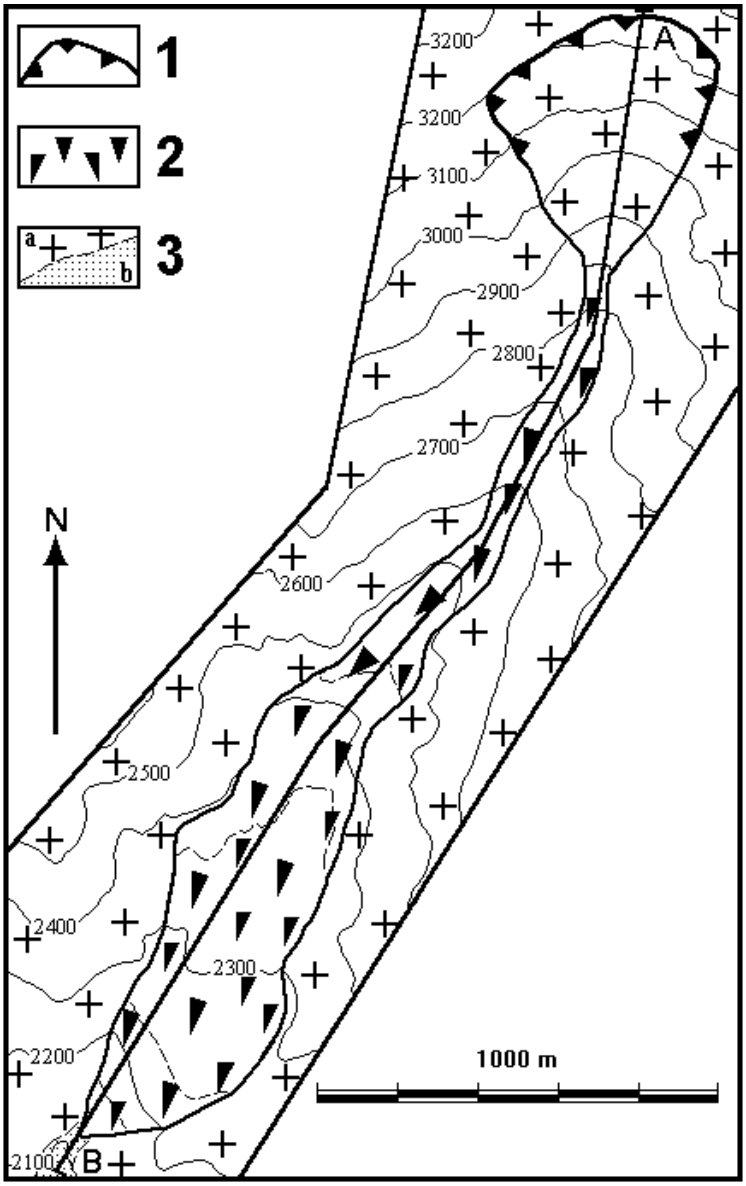

Figure 33. The schematic map of the Seit rock avalanche

1 – rock avalanche scar; 2 – rock avalanche debris; 3-a – bedrock granite; 3-b – pre-rock avalanche alluvial deposits

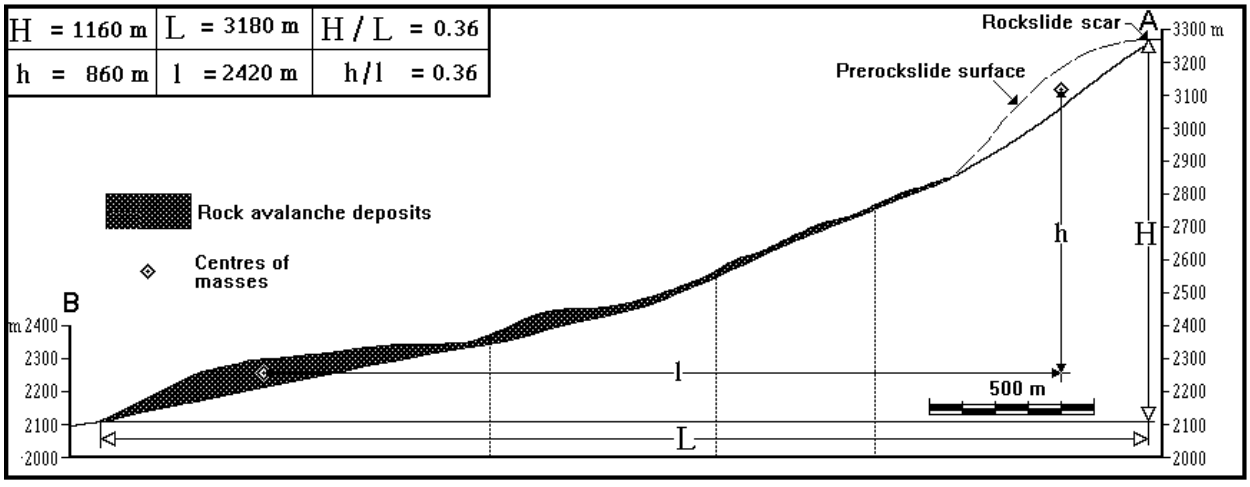

Figure 34. Longitudinal cross-section along the Seit rock avalanche

Figure 35. The Seit rock avalanche body fills the creek's channel and overlays the recent terrace left by pre-rockslide debris flows

Figure 36. Drilling of the ~300 years old Archa tree growing on the Seit rock avalanche deposits

Figure 37. The Seit rock avalanche headscarp and the debris-free upper part of the transition zone

Figure 38. 3D Google Earth image of the Seit rock avalanche with marked trimlines in the upper part of the transition zone which are 100-140 m above the gully bottom

Figure 39. Lower part of the Seit rock avalanche transition zone

The trimline marked by arrows rises up in the central part of the panorama blocking the small gully and then decreases gradually

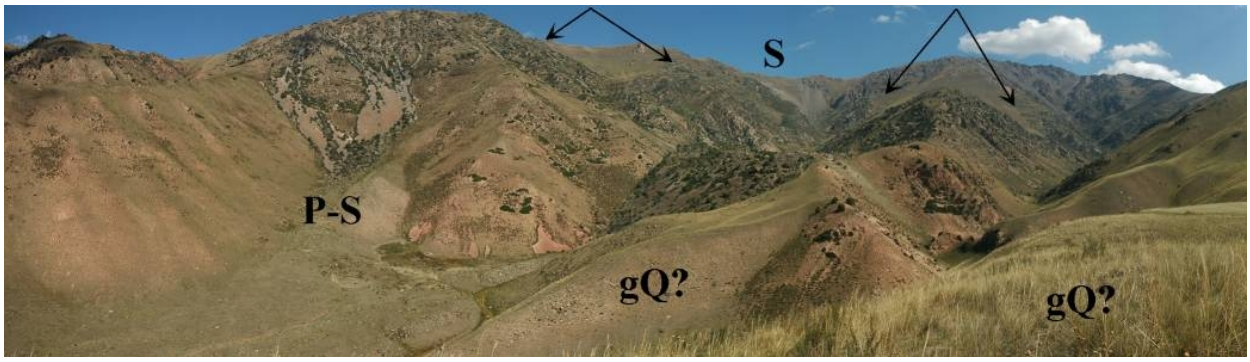

Figure 40. Overview of the Seit and the Pre-Seit rockslides area

S – Headscarp of the Seit rock avalamcje; P-S – headscarp and remnants of the body of the Pre-Seit rock avalanche; Arrows mark remnants of smooth older relief; gQ? – reworked glacial or very old rock avalanche deposits

Figure 41. Wavy surface of the Seit rock avalanche distal part

Longitudinal 'stripes' of coarser and finer debris can be observed on top of the rock avalanche body (Figure 43). Some of finer 'stripes' are even covered by soil and vegetation. Locally, molards – conical hills up to 1.0-1.5 m high are observed. Molards are composed of granite blocks that look finer than the surrounding big angular blocks (Figure 44), which is typical of 'classical' molards [Cassie et al., 1988] formed by ejection of the material from the internal part of rock avalanche debris. At some sites here it is apparent that molards originated due to *in-situ* destruction of very large fractured blocks pressed out or ejected upward from the rock avalanche interior. Such blocks, being subjected to the triaxial compression inside the moving debris, have been dilated when they appeared on the surface due to rapid disappearance of high uniform compression (Figure 45).

Figure 42. Angular fractured boulder that was broken just before motion halted
(otherwise its parts should be separated)

Figure 43. 'Stripes' of coarser (big boulders) and finer debris on top of the rock avalanche body

Figure 44. The molard on top of the Seit rock avalanche deposits at 42,12007º N, 74,14185 E
Its structure differs significantly from that of the surrounding chaotic blocks

Figure 45. Bigger molard with distinct evidence of its origin from a single large block

The Seit rock avalanche is not the only large-scale bedrock slope failure in this area. Just nearby at 42.102 N, 74.136º E there is a deep short gully with a small remnant of debris inside it and bouldery deposits in front of it (see Figure 40, Figure 46). It is quite unlikely that such coarse material could be left by debris flows – there is no catchment to produce a debris flow powerful enough to transport such blocks. It is also too low to be a moraine. The most likely explanation is that there was a much older (Pre-Seit) rockslide.

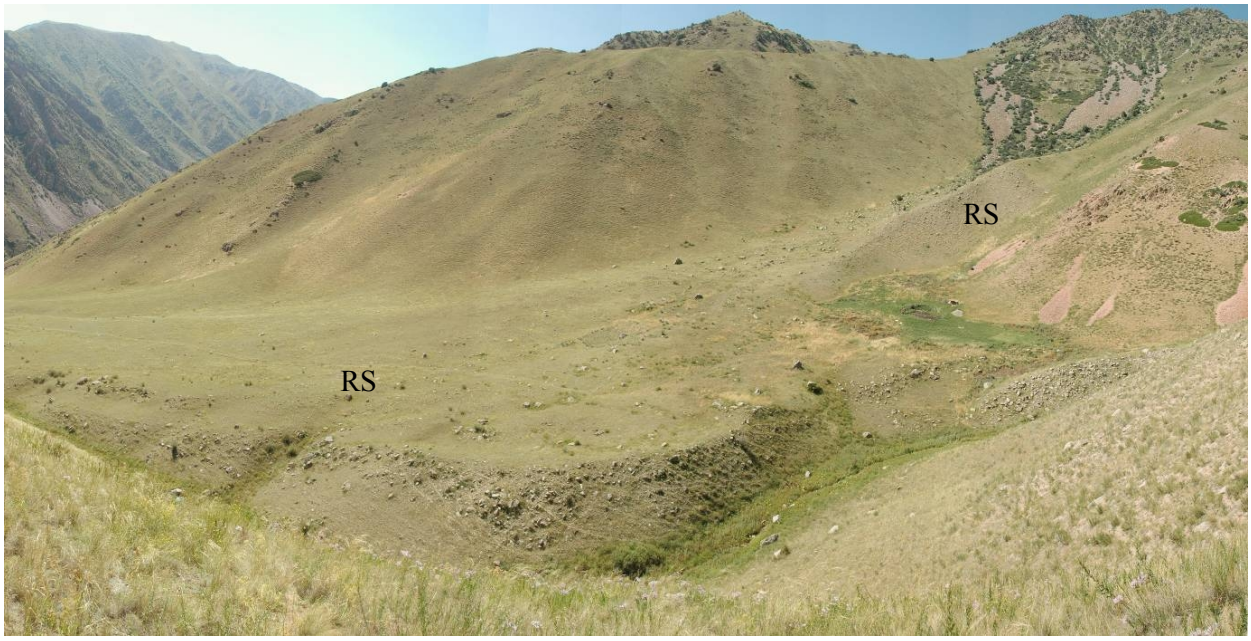

Figure 46. Remnants of the Pre-Seit rockslide deposits (RS) on the right bank of the gully filled by the Seit rock avalanche just downstream of the distal end of the Seit rock avalanche body

2.1.2 The Mini-Köfels rockslide

About 1 km upstream of the place where the Kokomeren River enters the Djumgal intermontane depression, at 41.906º N, 74.28º E, one can see a rockslide (No 3 on Figure 2) representing a smaller analog of the famous 2-3 km^3 Köfels rockslide [Erismann 1979]. The reddish-colored granite and gray-brownish gneiss debris that descended from the right slope of the valley rests on the left bank of the Kokomeren River composed of gray Palaeozoic terrigenous deposits (Figure 47).

As in the Köfels' case, the frontal part of this "Mini-Köfels" rockslide filled the prominent lowering at the opposite bank of the valley (Figure 48). It is a typical "primary" rock avalanche whose distal part is raised much above its proximal part, where the temporary dam was subsequently eroded by the river. However, unlike the Seit rock avalanche representing the Primary RA type in laterally confined conditions, the Mini-Köfels event occurred in frontally confined conditions – in a rather narrow, deep valley. Nevertheless, lengthwise debris distribution is the same – most of the collapsed material moved ahead without any prominent accumulation at its proximal part.

On the right bank of the river, immediately above the motorway, one can see intensively crushed rockslide debris overlaying alluvium of a low terrace (Figure 49).

The rockslide formed a dam several dozens of meters high. However, it was overtopped shortly after the event, since the lake was formed in the narrow gorge, and breached soon at its proximal part by the powerful Kokomeren River.

Though no lacustrine sediments have been found close to the dam, it is hypothesized that lacustrine sediments outcropping about 4.5 km upstream could be accumulated in the temporary lake dammed by the Mini-Köfels rockslide. It is known that reservoir sedimentation starts from the upstream part where a stream's velocity sharply decreases (it will be shown on Figure 153). Thus, even in short-lived, temporary lakes lacustrine sediments would accumulate far from the dam, rather than just near it where the lake was much deeper.

Figure 47. The Mini-Köfels rockslide deposits resting on the left bank of the Kokomeren River valley

Figure 48. Central and downstream parts of the Mini-Köfels rockslide body
Smooth hill left of the bedrock summit is the distal part of the rockslide that filled the abandoned valley

This phenomenon will be described in more detail later, along with the description of well-pronounced lake sediments of the Kokomeren rockslide dammed lake (Section 3.1.4).

The Mini-Köfels rockslide is characterized by distinct correlation of the lithologies visible in the headscarp area and in the deposits. The upstream part of its body is composed of reddish-colored granite debris (small light-red area at the extreme left part of the body on Figure 47), while the downstream part is of gray-brownish gneiss debris (most of Figure 48). These units correspond directly to the bedrock types of the source zone of this slope failure. This peculiarity of large-scale bedrock landslides will be described in section 3.

Figure 49. Comminuted Mini-Köfels rockslide debris (crushed granite) overlying alluvium of the Kokomeren River right bank terrace about 5 m high

2.1.3 The Ak-Kiol rockslide dam

One more impressive example of a Primary rock avalanche whose path is characterized first by lateral confinement and then by frontal confinement is the Ak-Kiol rockslide located in the southern part of the study region at 41.68 N, 74.28º E in the small Unkursay river valley that flows into the Minkush river a few hundred meters upstream of its junction with the Kokomeren River (Figure 50, No 2 on Figure 2). The rockslide still forms a dam with a beautiful lake behind it (Figure 51, Figure 52). Another large rockslide dammed the same valley 2.5 km downstream, but this dam has breached (see section 4.2).

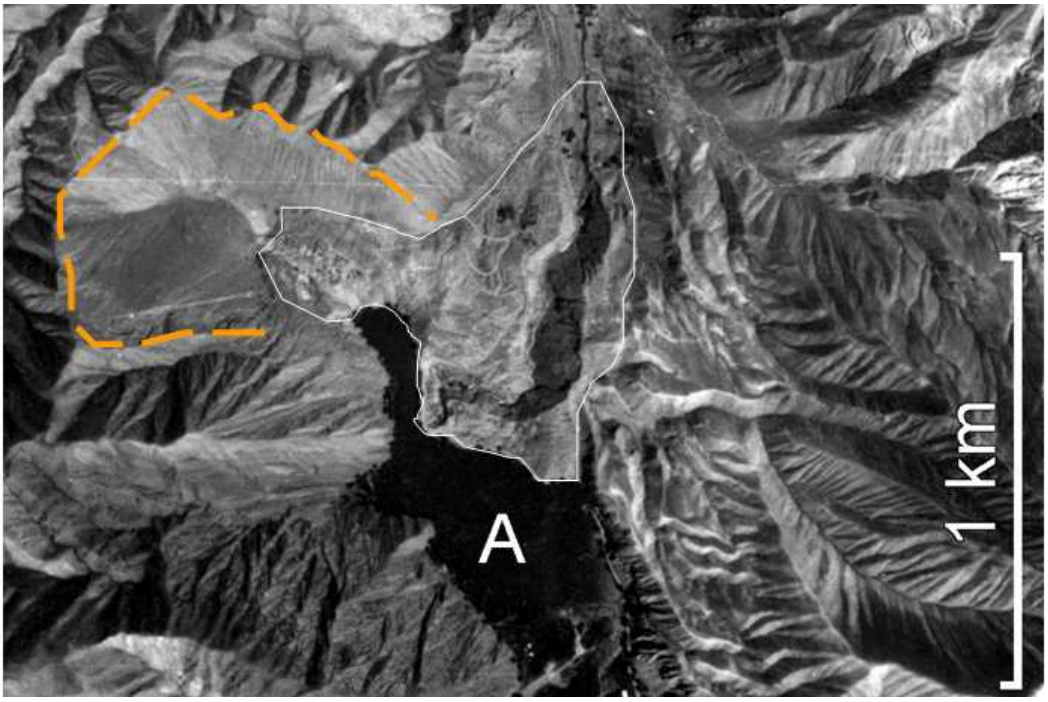

Figure 50. Air photo of the Ak-Kiol area

A – rockslide dammed lake; headscarp is marked by orange dashed line; rockslide body by thin white line

Figure 51. The Ak-Kiol Lake and deeply eroded rockslide body damming it

Figure 52. The Ak-Kiol rockslide-dammed lake from upstream

Notice that the right (distal) part of the dam is much higher than the proximal one, indicating the "Primary" type of this blockage

This rockslide originated in Paleozoic brown-red conglomerate and sandstone with thin gypsum interbeds and has a roughly 0.5 km deep headscarp (Figure 53) that affected the ridge far beyond its watershed (Figure 54). In fact, this was the collapse of a Paleozoic syncline core whose hinge line was dipping gently towards the river valley. The southern side of the headscarp (left on Figure 53) directly corresponds to the bedding and additional subsequent failures likely occurred from here later on (Figure

55). The opposite, left side of the headscarp is slightly steeper than the bedding. The presence of the gypsum in these strata should facilitate formation of a very deep rockslide scar, considering its low strength.

The initial thickness of the moving debris before it left the headscarp and entered the Unkursay valley can be reconstructed based on the presence of debris patches on both sides of the headscarp depression much above its present day base. On Figure 56 one can see the mouth of the dry gully joining the headscarp from its right side filled with debris. The surface of the rockslide deposits resting in this gully is 130-140 m higher than the surface of the rockslide body just below, according to a laser vector measurement. A small patch of debris at the opposite side of the headscarp outlet, approximately on the same level (see Figure 53) also marks debris thickness at the left outlet from the headscarp (Figure 57). The distinct lowering can be seen at the proximal part of the body partially filled by debris flows, some of which are quite recent (Figure 58). Moreover, some evidence indicates that the proximal part of the rockslide dam could be formed later than its main body. This can be assumed from the slightly different shape of small hills that form the dam's surface (see background part on Figure 51 and dashed line on Figure 59).

Figure 53. Panorama of the Ak-Kiol rockslide headscarp
The outlined areas are shown on Figure 56 and Figure 57

Figure 54. Distant view on the upper part of the Ak-Kiol rockslide headscarp

The distal part of the rockslide body is much higher than its proximal part (see Figure 52, Figure 59). Considering this, as well as the shape of the dam, which is much wider than the headscarp outlet, this rockslide can be classified as a Primary rock avalanche that was deposited in frontally confined conditions.

Though it is clear that the rockslide was formed from the core of a syncline with limbs dipping about 30° towards the axis, its body, well visible in the canyon eroded through the dam body, looks as if it is composed of nearly horizontal layers of sandstones and conglomerates (Figure 60). It can be hypothesized that initially the gigantic wedge slid down as a block slide following the fold hinge line, leaving patches of debris on the headscarp walls. As soon as it left the deep headscarp and lateral confinement provided by the headscarp walls, this synclinal structure was unfolded and, finally, the deposit rested in the valley with nearly horizontal strata. Finally, debris climbed the opposite bank of the river valley passing an equilibrium point and came to rest.

Figure 55. Right side of the headscarp coinciding with bedding where subsequent failures have occurred

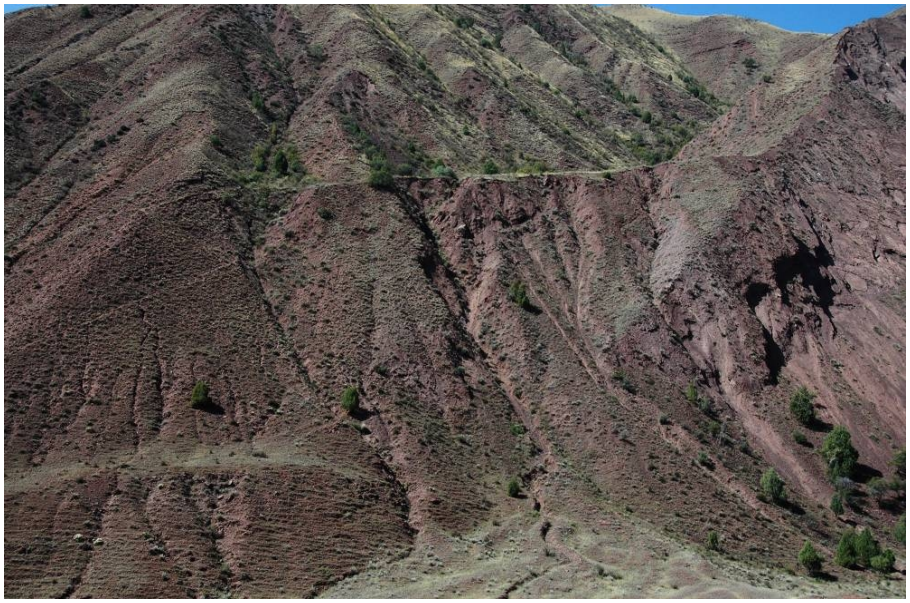

Figure 56. Mouth of the gully near the headscarp that was blocked by rockslide debris
Nearly horizontal top of this fill is about 130-140 m above the surface of the main body

Figure 57. Patch of rockslide debris on the left outlet of the headscarp

Figure 58. Proximal depression at the headscarp bottom partially filled by debris of the subsequent failures and debris flows

Figure 59. View on the Ak-Kiol rockslide dam from the downstream
Dashed black line shows the assumed initial dam's crest profile, before deposition of the proximal part of debris

Figure 60. Rockslide body composed of nearly horizontal strata despite the syncline structure of the host red beds

2.2 Jumping rock avalanches

2.2.1 The Kashkasu rockslide

An expressive rockslide 5-10 Mm^3 in volume collapsed from a ~700 m high, steep slope and blocked the Kashkasu River at 41.91º N, 74.17º E (No 4 on Figure 2, Figure 61). The landslide dam still exists while the small dammed lake has been filled with sediments forming a forested flat area surrounded by cliffs (Figure 62). This rock slope failure formed a compact body, the downstream part of which is much wider than the upstream part, and has a distinct convex shape with a nearly planar surface and steep frontal slope (Figure 63, Figure 64).

Besides the surface outflow used by the small stream and marked by dark-green bushes visible on Figure 63, there is a spring (marked by the white arrow on the figure), that releases groundwater filtering through the upper narrower part of the dam. No springs are visible in the lower part of the dam.

On Figure 63 one can see that the spoon-shaped sliding surface of this rockslide comes out on the slope at a level of the upper part of the dams' body, about 100 m above the valley bottom.

Slopes of both upper and lower parts of the blockage are either convex or planar. The upper one has a distinct lowering at its proximal part and poorly pronounced upstream widening, reflecting the action of the same process that resulted in the formation of the distinct downstream spreading of rockslide debris.

When climbing the upper part of this blockage along the path visible on Figure 63, one crosses sub-vertical belts of angular boulders of different lithologies. Most of them are gneiss-like granites, prevailing within the headscarp area, while between such zones are rather narrow belts composed of dark grey to black mafic igneous rocks (Figure 65). Later on, describing the Kokomeren and Ornok rockslides, we will focus on the retention of the structure typical of the host rock mass in the resultant rockslide/rock avalanche deposits. The formation of bouldery belts of different lithologies well expressed here reflects the same phenomenon.

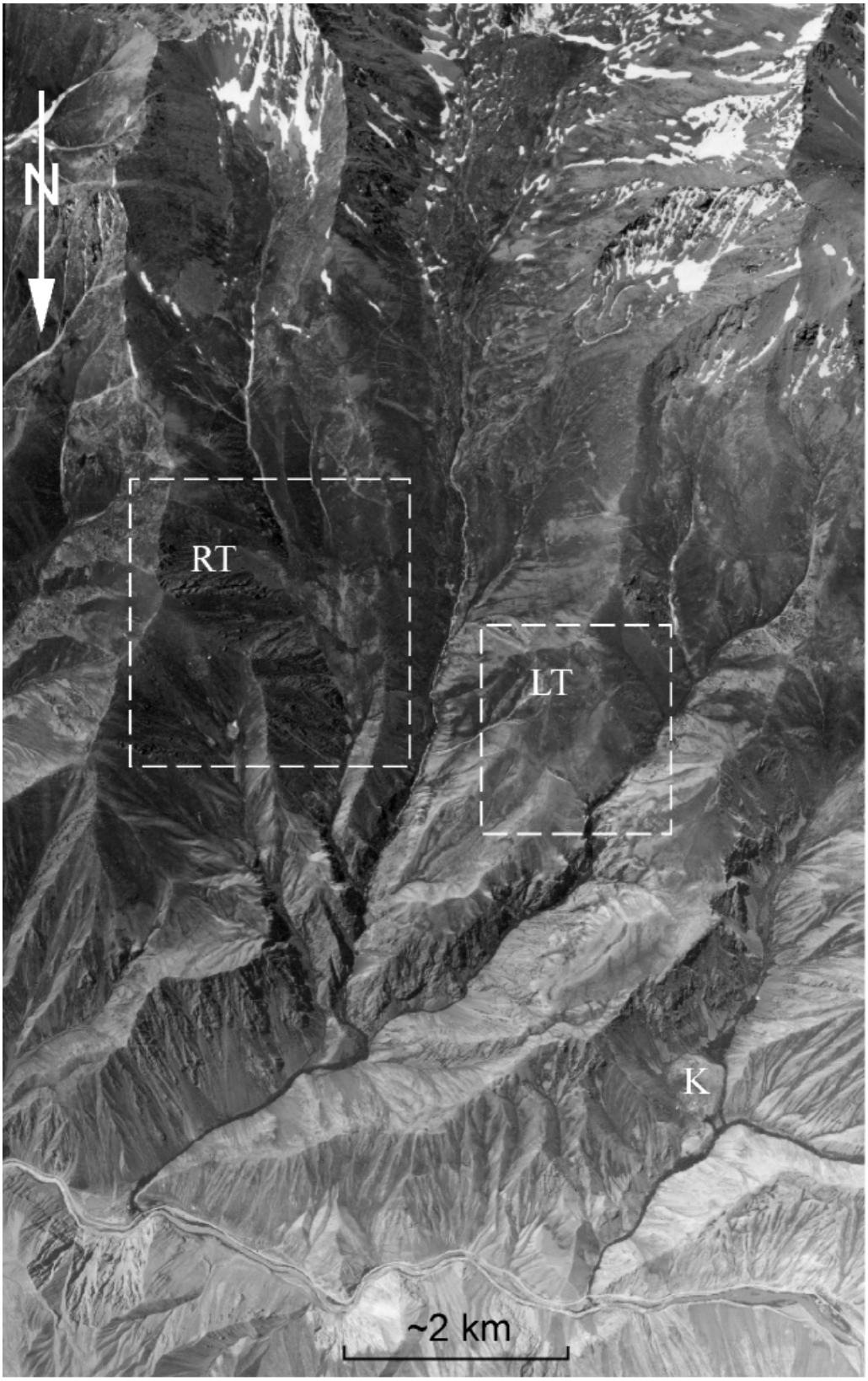

Figure 61. Aerial photograph of the Tuurakaing River basin and of the lower part of the Kashkasu River basin

LT – the Left Tuurakaing rock avalanche; RT – the Right Tuurakaing rock avalanche; K – the Kashkasu rockslide. Outlined hardly attainable rock avalanches are shown on Figure 189

Figure 62. The Kashkasu rockslide dam and a planar surface of the dammed lake filled by sediments

Figure 63. Kashkasu rockslide dam

The planar surface visible in front of the dam is the top of rockslide body lower part (see Figure 64). White arrow marks springs of water filtering through the upper part of the dam

Figure 64. View on the lower widened part of the Kashkasu rockslide dam from the path crossing its upper part (see Figure 63)

Figure 65. Main lithologies typical of the upper part of the Kashkasu dam body

One more rock avalanche – the longest one in the entire region was identified on space images at the Suusamyr Range in the upper reaches of the Kashkasu River in the recently glaciated zone (41.867° N, 74.15° E). The upper part of its valley bottom is filled by bouldery deposits with distinct striation (Figure 66). Both these deposits and the assumed headscarp differ significantly from what can be seen in the adjacent valleys at the same altitude (Figure 67). Microrelief of the deposits filling other valleys is totally different and their watershed slopes also are much more curved by nival processes than the smooth headscarp of this rock avalanche covered by talus. Combination of these morphological peculiarities indicate different origin of the Upper Kashkasu valley fill from that of all the surrounding valleys, which, in turn reflects difference of the processes that formed this relief. All these allows sound assumption that here we have the rock avalanche, which is the longest one in the entire Kokomeren River basin.

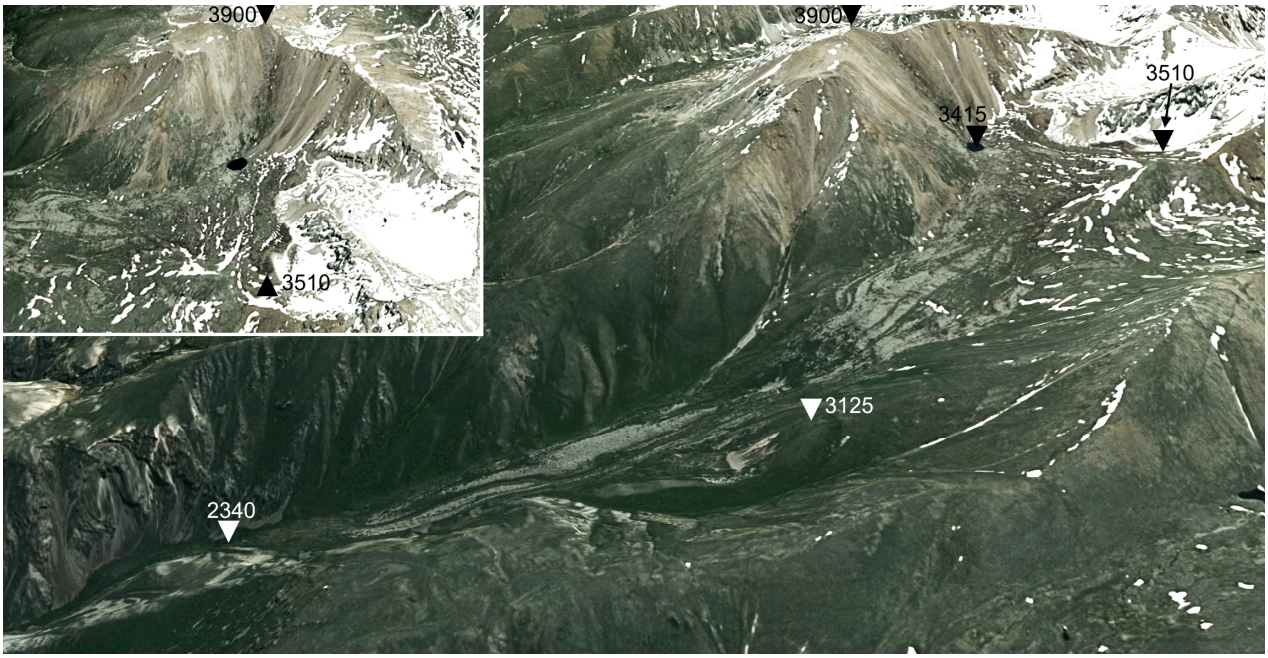

Figure 66. Assumed 5.7 km long Upper Kashkasu rock avalanche that originated in the recently glaciated part at the eastern termination of the Suusamyr Range. Its debris raised on the opposite slope up to 3510 m a.s.l. Freshness of the assumed headscarp, which relief differs from that of the adjacent slopes is visible on the inset. The elevation mark 3125 m a.s.l. indicated the headscarp crown of a smaller rockslide which body merges the main rock avalanche. 3D Google earth image

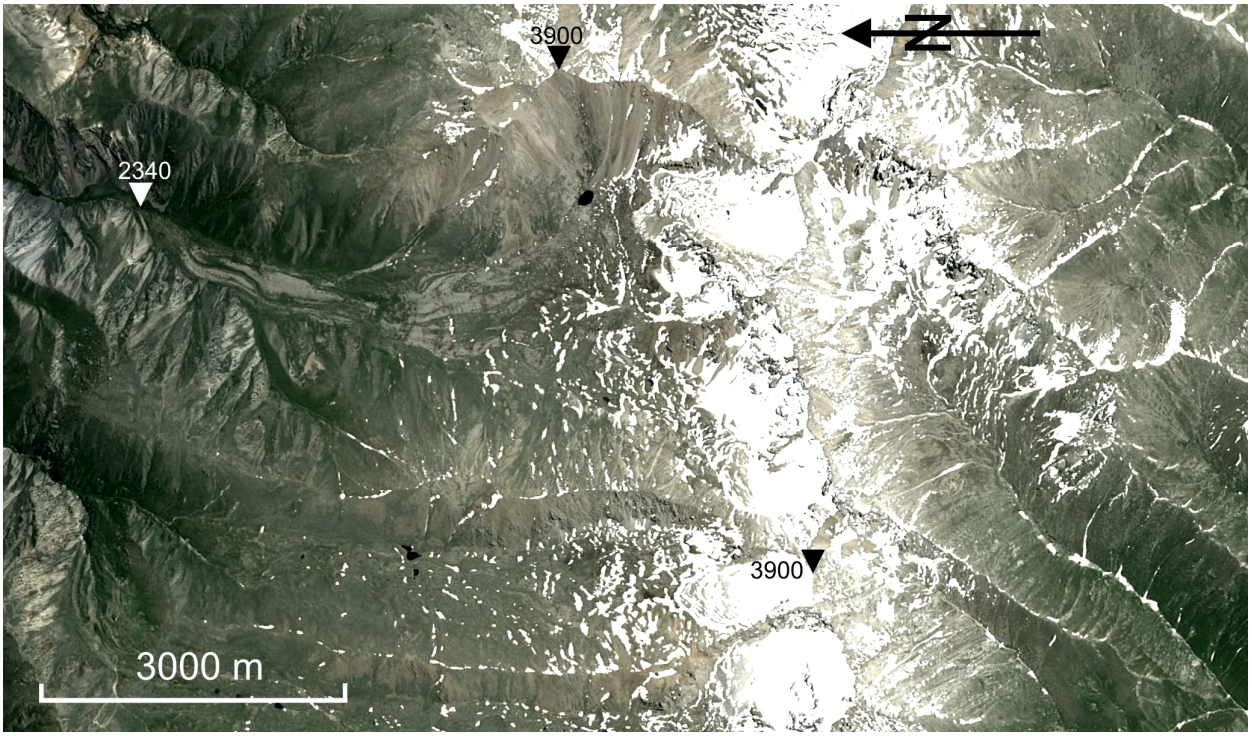

Figure 67. Google Earth space image of the part of the Suusamyr Range watershed

2.2.2 The Northern Karakungey rock avalanche

Another example of a Jumping rock avalanche is located in the Northern Karakungey creek valley at 41.87º N, 74.24º E (No 5 on Figure 2, Figure 68). It also has a compact body at the foot of the rockslide scar with convex slopes, including an elongated avalanche-like part (Figure 69). The sliding surface of this bedrock slope failure also comes out on the slope about 200 m above its base, approximately at the level of the topmost surface of its compact part (Figure 70). While jumping from this 'shelf' the descending rock mass of this Northern Karakungey rockslide divided into two parts – the larger one converted into a rock avalanche, and the smaller one formed a separate deposit upstream of the main dam (see map on Figure 69). The total volume of this rockslide is about 10×10^6 m^3.

As can be seen on Figure 71, the rock avalanche followed the creek's channel in a direction almost transverse to the direction of the initial slope failure (see Figure 69). It is interesting that it hugged the true left bank of the valley. Being ahead of the description of the Sarysu, Southern Karakungey and Chongsu Secondary rock avalanches (section 2.3) we want to point out that debris of the downstream part of the Northern Karakungey rock avalanche did not spread over the entire valley bottom as that of the Secondary rock avalanches. We hypothesize that such a difference reflects some differences in mechanisms of their mobility. As can be seen on Figure 63 and Figure 69, the sliding surfaces of both the Kashkasu rockslide and the Northern Karakungey rock avalanche came out on the slopes much above their feet, so that descending rock masses fell onto valley bottoms nearly at a right angle. This could result in squeezing of the rockslide frontal part by the overtaking material that originally rested at the upper part of the source zone (Figure 72). Just this squeezed debris could form the lower, more mobile part of the resulting rockslide dam.

Figure 68. Overview of the Northern Karakungey rock avalanche

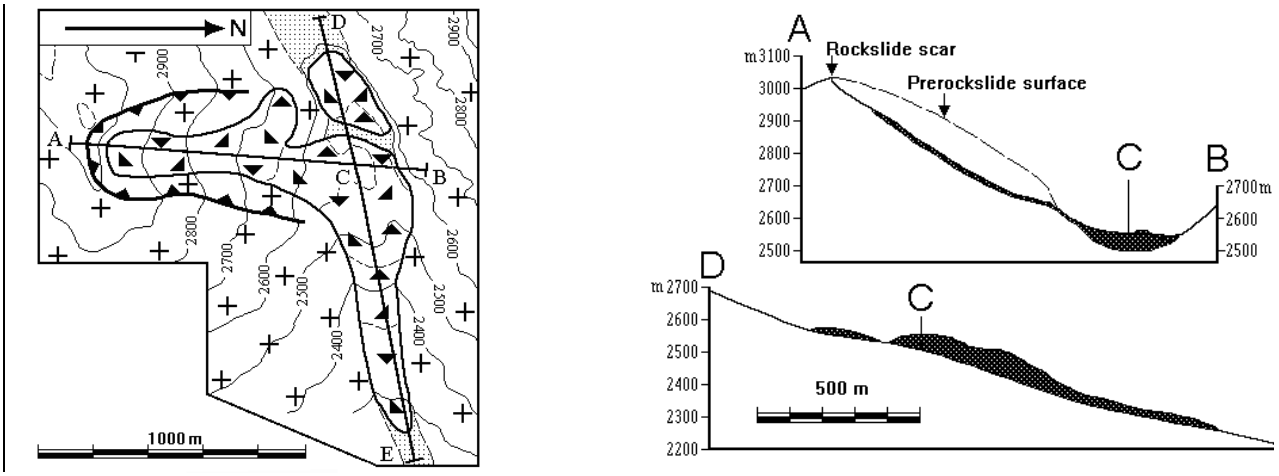

Figure 69. Schematic map and cross-sections of the Northern Karakungey rockslide

Figure 70. Headscarp of the Northern Karakungey rock avalanche
Vie from the top of the compact part of its body

Figure 71. Northern Karakungey rock avalanche
Compact blockage with convex slopes in the background and the avalanche-like part in the foreground. Note that the latter fills the valley only partially, following its most recently incised gully

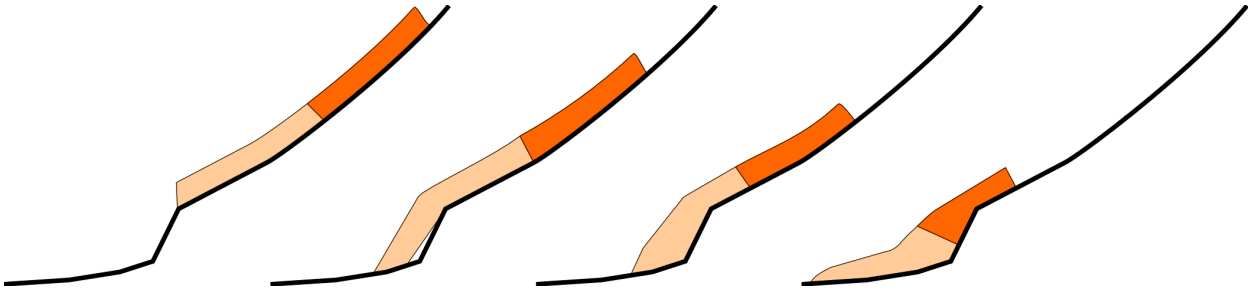

Figure 72. Schematic model of the successive stages of "Jumping" rock avalanche formation

2.3 Secondary rock avalanches

2.3.1 The Southern Karakungey Secondary rock avalanche

The western termination of the Djumgal intermontane depression where the abovementioned Northern Karakungey rockslide is located has been subjected to numerous landslides and rock avalanches that occurred repeatedly in the Late Pleistocene and Holocene. Two gullies (Northern and Southern Karakungey) dissect the range that rises above the Djumgal depression termination, and both of them have been dammed by rockslides. Although both the Northern and Southern Karakungey Holocene rockslides occurred on slopes of similar height (~600 m) and steepness, composed of the same granite and facing north and north-east (No 6 on Figure 2, Figure 73, Figure 74), their morphology and mechanism of emplacement differ significantly. It can be assumed that both failures occurred simultaneously due to a strong earthquake, though neither of these features has been dated by any quantitative method yet. Tree ring dating provided an age of about 250 years for both (thus, younger than the Seit rock avalanche dated by the same method), which corresponds to the upper age limit. It is most likely that in fact they are older, but how much older is still questionable. One more significantly eroded scar can be identified between these gullies on the east-facing front slope (KK-O on Figure 74). Corresponding deposits have been significantly reworked and can hardly be distinguished from bouldery alluvial fans that form the uppermost part of the depression fill. Such peculiarities show that this failure should be much older than the well-expressed Karakungey rock avalanches.

Besides above-mentioned bedrock landslides that can be identified morphologically, there is evidence of one more much older rock avalanche. A large amount of unrounded granite boulders rests several kilometers east of the Southern Karakungey rock avalanche (P-KK on Figure 73). This material differs from the semi-rounded boulders of, likely, reworked glacial origin typical of the Quaternary fill of the Djumgal depression western termination. However, the assumption that it is the remnant of a very long runout, old rock avalanche requires additional proof.

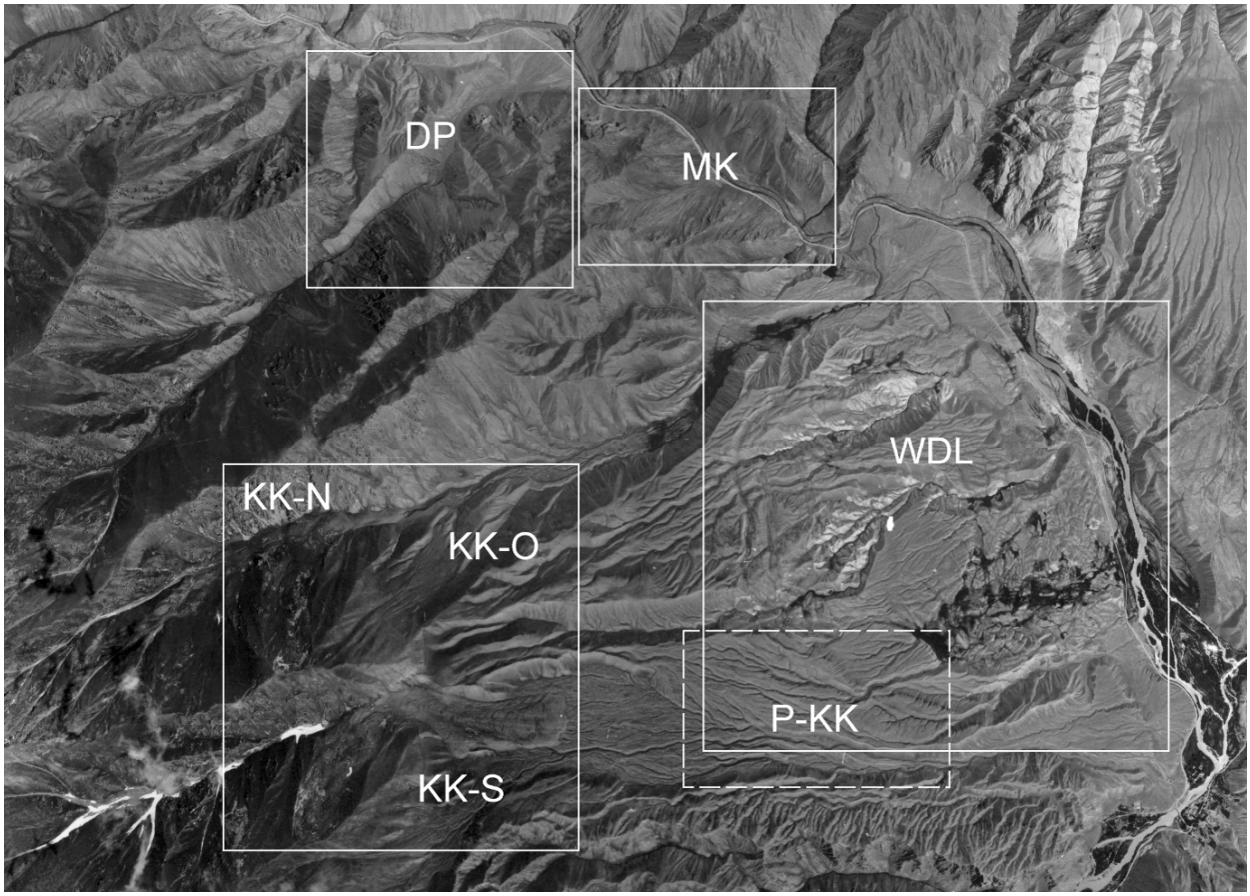

Figure 73. Landslides, rockslides and rock avalanches at the western termination of the Djumgal intermontanee depression and the surrounding ranges

DP – Displaced Peneplain RS, MK – Mini-Köfels RS, KK-N – Northern Karakungey RA, KK-S – Southern Karakungey RA, KK-O – Old Karakungey RA, P-KK – area where deposits of the assumed Pleistocene Pre-Karakungey RA has been found, WDL – Western Djumgal landslide about 10 km^2 in Neogene and Quaternary deposits bounded by a distinct horseshoe-shape escarpment

The Southern Karakungey rock avalanche (41.86º N, 74.25º E), about 20×10^6 m^3 in volume, is a classic example of the secondary type of long runout bedrock slope failure. Unlike the Chongsu and Sarysu rock avalanches that will be described hereafter, the direction of the avalanche-like debris motion in this case is not in line with the direction of the initial slope failure (Figure 75, Figure 76). The deposit formed a compact dam just at the foot of the scar that blocks the valley and has an expressive concave secondary scar on its downstream slope (Figure 77). The frontal part of this blockage rises 10-15 m above the dam's crest.

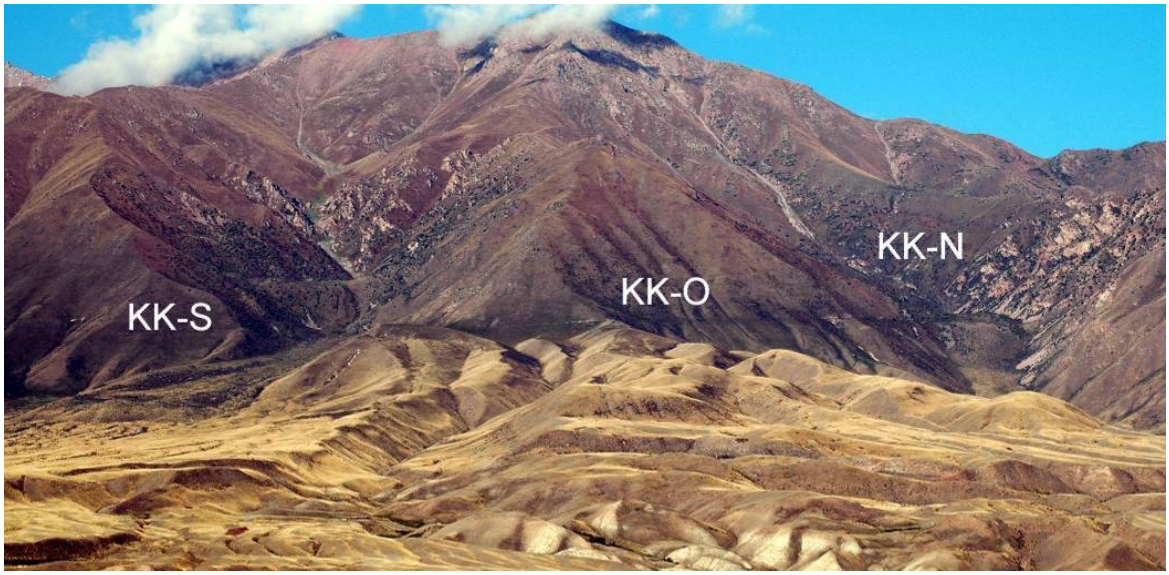

Figure 74. The Karakungey rockslides and rock avalanches at the western frame of the Djumgal depression

KK-S – the Southern Karakungey RA, KK-N – the Northern Karakungey RA, KK-O – Scar of the Old Karakungey RS

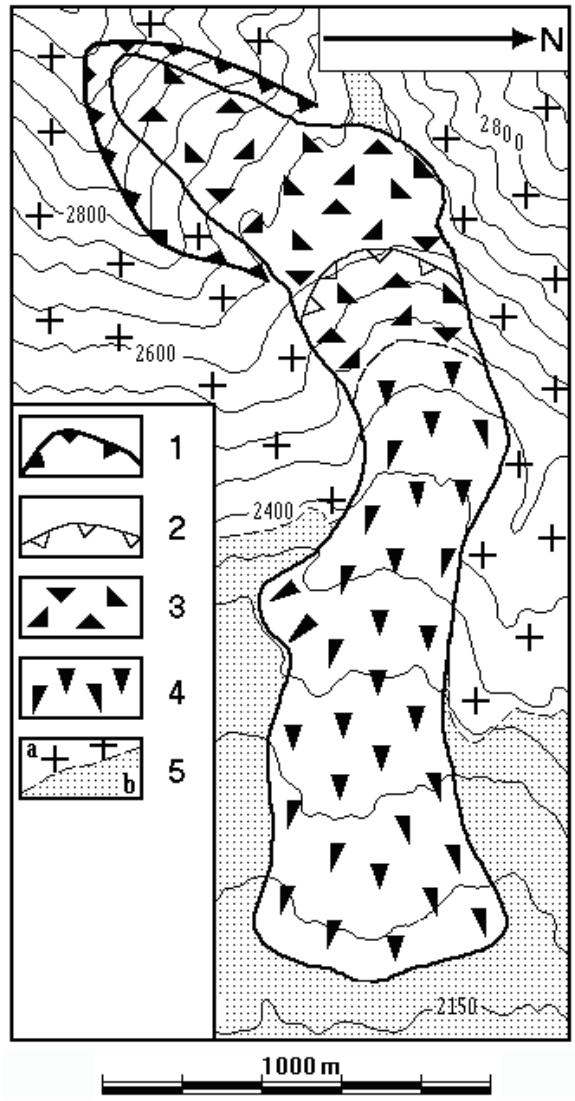

Figure 75. Schematic map of the Southern Karakungey rockslide

Legend: 1 – Main scar; 2 – Secondary scar; 3 – Rockslide deposits; 4 – Rock avalanche deposits of the secondary rock avalanche; 5 – Bedrock (a) and Quaternary deposits (b)

The collapsing rock mass hit the opposite slope at a rather sharp angle (about 40º) and deflected down-valley. The rock avalanche that originated after this collision was 2000 m long, 300-600 m wide and 15-20 m thick (Figure 76). A distinct secondary scar highlights the boundary between the compact and long runout parts of the rockslide deposits (see Figure 77). Since the latter seems to be more voluminous than the assumed volume that could be stored in the secondary scar, it could not have descended from the dam with a significant delay, thus the secondary scar just marks the transfer from the first stage of emplacement to the second one.

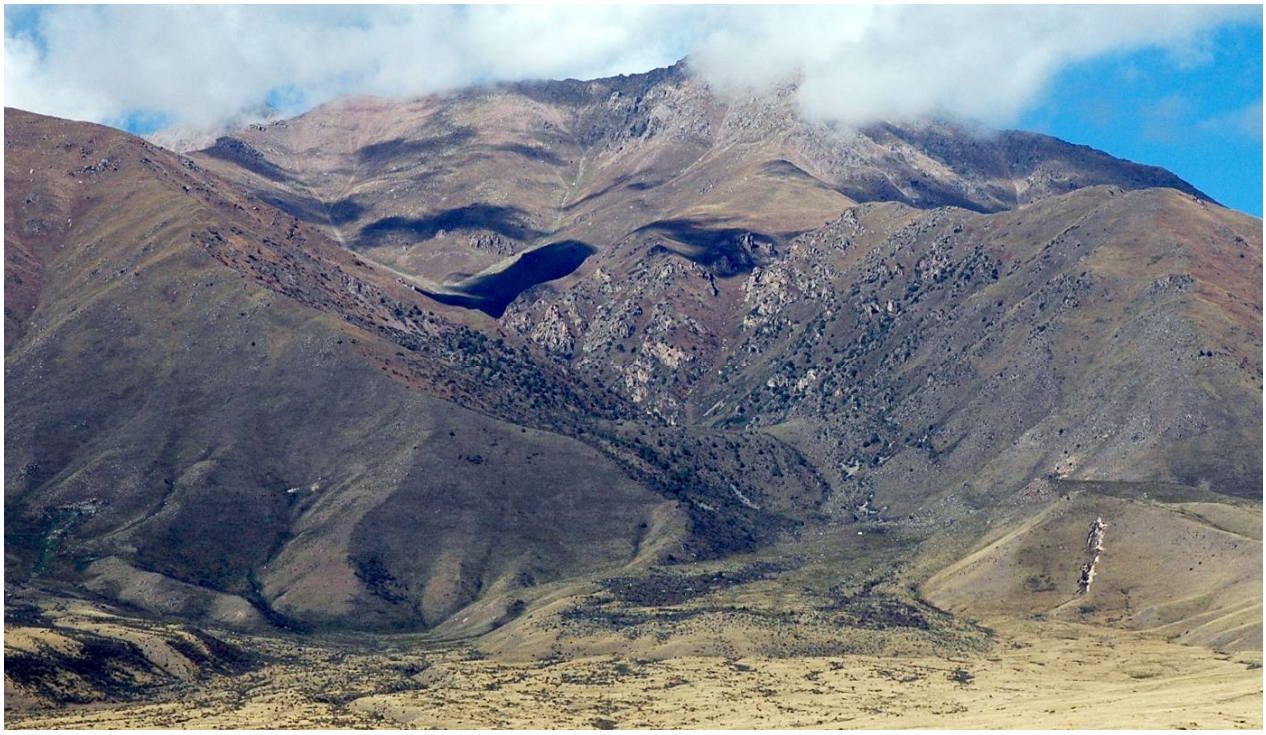

Figure 76. The frontal view on the Southern Karakungey rockslide

Figure 77. Secondary scar of the southern Karakungey rockslide
Headscarp is visible in the background, while compact blockage with raised frontal part and the concave downstream slope – the secondary scar – is in the foreground

A distinct headscarp marks the initially convex spur that collapsed during this slope failure. The resultant blockage has a straight steep upstream-facing slope indicating the absence of any upstream spreading of debris (Figure 78), contrasting long downstream motion.

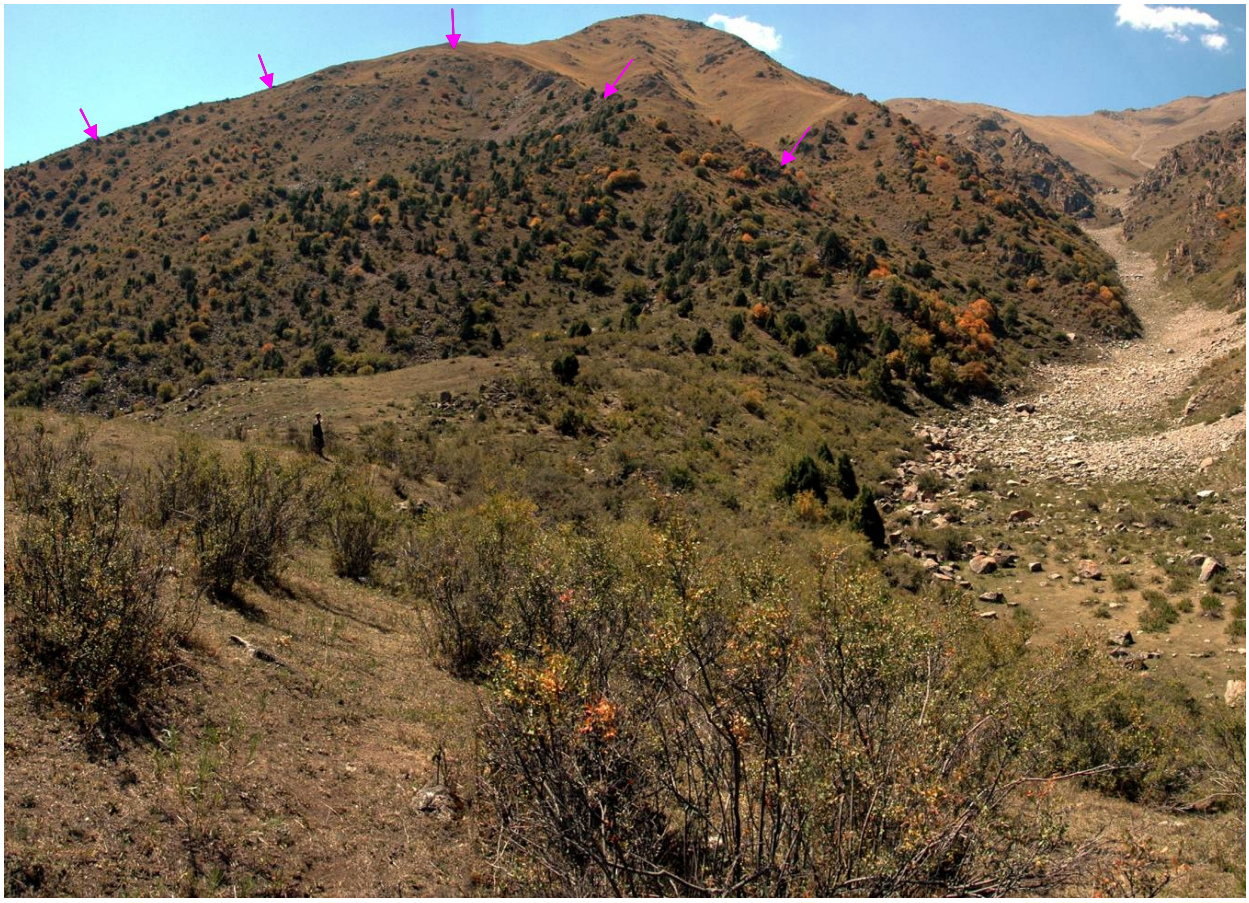

Figure 78. Headscarp (arrows) and sharp upstream edge of the Southern Karakungey rockslide body
View from the front of the compact part

The outer boundary of the long runout rock avalanche (which is several dozen meters wide) is composed of huge angular boulders, whereas its axial part and boundary slopes are composed of finely crushed debris (Figure 79). The central part of this "tongue" is lower than the outer bouldery belt.

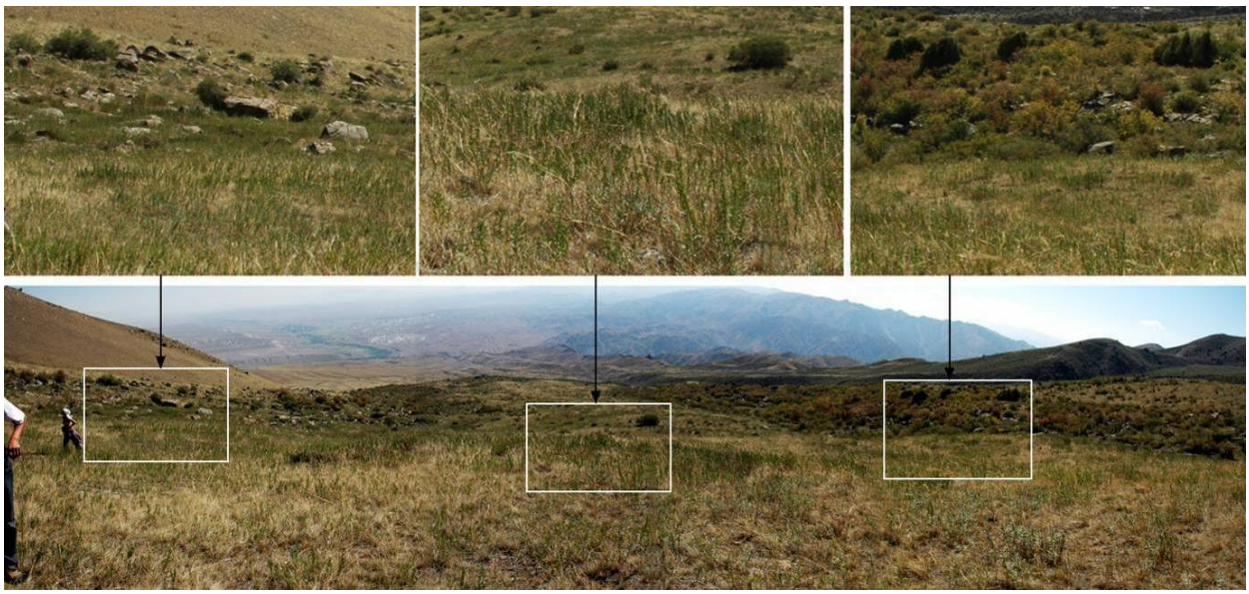

Figure 79. Surface of the Southern Karakungey rock avalanche
(view "downstream"). Levees composed of angular granite boulders are shown on the left and right insets while smooth matter in the axial zone is shown on the central inset

On the true right side of the avalanche, where it leaves the rather narrow deep valley, one can see the remnant of older bouldery deposits (O on Figure 80) overlain by the deposits of Southern Karakungey rock avalanche (S-KK, ibid). Though its origin is questionable, it could be hypothesized that it is a remnant of a much older rock avalanche.

Figure 80. Remnant of older bouldery deposits (**O**) overlain by debris of the recent Southern Karakungey secondary rock avalanche (**S-KK**)

On its path, the secondary rock avalanche left trimlines that are most obvious on the true left slope (Figure 81). Moreover, there is a patch of coarse angular boulders above the distinct trimline resting on the slope composed of much finer material (Figure 82). Since all Quaternary deposits here are composed of granite debris washed out from the adjacent slopes it is difficult to make a distinction between angular boulders of different ages and origins. However, in this case it can be assumed that this patch was formed by boulders ejected from a rapidly moving rock avalanche that had turned here about 30° from E-N-E to E-S-E (see Figure 75 and Figure 81). Similar phenomena at the Chongsu rock avalanche will be described in the next section.


Figure 81. Distinct trimline (arrows) left by the secondary rock avalanche

Figure 82. Patch of angular boulders above the left-side trimline

2.3.2 The Chongsu Secondary rock avalanche ("classical" subtype)

This rock slope failure of about 20×10^6 m^3 in volume descended at 41.99º N, 74.02º E from the ridge bounding the Kyzyl-Oi intermontane depression from the north. It is located in the upper reaches of the Chongsu River (No 7 on Figure 2). The mountain range and depression are separated by a neotectonic fault (see Figure 10), which is visible in the outcrop near the distal end of the Chongsu rock avalanche (Figure 83, Figure 84). The collapsed spur in the upper reaches of the unnamed gorge as well as the entire ridge are composed mostly of granite.

This event is another excellent example of the "classical" subtype of the Secondary rock avalanche type [Strom, 1996, 2006] the characteristic feature of which is the distinct separation of the collapsed rock mass into a compact body immediately at the foot of the failed slope and a long runout rock avalanche that descended from a concave (secondary) scar on the frontal or downstream side of the compact body (Figure 85, Figure 86). It seems that the volume of the secondary rock avalanche exceeds the volume of the secondary scar, similar to the Southern Karakungey case. This excludes the possibility that the secondary rock avalanche could collapse later, some time after the initial slope failure. The secondary scar just marks the abrupt change in debris motion mode.

The Chongsu rock avalanche morphology provides a good chance to reconstruct the process of debris motion and, thus, to make some assumptions on the mechanical processes that took part during rock avalanche emplacement.

Expressive trimlines on the valley slopes that confined the rock avalanche transition zone downstream of the secondary scar are visible much above the final rock avalanche surface (Figure 86 – Figure 88). They stretch parallel to it for a long distance – about 700 m on the left slope and up to 1 km on the right slope. Since they are visible on both sides of the transitional zone it is unlikely that the trimlines mark inertial run-ups, when rockslide debris splashes either on one or on another slope like the Karmadon rock-ice avalanche [Nikitin, et al., 2006] or like the Pandemonium Creek rock avalanche [Evans, et al., 1989]. In this case, we assume that the trimlines indicate constancy of moving debris thickness up to its section shown on Figure 88 where the trimline level sharply decreases so that it meets the resultant rock avalanche surface. This means that at some stage of motion the thickness of moving debris decreased rapidly. Moreover, since the final level of debris within the proximal part of rock avalanche is much lower than the initial one, it is obvious that most of the material "flowed out" leaving just patches of debris on the slopes.

At the site shown on Figure 87 where the rock avalanche turned to follow the valley direction, its right trimline rises about 60 m above its general level indicating the velocity of the moving debris of about 125 km/h. Besides, there is an apron of angular granite boulders on the right slope of the valley above the trimline represented by a nearly horizontal bench (see Figure 87). This apron is very thin, "one boulder thick" in general, and rises up to 15 m above the bench. Moreover, several boulders rest on the slope outside the main apron (Figure 89), allowing the assumption that they moved by ballistic

trajectory. Similar phenomena were observed at the Avalanche Lake rock avalanche in the Mackenzie Mountains in Canada [Evans, et al. 1994]. It can be hypothesized that boulders that formed the apron itself moved in the same way. The position of both the thin continuous apron and separate angular boulders is not random – this splash of debris outside the main mass occurred just at that section where moving debris had to turn sharply. Evidence of similar phenomena can be observed at the Southern Karakungey rock avalanche (see Figure 82). We should note that the velocity estimates based on simple equating of the potential and the kinetic energy are quite rough. More comprehensive analysis that takes into consideration the real geometry of the flow-path was proposed by Rahman and Konagai (in press). However, considering that, as they pointed out, velocity estimated based on mud-marks far from the source area are close to those obtained by the numerical modeling our estimate of 125 km/h seems to be more or less realistic.

"Downstream" of the point where the left trimline level decreases the rock avalanche formed a distinct mound-like body about 5 m high (Figure 90), while its distal part rests as a fan-like body from 3-5 to 7-10 m thick and is composed of huge angular boulders with distinct lateral and frontal edges (Figure 91), which indicate that motion halted abruptly. It should be noted that we can see the grain size composition of its debris from the surface only. No one outcrop exists where its internal structure is observable. The frontal part of the rock avalanche deposits overlays a small levee composed of granite boulders of the same size, which, unlike those described above, are sub-rounded (Figure 92). Most likely it was formed by a pre-rockslide debris flow, which, by the way, should be quite powerful, judging from the boulders' sizes.

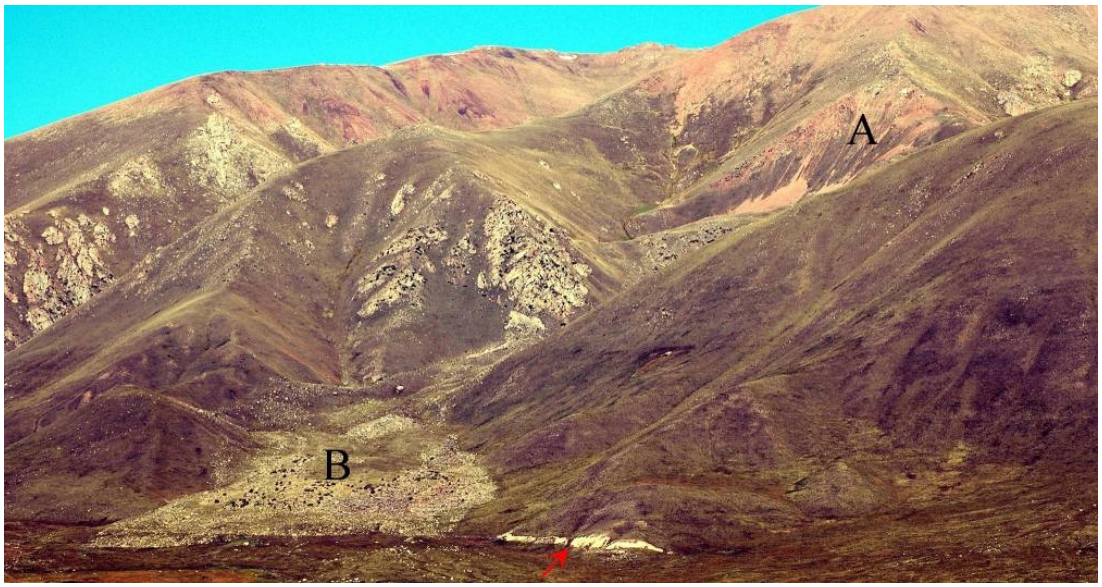

Figure 83. Overview of the Chongsu rock avalanche

A - headscarp, B - distal accumulation. Red arrow marks the outcrop of neotectonic reverse fault (Figure 84)

A few kilometers east of the Chongsu rock avalanche at 42.01º N, 74.05º E at the north-western boundary of the Kyzyl-Oi depression there is one more large rock slope failure. Unlike the above Chongsu case this bedrock slope failure, named Chongsu-2, did not transform into a long runout rock avalanche. Its deposits formed a convex, compact body (Figure 93). Failure occurred a few hundred meters north of the surface rupture shown on left zoomed fragment of Figure 10. Such a coincidence gives grounds for the assumption that both rockslides occurred due to a strong earthquake that produced this rupture as well. To prove (or disprove) this assumption, precise dating of both rockslides and of rupturing events should be carried out.

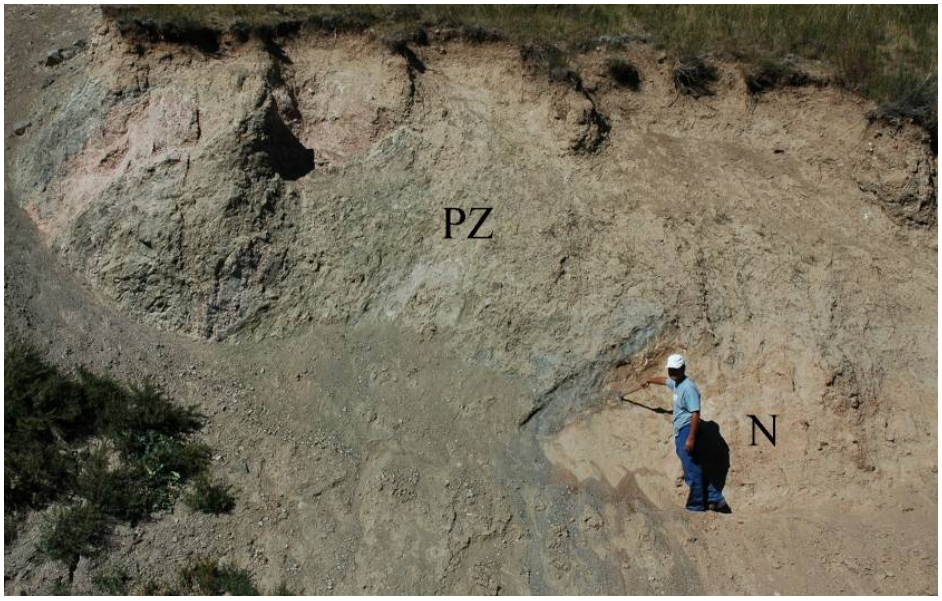

Figure 84. Neotectonic reverse fault
PZ – crushed Paleozoic rocks; N – Neogene deposits

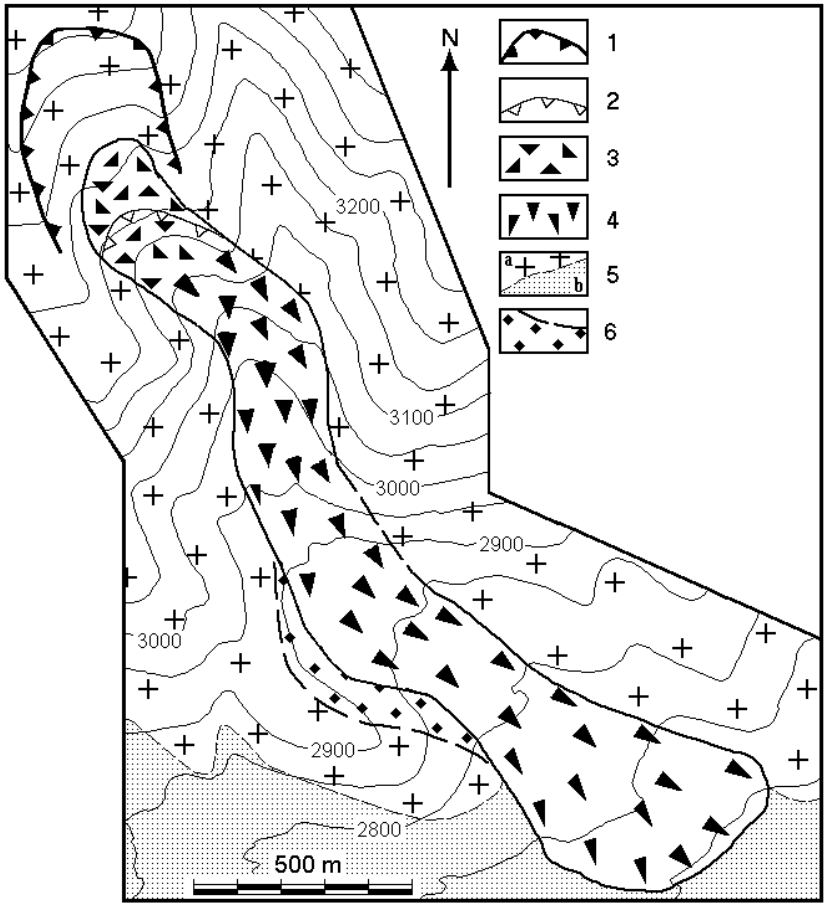

Figure 85. The schematic map of the Chongsu rock avalanche
Legend: 1 – Main scar; 2 – Secondary scar; 3 – Rockslide deposits; 4 – Rock avalanche deposits, including those remaining on the slopes above resultant surface of the deposits; 5 – Bedrock (a) and Quaternary deposits (b); 6 – Remnants of rock avalanche splash above the main deposit surface

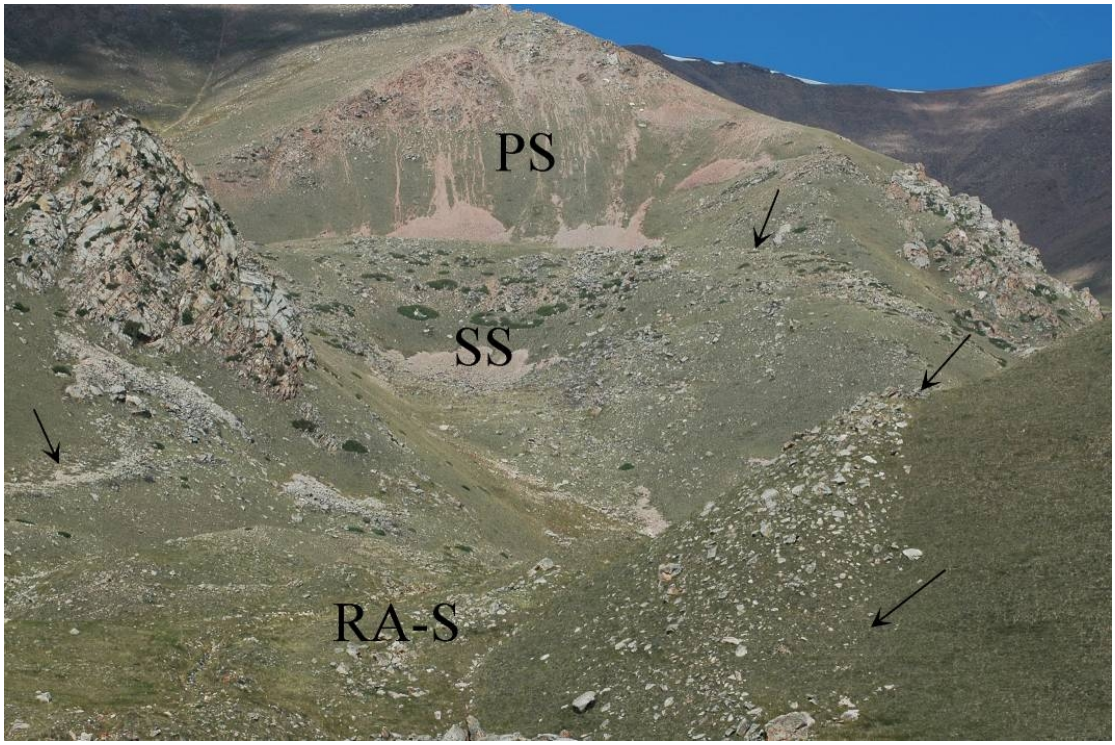

Figure 86. Primary (PS) and secondary (SS) circus-like scars of the Chongsu rock avalanche
Arrows mark the trimlines on the valley slopes much above than final rock avalanche surface (RA-S)

Figure 87. Trimline on the right slope of the Chongsu rock avalanche transit zone
Arrows mark a narrow bench corresponding to the initial thickness of moving rock avalanche. Splash of debris above the trimline is visible at the left part of the photograph

Figure 88. Abrupt decrease of the trimline level at the Chongsu rock avalanche transit zone

It indicates change of rock avalanche initial thickness. Note constant trimline level "upstream"

Figure 89. Angular boulder (black arrow) outside the splash indicating the ballistic trajectory of debris now resting above the nearly horizontal bench (HB)

Figure 90. The Chongsu rock avalanche left boundary downstream from the site shown on Figure 88
Person marked by the circle is about 1.6 m high

Figure 91. Lateral and frontal edges of the Chongsu rock avalanche indicating abrupt halt of its motion

Figure 92. The Chongsu rock avalanche front overlaying pre-rock avalanche debris flow
(levee composed of roughly rounded boulders in the foreground)

Figure 93. The Chongsu-2 rockslide

2.3.3 The Sarysu Secondary rock avalanche

One more Secondary rock avalanche ascribed to the "classical" subtype occurred at the eastern part of the Kyzyl-Oi depression (41.96º N, 74.22º E) (No 8 on Figure 2). A huge block of metasediments descended from the same watershed as the gigantic Kokomeren rockslide, which will be described hereafter (section 3.1), but from its opposite, northern slope. The initial descent of this block was rather small, ~200 m only (Figure 94), but it resulted in a 4.5-km long rock avalanche, which traveled along the dry gully at a mean angle of about 11º.

The rock avalanche body resting in the rather narrow valley has a smooth, partially soil-covered surface with expressive trimlines rising 10-20 m above the main part of the rock avalanche debris. Unlike the Seit and the Chongsu rock avalanches where parallel trimlines follow both sides of the path, in this case remnants of debris above the resultant surface are visible, first, along the right side, and then along the left one (Figure 95), thus indicating rapid liquid-like motion of debris accompanied by its "swinging" from one side to another, similar to the abovementioned Pandemonium Creek rock avalanche [Evans, et al., 1989], though not so intensive.

"Downstream" of the rock avalanche path the left trimline descends and joins the "mainstream" (Figure 96), which follows down up to the rock avalanche termination (Figure 97). Most of its body is composed of intensely crushed debris (Figure 98), locally, on top, mixed with larger angular boulders (Figure 99). The much more intensive crushing of debris than at many other rockslide described in this guidebook is, most likely, due to the much lower strength of the metasediments involved in this slope failure in comparison with granite or gneiss of the Seit, Chongsu, or Karakungey rock avalanches.

We classified the Sarysu rock avalanche as a "secondary classical" subtype conventionally, because the "secondary scar" above the avalanche-like part of this feature is not well-expressed (see Figure 94). It could not be excluded that it originated due to the "bottle-neck effect" as the Snake-Head rock avalanche described in section 2.3.5.

Besides this very long runout rock avalanche, it is assumed that several smaller bedrock slope failures collapsed from the ridge in the past, bounding the Kyzyl-Oi depression from the south, east of the Kokomeren River. Some evidence of such failures could be found both in the deposits of the merged alluvial fans west of the gully along which the Sarysu rock avalanche passed through (Figure 100), and in the slope morphology (Figure 101).

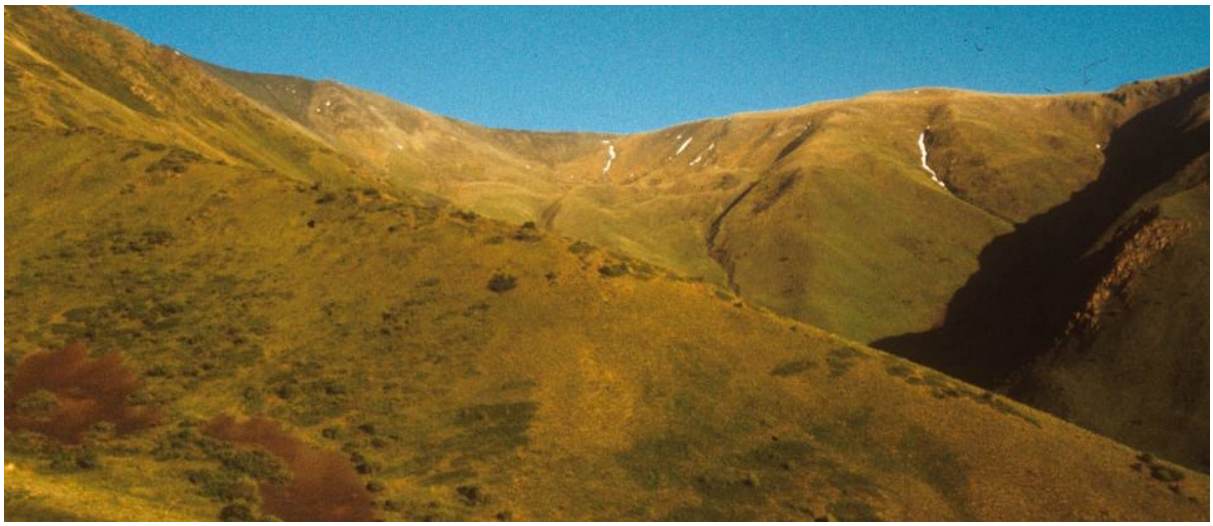

Figure 94. The Sarysu rock avalanche headscarp and proximal (compact) part of its body

Figure 95. Upper part of the Sarysu rock avalanche
Arrows mark trimlines left by moving debris first on the right side and then on the left side of the rock avalanche path

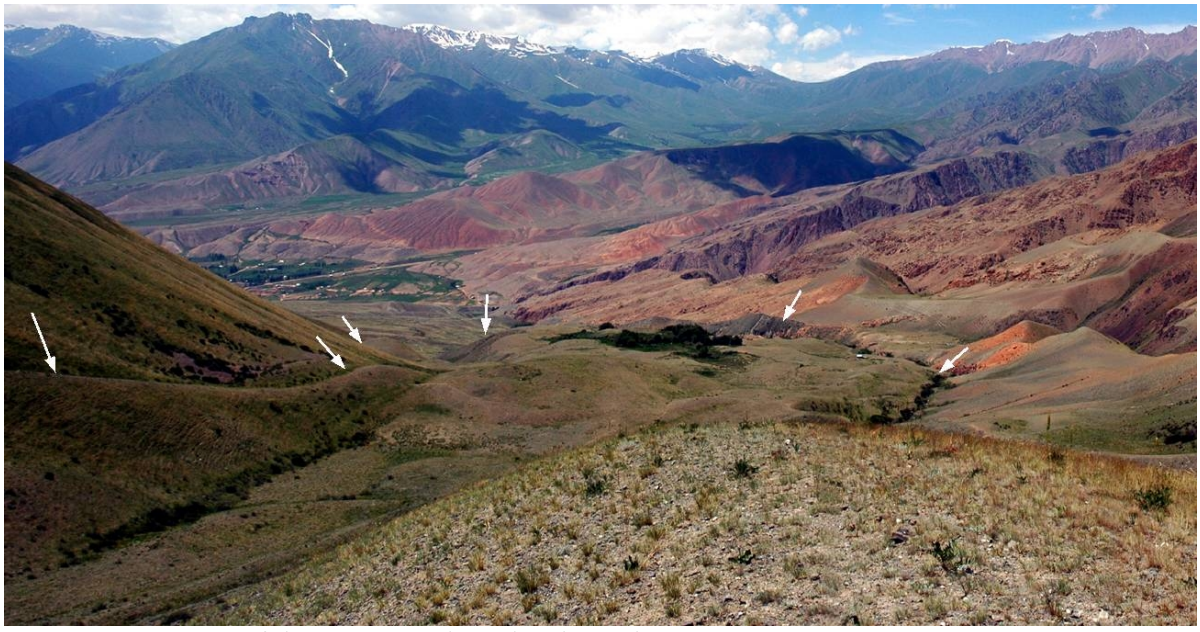

Figure 96. Lower part of the Sarysu rock avalanche path
Small arrows mark rock avalanche side boundaries and its distal limit. The distinct trimline is visible at the left side

Figure 97. Distal end of the Sarysu rock avalanche
smooth hill in the center of the panorama

Figure 98. Intensively crushed grey debris at the right side of the Sarysu rock avalanche distal part

Figure 99. Large angular clasts (on the foreground) on top of the Sarysu rock avalanche distal part

Figure 100. Unusually large angular clasts (at the foreground) in the Quaternary fill of the Kyzyl-Oi depression west from the Sarysu rock avalanche termination

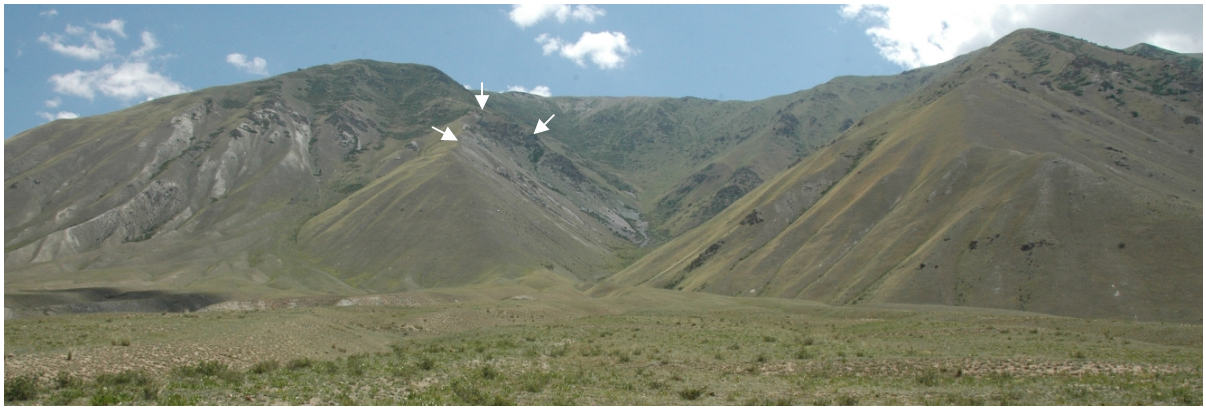

Figure 101. Possible headscarp of the assumed rock avalanche (arrows) west of the Sarysu rock avalanche path

2.3.4 Mingteke rock avalanche

One of the longest rock avalanche in the study region (No 9 on Figure 2) descended at 42.01º N, 74.34º E from the hanging wall of an active fault bounding the Djumgal depression from the north and shown on Figure 14 and traveled for about 5500 m (Figure 102). It is considered as one more example of the secondary rock avalanche.

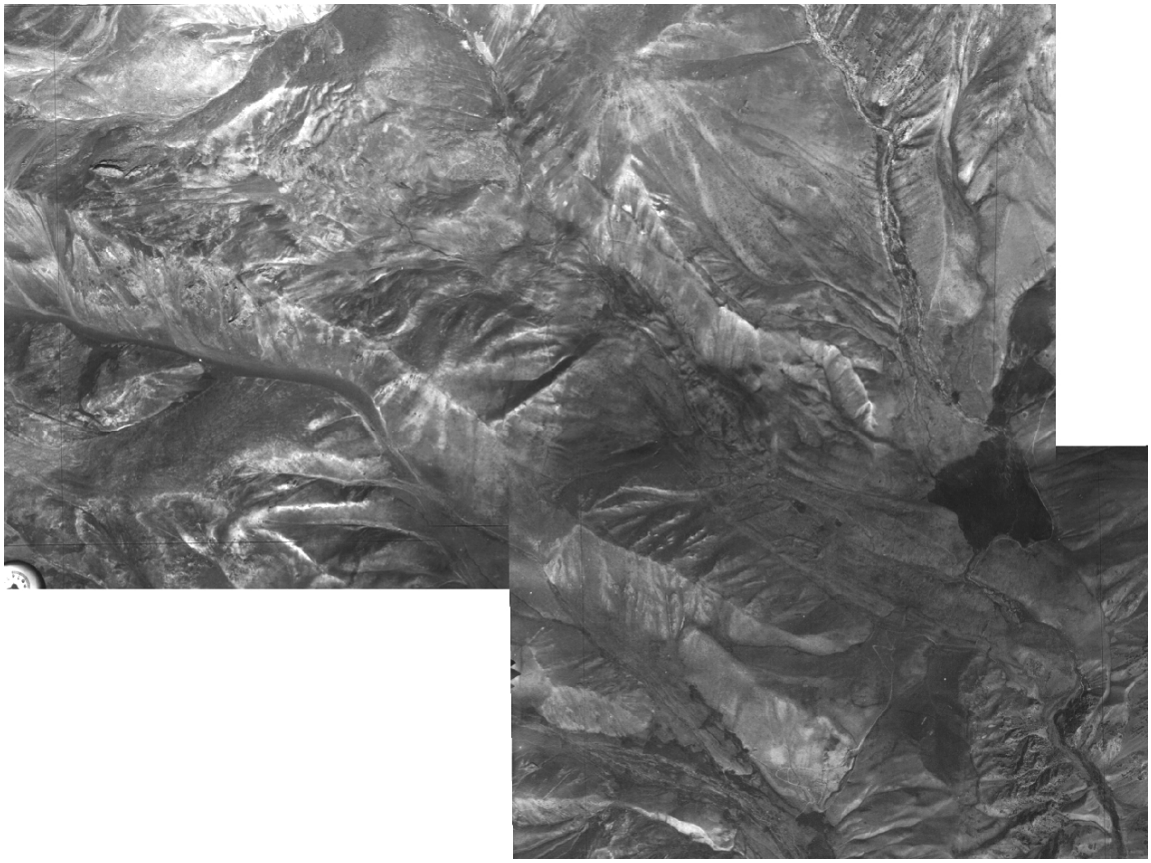

Figure 102. The Mingteke rock avalanche
Assemblage of aerial photographs

This rockslide, about 80 Mm^3 in volume, failed from a slope composed of highly metamorphosed sediments, mainly jasper-like quartzite. A large amount of material accumulated at the foot of its headscarp, while most of it turned right almost at a right angle (see Figure 102) and was involved in the flow-like motion that resulted in the formation of this long runout rock avalanche.

The headscarp backwall is a nearly planar surface rising from about 3350 to 3700 m a.s.l. (Figure 103). The absence of sidewalls, and large amount of rock mass involved in this rock avalanche, indicates that almost the entire spur (several hundred meters long and high) collapsed, very similar to the Ananievo rockslide triggered by the 1911 M8.2 Kemin Earthquake in Northern Kyrgyzstan [Delvaux et al., 2001, Havenith et al., 2003]. The latter, however, did not convert into a long runout rock avalanche.

After travelling nearly 5 km from the headscarp crown, the debris rose for about 90 m on the left bank of the Mingteke Creek valley (Figure 104) indicating a velocity of more than 150 km/h (it could be not so high, however, considering that rather small amount of debris was pushed up by much larger rock mass) . It dammed the valley and this dammed lake, along with a small depression in the lowermost part of the rock avalanche, were filled by alluvium and debris flow deposits (see small flat areas on Figure 104 and Figure 105).

This rock avalanche has very impressive and informative trimlines, allowing sound assumptions on the mechanism of its motion. The left trimline, clearly visible on Figure 106, is much higher than the final rock avalanche surface. The upper-most level of rockslide debris at the opposite side of the transition zone is much lower. If we make a cross-section at this part of the rock avalanche we see that the higher the trimline, indicating the maximum thickness of moving debris, the lower the resultant surface of the rock avalanche body. This allows the assumption that the thickness of debris is somehow proportional to its mobility.

Figure 103. Headscarp and proximal compact part of the Mingteke rock avalanche

Figure 104. Frontal part of the Mingteke rock avalanche with ~90 m runup (arrow)

Figure 105. Overview of the Mingteke rock avalanche from its raised frontal lobe

The secondary scar of this rock avalanche marking the boundary between its compact and mobile parts is not as well defined as in the Southern Karakungey and Chongsu rock avalanches. This transition zone is characterized by several steps with slightly concave frontal slopes (Figure 107).

Figure 106. Trimlines (marked by arrows) at the central part of the Mingteke rock avalanche

Note that they are much above the resultant surface. J – small portion of debris that jumped over the short low spur visible in the central part of the photo

Figure 107. The upper part of the Mingteke rock avalanche

Besides this impressive rock avalanche a suspicious site was identified in the upper reaches of a recently glaciated valley about 2 km south-west from its headscarp. A well-defined tongue-like body crosses the distinct glacial cirque, thus being much younger than this geomorphic feature. This allows the assumption that we could have another bedrock landslide here. The spatial proximity of the two rock slope failures and of an active fault shown on Figure 14 strengthen the assumption of their origin due to a large prehistoric earthquake.

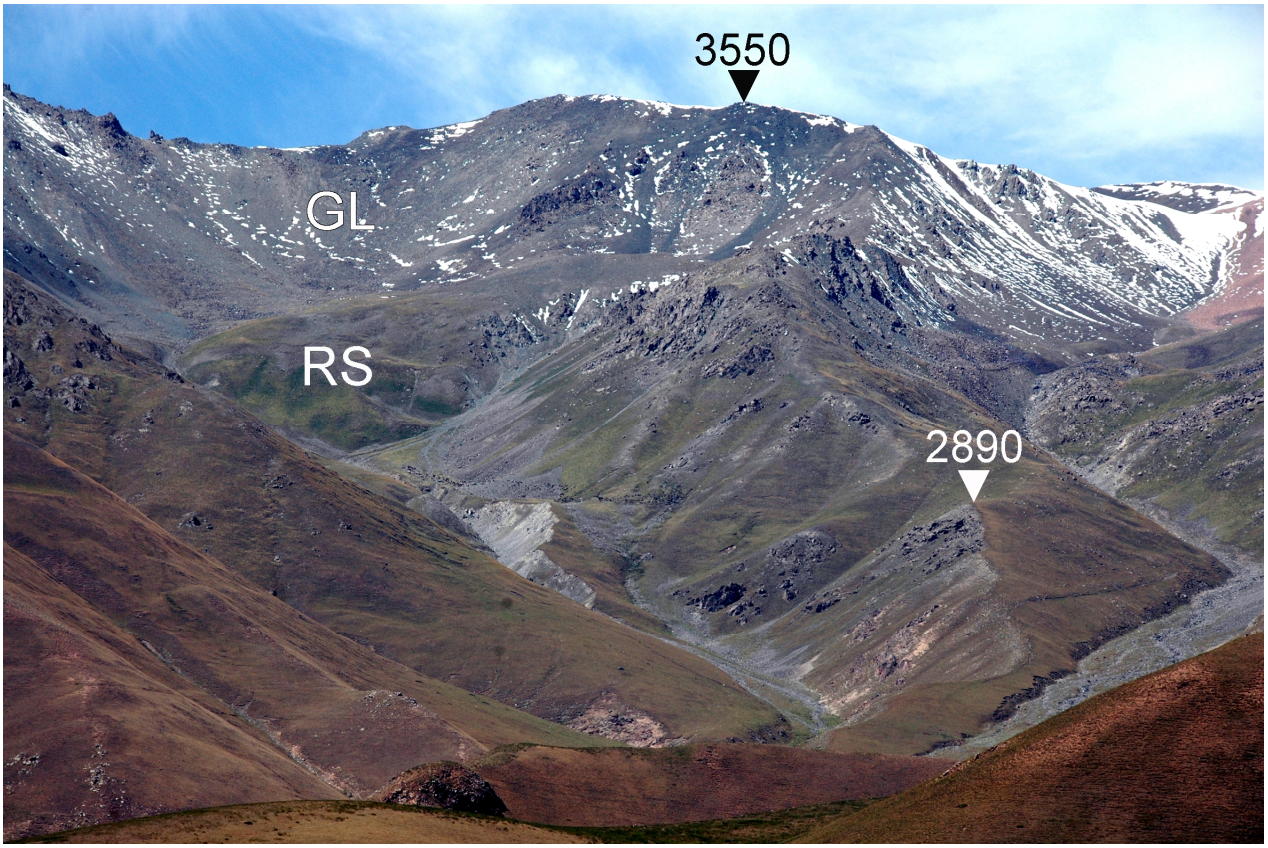

Figure 108. Possible rockslide in the recently glaciated zone

2.3.5 The Snake-head secondary rock avalanche ("bottleneck" subtype)

An interesting and in many respects still mysterious bedrock slope failure occurred in prehistoric times (most likely in the Late Holocene) in the eastern part of the Suusamyr intermontane depression, in the upper reaches of a small unnamed gully on the right bank of the Karakol River valley (42.35º N, 74.34º E) (No 11 on Figure 2).

This rock avalanche is an expressive member of a large cluster of landslides and rockslides in a limited area about 10 km long from east to west and 3 km wide from north to south (Figure 109). It includes both well-developed landslides and slopes with indications of ongoing deformations (Figure 110, Figure 111). Several similar clusters divided by the same-size gaps without prominent slope failures have been identified along the northern boundary of the Suusamyr depression [Strom, Abdrakhmatov 2004; Havenith et al. 2006]. These clusters coincide with recent surface ruptures (see Figure 9) that give grounds for the hypothesis of their origin due to strong earthquakes.

The initial failure of about 5×10^6–7×10^6 m^3 of Devonian sandstone converted into a rock avalanche that traveled 2815 m (runout measured from the head-scarp crown towards rock avalanche tip) along a narrow and gently inclined valley. After reaching an alluvial fan, the rock avalanche debris formed an elongated blade bounded by longitudinal levees with transverse levees and furrows between them (B on Figure 112).

The initial rockslide at the site in question has a very unusual asymmetric head-scarp (Figure 113) about 400-500 m long and only 300-350 m wide, so that the horizontal "depth" of this "bite" exceeds its width (Figure 114). Destruction affected almost the entire hillside but the rockslide mass moved more along the slope rather than towards its dip direction (Figure 115). We assume that this could be due to high southward-directed seismic acceleration that had caused the rock mass failure.

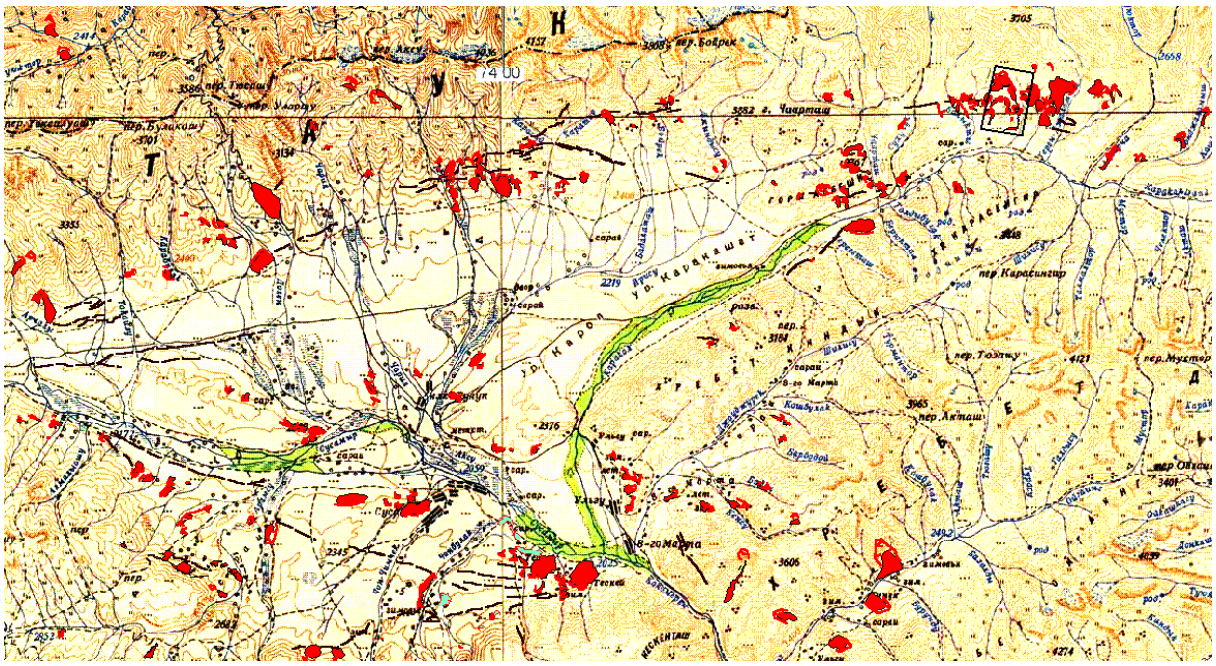

Figure 109. Spatial distribution of rockslides, landslides and recent faults of the Suusamyr intermontane depression

The Snake-head rock avalanche, shown on Figure 112 is marked by a rectangle

The proximal part of the rockslide is several dozens of meters thick and about 800 m long; it rests at the scar's base and at the rather wide upper reaches of the unnamed creek (see area A on Figure 112, Figure 113). It has an expressive wavy surface with several small closed depressions. At the western, lower, part of the headscarp a low "pressure ridge" can be identified (Figure 116). Following this "outer" zone of this compact rock avalanche part we can see a rather sharp boundary between the inner zone composed of crushed bedrock, and its outer zone composed of heavily weathered surficial material, likely bulldozed by the descending rockslide mass (Figure 117), similar to the above pressure ridge.

This "compact" body with a wavy surface extends to the rather sharp narrowing of the valley (Figure 118), which formed an obstacle to the rapidly moving rockslide debris. But motion did not halt completely. Rather, a small part of the debris continued moving and formed a long runout rock avalanche. The latter traveled nearly 2000 m along the creek's valley with a mean angle of about 5º only. Rock avalanche debris fills the creek's bottom and the deposits have a more or less planar surface (Figure 119). Though there is a minor stream at present, it has not produced any prominent erosional

features. The rock avalanche surface is turf-covered and boggy in some parts. Locally, angular clasts and boulders can be seen through the grass (Figure 120).

Several hundred meters downstream, at a local widening of the creek's valley, small landslides on valley slopes added some material to this rock avalanche (see Figure 112, area C). At the foot of the hilly area the rock avalanche sharply turned to the right along the lowermost part of the pre-existing alluvial fan and finally formed an elongated palm-like body 650 m long, up to 150 m wide and, as well as can be estimated, 4-6 m thick (Figure 121). It looks from above like the head of a snake, hence why we called the entire feature the Snake-head rock avalanche. The total volume of this distal part of the rock avalanche can be roughly estimated as $\sim 3 \times 10^5$ m^3. The volume of deposits that filled the narrow bottom of the creek is of the same order. Thus, only ~10% of the collapsed rock mass was involved in the avalanche-like motion.

The palm-like blade is bounded by levees that rise up to 4-5 meters above the surrounding alluvial fan surface and 1-2 m above the internal part of the rock avalanche deposits (Figure 122). The latter represents a system of levees and furrows, which strike transverse to the direction of rock avalanche motion (Figure 123). Such relief is completely different from that typical of debris flow deposits and, at the same time is not typical of most of the "classical" rock avalanche deposits. However, similar morphology, though at a much larger scale, was described at the distal part of the gigantic, 43 km long and up to 15 km^3 in volume Pleistocene Cerro Caquilluco–Cerrillos Negros Rock Avalanche in Peru [Crosta et al., 2015]. In the outcrops along the small spring that has eroded the right edge of the distal part of the rock avalanche one can see that it is composed of intensively shattered debris (3-5-cm fragments in fine matrix), whereas the surface of the blade is covered by angular boulders 20-30 and, rarely, 40-50 cm in size. The rather steep edges of the distal blade (see Figure 122) indicate that it was formed, most likely, by dry material. If it would move as a debris flow with high water content, it would spread much wider forming a fan-shape body.

Figure 110. Landslides east from the Snake-head rock avalanche

We hypothesize that the extreme mobility of this relatively small rock avalanche could be caused by the "bottle-neck effect" – transfer of momentum of the abruptly decelerating entire rock mass to the small portion that passes through the prominent narrowing (see Figure 118) [Strom, 2010a]. It should be noted, however, that further investigations should be carried out to explain the mechanism of the Snake-head rock avalanche formation from the very beginning of the rock slope failure to the final halt of debris motion.

Several rockslides can be seen on the opposite (left) bank of the Karakol River valley (Figure 124). It is evident that rockslide bodies that can be identified on this photograph have different ages, thus indicating recurrent slope failures.

Figure 111. Landslides west of the Snake-head rock avalanche headscarp (S-H)

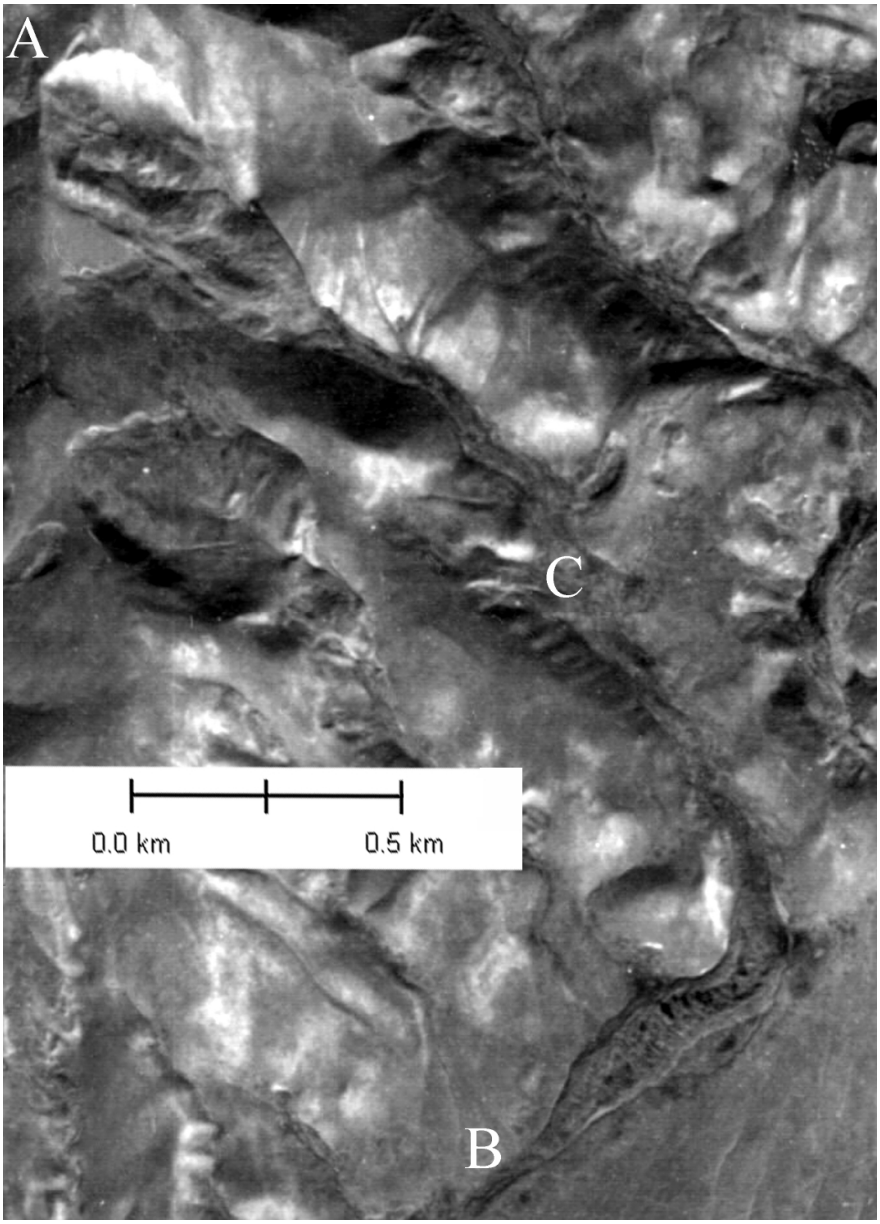

Figure 112. Long runout Snake-head rock avalanche

The initial massive rock slope failure at **A** was accompanied by a rock avalanche that traveled along the narrow gorge about three kilometers up to **B**. **C** – part of the transitional zone where debris of additional landslides "fell into" the main rock avalanche

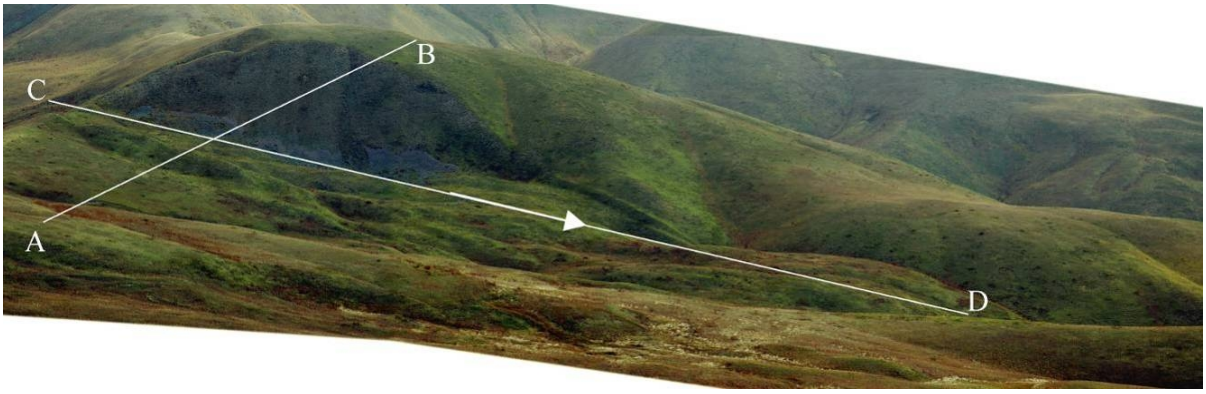

Figure 113. Head-scarp of the Snake-head rockslide and the proximal part of rock avalanche deposits

Note quite asymmetric form of the head-scarp that destroyed the entire hillside, while rockslide mass moved right (arrow) more along the slope rather than towards its dip direction. Schematic cross-sections AB and CD are shown on Figure 114.

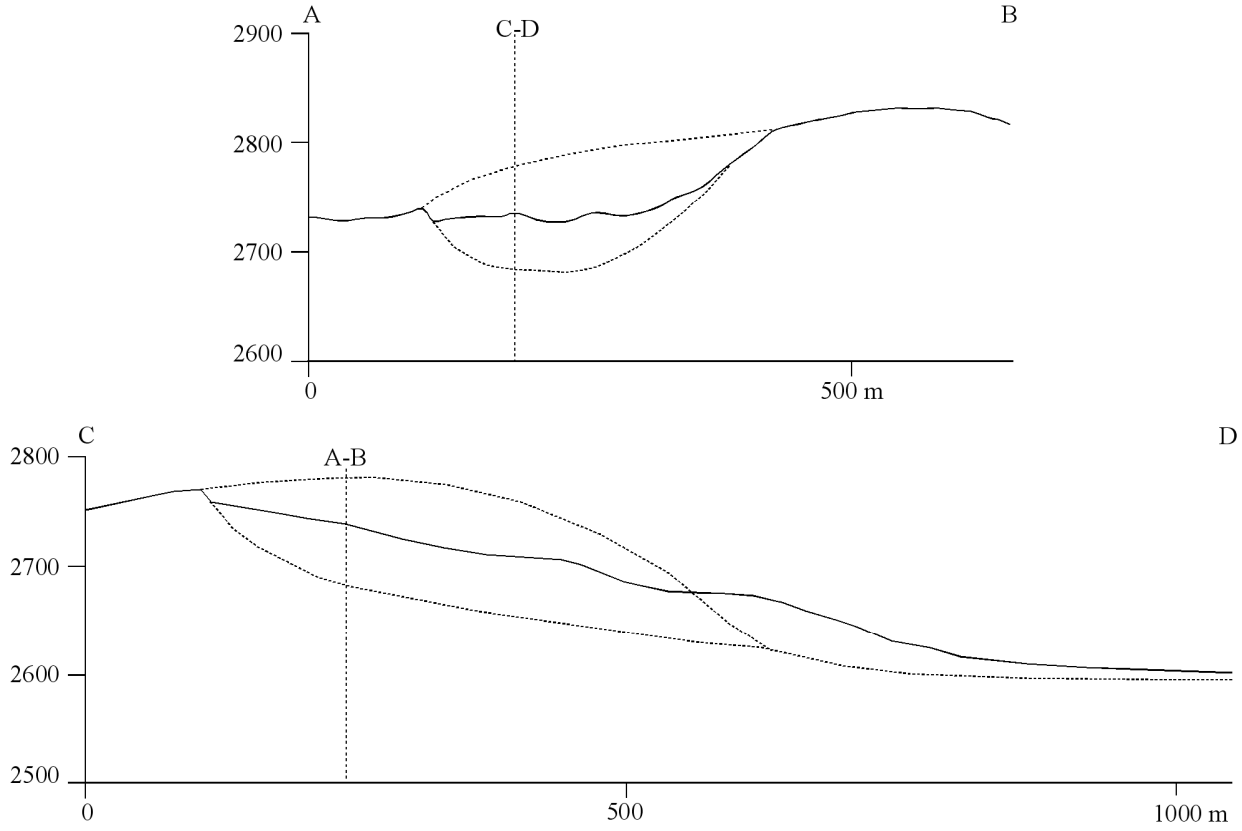

Figure 114. Schematic cross-sections of the Snake-head rockslide scar

Figure 115. Headscarp main wall and direction of downslope motion (dashed arrow) and the direction of the initial debris motion (solid arrow)

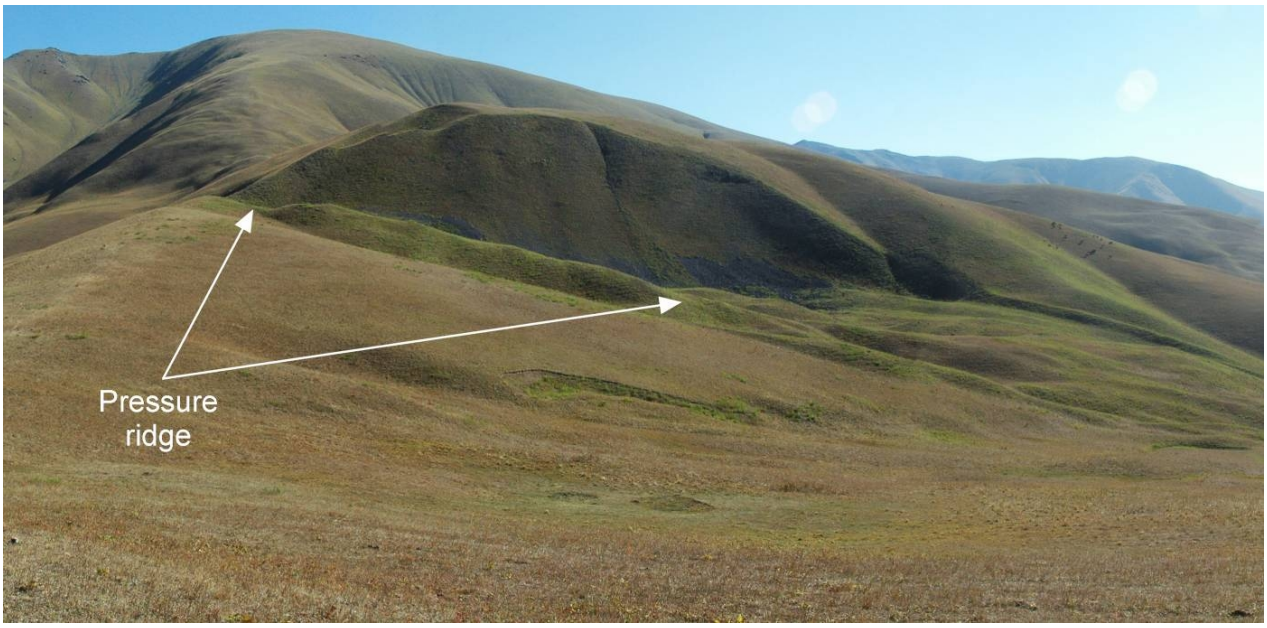

Figure 116. Pressure ridge at the lower part of the Snake-head headscarp area

Figure 117. Sharp boundary between the inner zone of the rockslide body composed of crushed bedrock (left, see also the inset) and the outer zone composed of weathered superficial material (right)

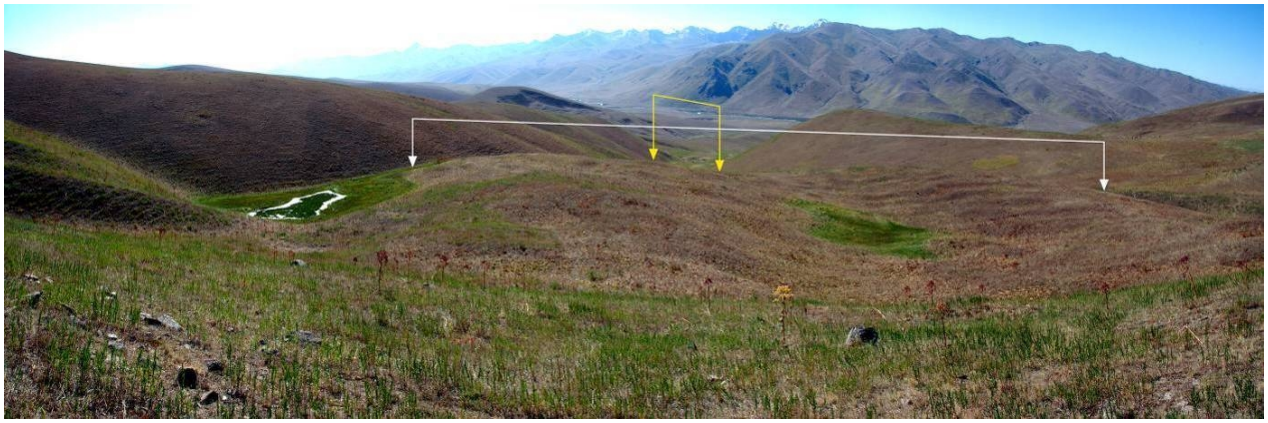

Figure 118. Sharp transition from the wide compact part of rockslide (white arrows) to the narrow avalanche-like part (yellow arrows)

Figure 119. Nearly horizontal surface of the Snake-head rock avalanche upper part immediately below its compact part

Figure 120~~118~~. Angular clasts at the central part of the Snake-head rock avalanche transition zone

Figure 121. The Snake-head rock avalanche palm-like distal blade

Figure 122. Boundary levees of the Snake-head rock avalanche distal blade
Left-site (above) and right-side (below)

Figure 123. Transverse levees and furrows at the central part of the Snake-head rock avalanche distal blade
General view above and zoomed outlined section below

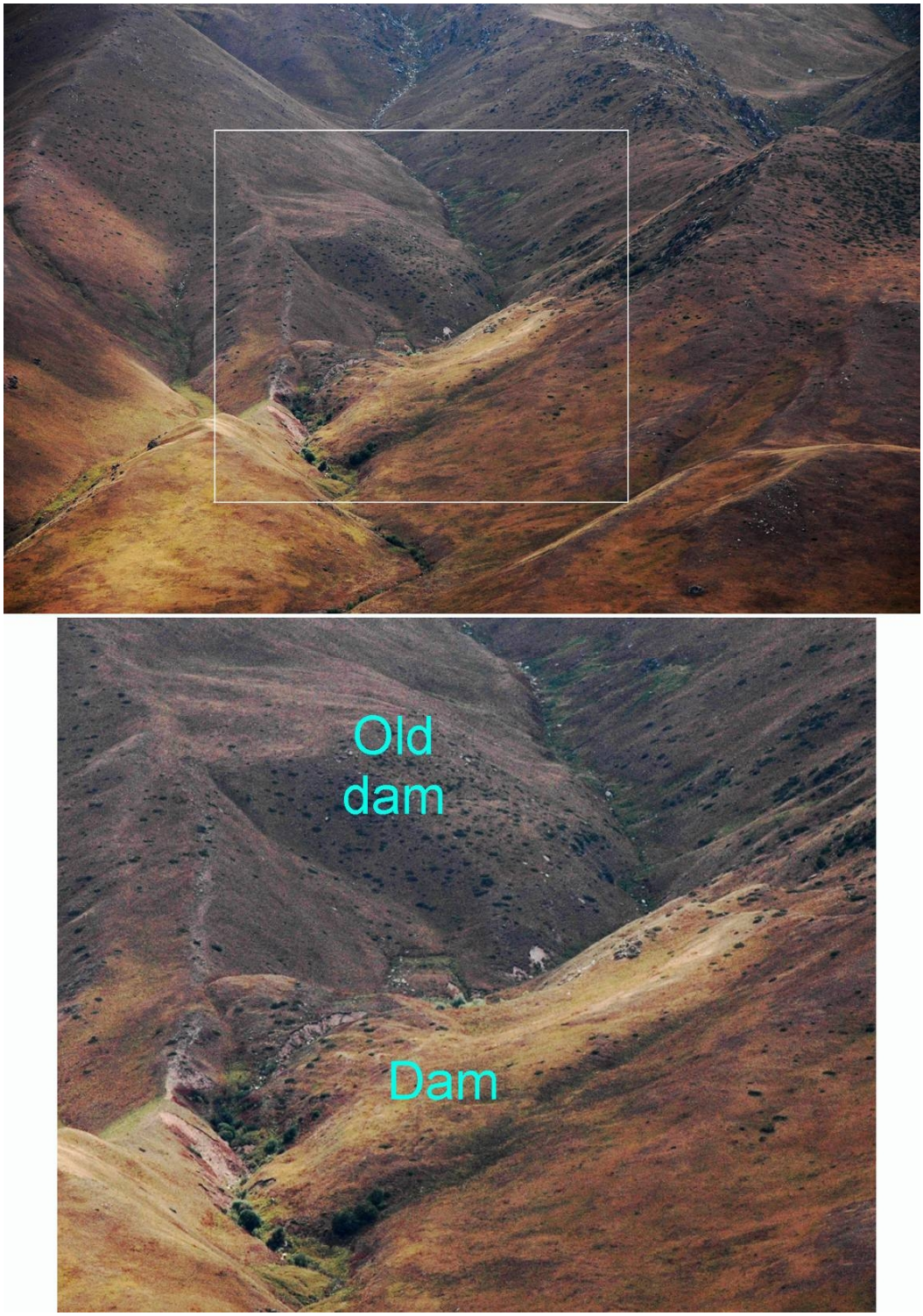

Figure 124. Recent and old (significantly eroded) rockslide dams
in the gully at the left bank of the Karakol River valley opposite the Snake-head rock avalanche site

3 INTERNAL STRUCTURE AND GRAIN-SIZE COMPOSITION OF LARGE-SCALE BEDROCK LANDSLIDES

3.1 The Kokomeren rockslide

One of the most interesting features in the entire Kokomeren River basin is the gigantic Kokomeren rockslide approximately 1.0 km^3 in volume (Figure 125 – Figure 127). It collapsed in the Pleistocene from the left bank of Kokomeren River at 41.93º N, 74.23º E (No 13 on Figure 2). A tremendous amount of rock debris collapsed onto the wide river terrace that was about 100 m above the riverbed at the time of failure (more than 150 m above the present riverbed) (see Figure 126), crossed it and filled the river channel, remnants of which can be found about 50 m above the present-day riverbed.

3.1.1 Rockslide description

Rockslide deposits resting on the left-bank terrace are up to 400 m thick. The river channel that existed at that time was blocked, but the thickness of the landslide dam in this zone could be estimated based on the elevation of lacustrine deposits. After this event, the river incised the landslide dam material and 50 m of bedrock below its bed. Locally, it eroded a new gorge that bypassed the blocked channel (Figure 128). At present the rockslide deposit base can be found on the right bank of Kokomeren River at a level of about 1700-1710 m a.s.l., while the top of deposits that filled the past river channel is at ~1900 m a.s.l. Lacustrine deposits upstream can be found at a level up to 1880-1890 m. a.s.l. Thus, we can expect that the blockage's effective height was at least 200 m (Hartvich, et al. 2008). The main part of the deposits that rests on the left-bank terrace is hardly accessible. However, the remnant of its frontal part on the right bank of the Kokomeren River just above the road at 41.92º N, 74.20º E is accessible and its internal structure and grain-size composition could be studied in detail.

The 1600-m high rockslide scar is composed of alternating, multicolored metasediments and igneous rocks – dark-gray metasediments, reddish granite, alternating red granite and dark-gray sandstone sheets, possibly with some fault zones (Figure 129). Both the lower part of the slope and left bank terrace basement are composed of reddish granite (see Figure 127).

The emplacement mechanism, a model of which is presented on Figure 130, could be reconstructed due to the positions of rock types involved in this rockslide (Figure 131) allowing the comparison of their original and final (after rockslide) position.

Two major zones may be distinguished in the main part of this natural dam (see Figure 131). The upper one, about 200-250 m in thickness, is composed of blocks and large massifs of fractured reddish granite, overlain, in turn, by a gray "layer" of metasediment blocks and big fragments (Figure 132, upper part). The lower one, up to 150-200 m in thickness, consists of highly fractured rocks, divided into some "layers" of granite and metasediment fragments (Figure 132, lower part). It is clearly visible that these "layers" are inclined 20 to 30º inside the slope – towards the scar base (Figure 133). Some large angular boulders are present in the lower part as well, but the extent of rock crushing here is much higher than in the upper part (Figure 134). The succession of the "layers" corresponds to the stratification in the slide scar, so that the structure of the bedrock outcrops (see Figure 129) is retained in the rockslide deposits (see Figure 132, Figure 133). Hence, this part of the sliding mass, up to 150-200-m thick, likely moved as a viscous body, parts of which did not undergo mixing. It can be assumed that the intensive shattering typical of the lower part of the rockslide body took place during the entire emplacement process, not just at a moment of its impact with the opposite valley floor as was proposed by Erismann [1979] for Köfels.

Practically the same succession of lithologies can be found at frontal part of the rockslide body on the right bank that filled the old river channel (see Figure 128). Its basal unit is composed of intensively shattered granite overlaying bouldery alluvium (Figure 135). This "former" granite looks like a compact, homogeneous mass, but it disintegrates in water. Its separate particles represent angular quartz and feldspar grain fragments usually with conchoidal surface texture. Most of the smallest particles are the quartz scales.

The grain size composition of shattered granite sampled from this unit corresponds to fine sand (!) with a specific gravity of 2.67 - 2.68 g/cm^3 (Table 1). The method of sample preparation practically has no impact on the grain size composition due to the lack of clay minerals. The latter indicates that such

grain size composition is the result of mechanical crushing but not of subsequent weathering. Being compacted in the laboratory to a relative density of 1.90 g/cm^3 it has a filtration coefficient of 0.05 m/day only. Thus, we can say that this material is practically impermeable.

Above this completely shattered granite we can see the succession of crushed granites and metasediments that remains unmixed (Figure 136) though it underwent intensive crushing and was displaced for more than 2 km from the source zone.

Table 1. Grain size composition of shattered granite from the basal unit of the Kokomeren blockage, right-bank part

			Fractions (mm)								
	spec. gravity	*prep. method	1.0-0.5	0.5-0.25	0.25-0.1	0.1-0.05	0.05-0.01	0.01-0.005	0.005-0.002	0.002-0.001	<0.001
			Content (%)								
Sample 1/91	2.67	A	11.9	27.9	27.6	8.4	17.1	2.7	2.4	0.4	1.6
		B	6.9	31.6	27.6	10.5	14.1	3.7	0.4	1.6	3.6
Sample 2/91	2.68	A	6.4	28.7	25.2	11.2	21.8	3.7	–	1.4	1.6
		B	7.8	24	22.5	15.3	17.1	4.6	1.4	2.5	4.8

*Methods of sample preparation: A – to specify microaggregation content (shaking in water); B – to specify grain content of maximum dispersion (boiling in water with natrium pyrophosphate)

The frontal part of this unit has a direct contact with bouldery alluvial (reworked moraine?) deposits that comprise the lower part of the valley slope. Crushed debris adjacent to this contact is intensely cemented (Figure 137) and is composed, locally, of a one-metre-thick mixture of crushed granite and metasediments with distinct boundaries between these lithologies (Figure 138). We assume that this part of the rockslide debris originated from the apical zone of a granite intrusion where small granite veins had intruded the host massive.

Typical crushed material of the granite-metasediments alternating layers can be seen on Figure 139. Results of grain-size analysis of material sampled from these outcrops are presented in Table 2.

Table 2. Grain size composition of crushed granite and metasediments' alternation of the Kokomeren blockage right-bank part

	Fractions (mm)														
	>80.0	80.0-40.0	40.0-20.0	20.0-10.0	10.0-5.0	5.0-2.0	2.0-1.0	1.0-0.5	0.5-0.25	0.25-0.1	0.1-0.05	0.05-0.01	0.01-0.005	0.005-0.002	<0,002
	Content (%)														
Sample 1/2005	1.8	1.1	3.35	5.9	14.35	19.6	17.0	5.5	13.2	8.3	3.55	4.1	0.8	0.3	1.2
Sample 2/2005	2.9	8.0	12.4	14.3	15.0	16.7	12.2	1.1	4.35	2.7	2.0	3.7	1.75	1.3	1.6

Sample 1/2005 – 44.7 kg of crushed granite; Sample 2/2005 – 42.7 kg of crushed metasediments; spec. gravity = 2.66 g/cm^3

The analysis of these samples was performed in three steps – field sieving and extraction of <5-mm fraction; dry sieving and extraction of <1-mm fraction and further laboratory sieving with washing and aerometric analysis. Table 2 presents the combined results of these three stages.

This material forms a large part of the right-bank rockslide deposits (Figure 140). The inclination of separate "layers" within the lower part of the right-bank body increases up to 30 - 40º (see cross-sections on Figure 131.

Figure 125. Aerial photograph of the Kokomeren rockslide

Figure 126. Dissected body of the Kokomeren rockslide

View from the Tuurakaing fan. 1 – granite basement; 2 – river terrace alluvium; 3 – rockslide deposits

Figure 127. The Kokomeren rockslide overview

Arrow in the right lower corner marks active fault that will be described later and shown in detail on Figure 145

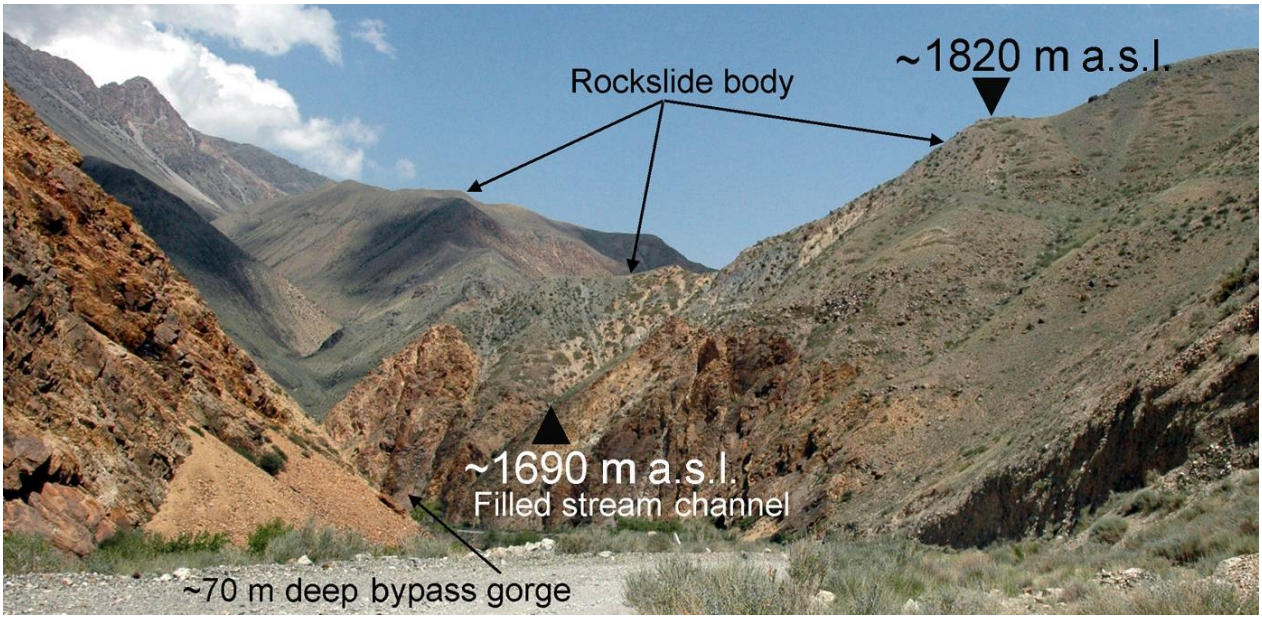

Figure 128. New gorge of the Kokomeren River that was incised after the blockage

Old river channel above 1690 m a.s.l. is filled with comminuted debris of the frontal part of the rockslide body. Benches at 1820 m a.s.l and above it are formed in the blocky carapace that overlays bouldery terrace alluvium visible at the right center of the photograph

These deposits are overlain by "layers" composed of much coarser angular boulders with very few, if any, fines. Similar to the comminuted debris these units do not feature any mixing – just above the comminuted material there are granite angular boulders (Figure 141), overlain, in turn, by layers of metasediments, whose extent of comminution strongly depends on the lithology. They are generally much coarser than those from the lower part of the body.

The boundary between the blocky and shattered zones is abrupt, without any transitional zone that may be interpreted as the evidence of sharp change of deformational conditions in the superficial and internal parts of the moving rockslide.

Figure 129. Alternating bedrock succession in the Kokomeren rockslide source zone
White arrows mark eastern boundary of the rockslide scar

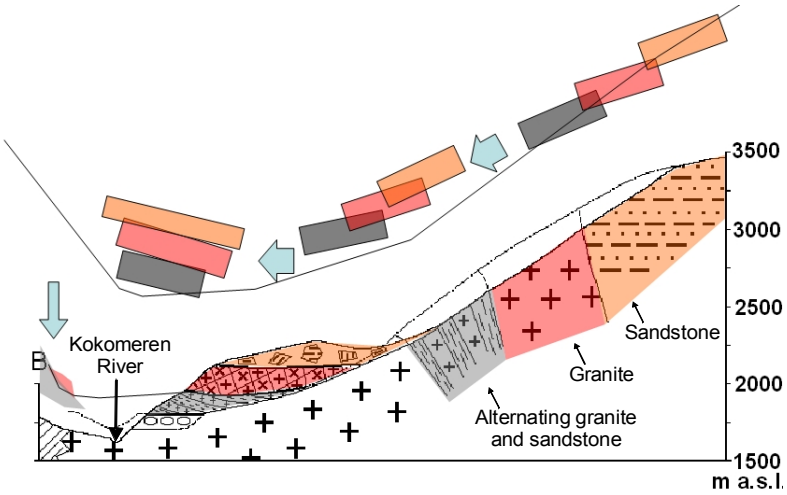

Figure 130. Reconstruction of the Kokomeren rockslide emplacement mechanism
(after Hartvich, et. al. 2008)

3.1.2 The Kokomeren rockslide 'satellites'

The gigantic bedrock slope failure that formed the Kokomeren rockslide was accompanied by a much smaller rockslide about 2 km upstream (41.92º N, 74.19º E) that descended from the left bank of the Kokomeren River valley just opposite the Kashkasu River mouth (Figure 142). Remnants of its deposits can be found on the river's right bank, where a large amount of angular boulders of the same material that forms the upper part of the scar area rests on the terrace-like surface several dozens of meters above the riverbed. We named this feature the Kashkasu-mouth rockslide.

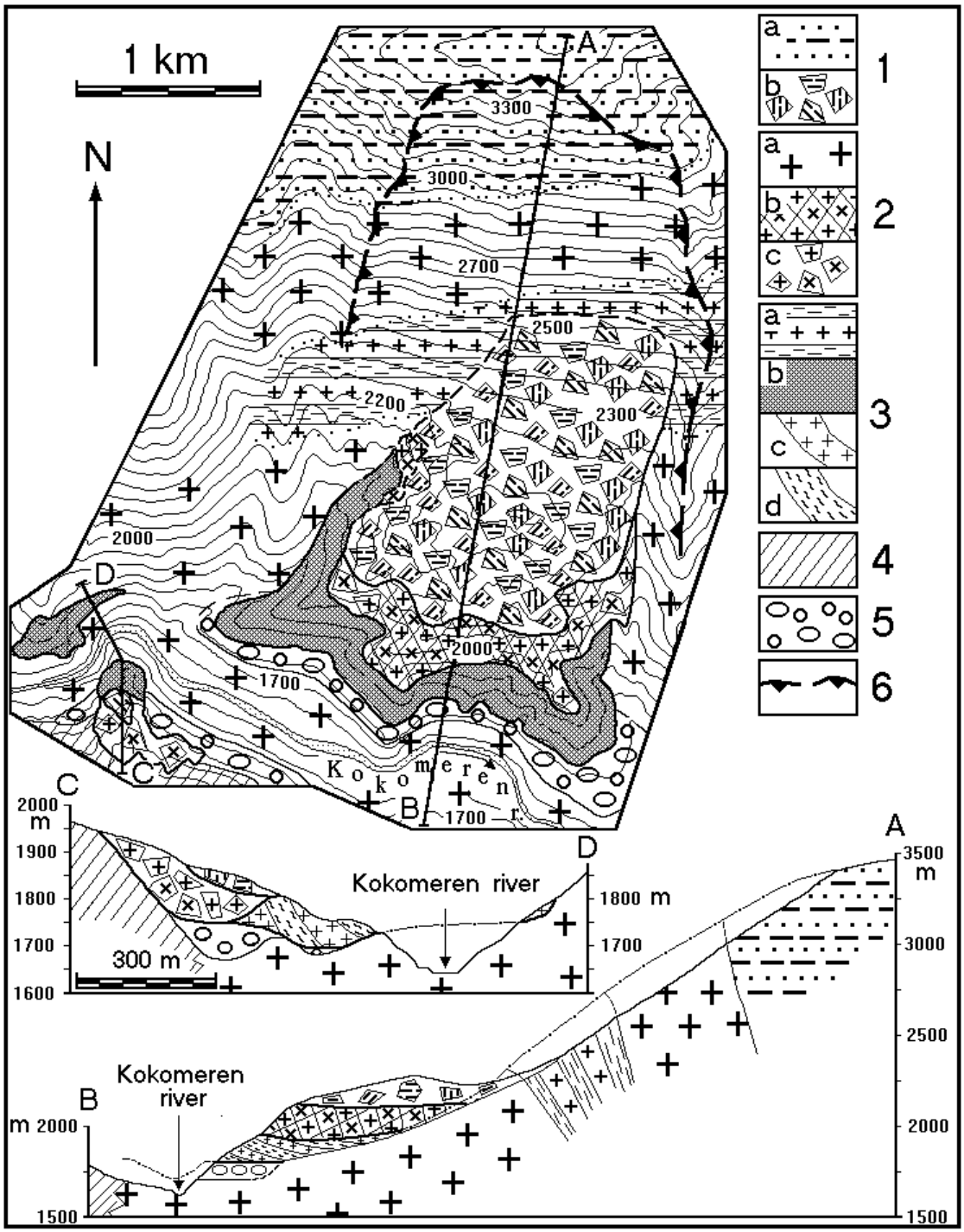

Figure 131. Schematic map and cross-sections of the Kokomeren rockslide blockage

Legend: 1a - Sandstone, 1b - Sandstone fragments in rockslide deposits; 2a - Granite, 2b, c - Granite in rockslide deposits, forming a huge massif (b) and crushed into blocks (c); 3a – Alternating granite and sandstone, 3b-d - Shattered granite and sandstone in rockslide deposits (b - on the map, c, d - on the cross-sections, where c - shattered granite, d - Shattered sandstone); 4 - Limestone, schist and diabase alternation; 5 - Alluvium; 6 - Rockslide scar

The geomorphic position of the rockslide deposits on the slope of the Kokomeren River valley is very similar to the position of the right-bank part of the Kokomeren rockslide body, thus, it is likely that both failures occurred simultaneously.

Figure 132. Vertical cross-section of the left-bank part of the Kokomeren rockslide body
Its characteristic features are preservation of the unmixed lithological units and presence of coarse debris in the upper part of the cross-section and of the intensively comminuted material in its lower part

Figure 133. Lower part of the Kokomeren rockslide body resting on the high left-bank terrace
Notice the inside-slope inclination of multicolored debris units

Figure 134. Shattered granite debris at the lower part of the Kokomeren rockslide body
Notice the succession of finer and coarser units

Figure 135. Pleistocene channel fill of the Kokomeren River (well-rounded boulders) resting on the bedrock and overlain by shattered granite of the Kokomeren rockslide right-bank part basal unit

Figure 136. Alternating "layers" of crushed rockslide debris on the right bank of the Kokomeren River
Crushed metasediments (gray) and granites (pink) that form unmixed units being displaced more than 2 kilometers from the source zone

One more rockslide (Figure 143) had blocked the small gully east of the Kokomeren rockslide at 41.92º N, 74.25º E (see also Figure 127). Since it forms a rather well-preserved dam it can be assumed that this slope failure is much younger than the main gigantic slope failure. It can be hypothesized that this rockslide was caused by a strong earthquake associated with surface faulting later than the earthquake that possibly triggered the giant Kokomeren rockslide failure. Evidence of such recurrent faulting was described in section 1.2 and will be described hereafter.

Figure 137. Contact of the cemented rockslide breccia and bouldery alluvium of the Kokomeren River valley right bank

Figure 138. Meter-size succession of crushed but unmixed granites and metasediments
They form cemented breccia at the frontal edge of the right-bank part of the Kokomeren rockslide

Figure 139. Typical grain-size composition of crushed granite (above) and metasediments (below) of the Kokomeren rockslide right-bank body lower part

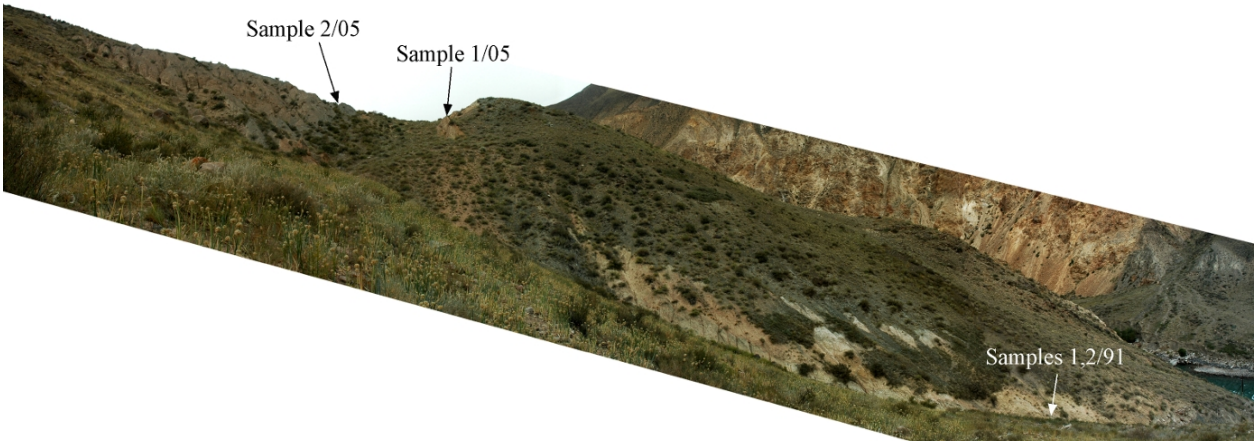

Figure 140. Overview of the shattered zone of the Kokomeren rockslide right-bank part
Arrows show where samples for grain-size composition were taken in 1991 (Table 1) and 2005 (Table 2)


Figure 141. Angular granite boulders on the top of the Kokomeren rockslide right-bank part

3.1.3 Active fault at the Kokomeren rockslide site

About 1.5 km downstream of the eastern end of the Kokomeren rockslide (41.91º N, 74.25º E) an expressive recent fault can be seen on the left bank of the Kokomeren River (Figure 144 - Figure 146). It is a north-north-west trending reverse fault with the western side up that displaces the Holocene terrace (see Figure 146) and overlying bedded silt sediments most likely of lacustrine origin.

The thickness of bouldery alluvium in the hanging wall is about $^{2}/_{3}$ of that in the footwall, whereas the lacustrine silt thickness is constant within the entire outcrop; hence it can be concluded that offsets occurred at least twice – during alluvium accumulation and after silt deposition. A bedrock block among boulders in the lower part of the alluvium in the footwall (outlined on Figure 146) could have fallen from the top of the uplifted block during the first event. Though it was difficult to measure offsets precisely from across the Kokomeren River, it is obvious that the cumulative vertical separation is about 6.6 m and that the second event likely displaced the silt about 2 m.

Figure 142. Strongly eroded rockslide scar opposite the Kashkasu River mouth

Figure 143. Partially eroded rockslide dam in the creek east from the Kokomeren rockslide

Collapsed slope is composed of Paleozoic granites. Part of the Kokomeren rockslide body can be seen at the upper left corner of the image

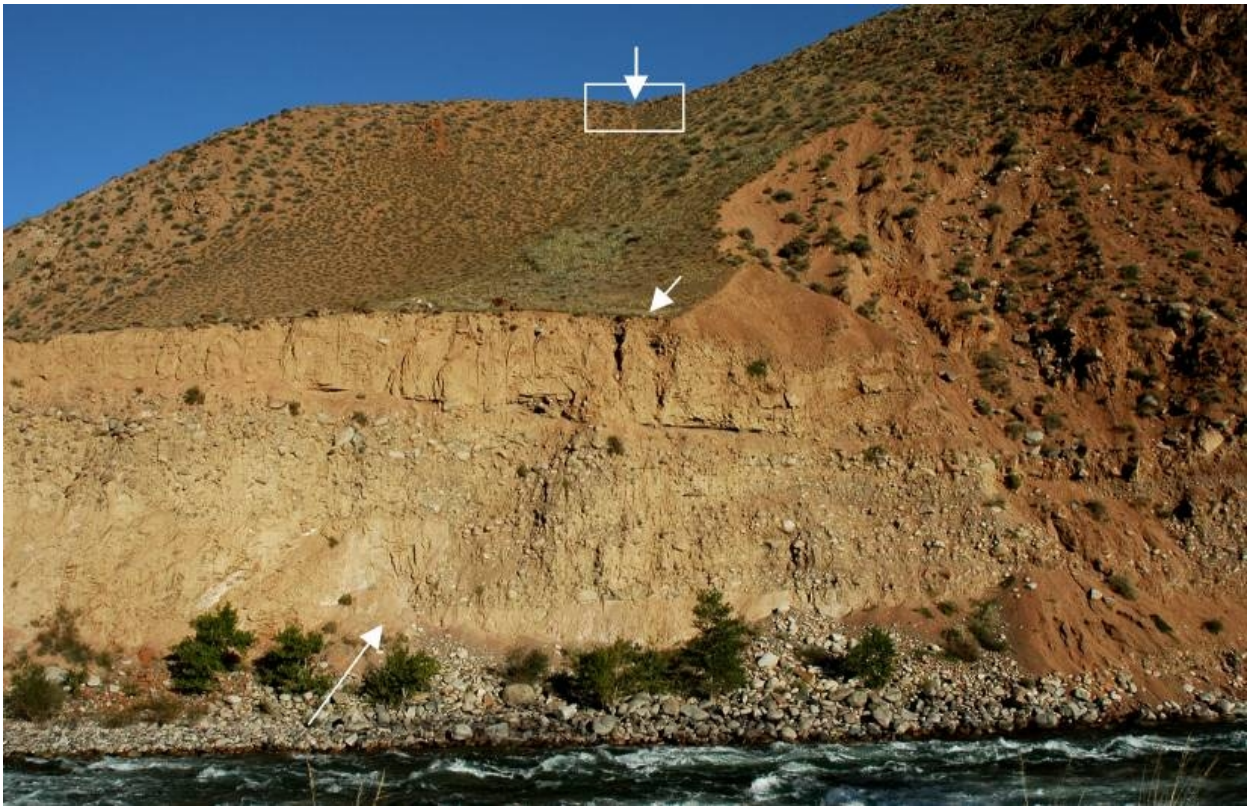

Figure 144. Recent fault rupturing left bank river terraces downstream of the Kokomeren rockslide
Inclined arrows mark rupture surface in the low terrace; vertical arrow shows the position of this fault where it crosses the remnant of the high terrace (see zoomed outlined area on Figure 145)

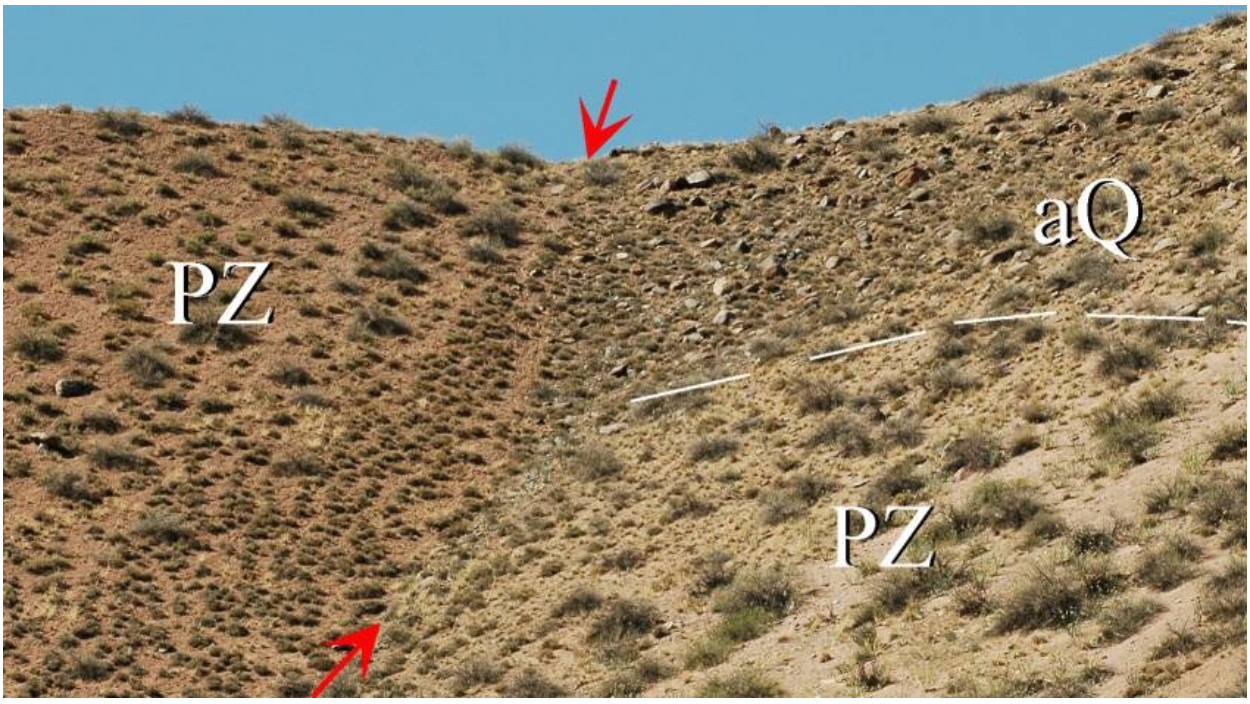

Figure 145. Displaced alluvium of high (Pleistocene) river terrace
Alluvium base at the footwall is marked by dashed line. Red arrows mark active fault

Figure 146. Detail of recent reverse fault shown on Figure 144
Piece of bedrock among the alluvium is marked

Both events should be younger than the failure of the Kokomeren rockslide, since at that time the Kokomeren riverbed was much higher than the displaced 12-15 m high terrace, which did not exist at the time. However, the displaced alluvium of the high river terrace (approximately the same that

underlay the left-bank part of the Kokomeren rockslide) indicates earlier offsets. The amount of its separation (see Figure 145) is much bigger than that of the low terrace (about 14 m, according to laser measurements).

The north-western continuation of this fault stretches directly towards the foot of the Kokomeren rockslide scar and we assume that one of the rupturing episodes on this fault, most likely associated with a strong earthquake, could have triggered or even caused this gigantic slope failure [Strom, Stepanchikova, 2008].

In the opposite direction, on the right bank of the Kokomeren River, this recent fault can be observed in the small open pit at the base of the smooth slope just above the road (Figure 147). Unfortunately, it is the only outcrop on the right bank of the valley where the fault could be found until now. The remaining part of the slope composed of the heavily weathered granite is covered by outwash.

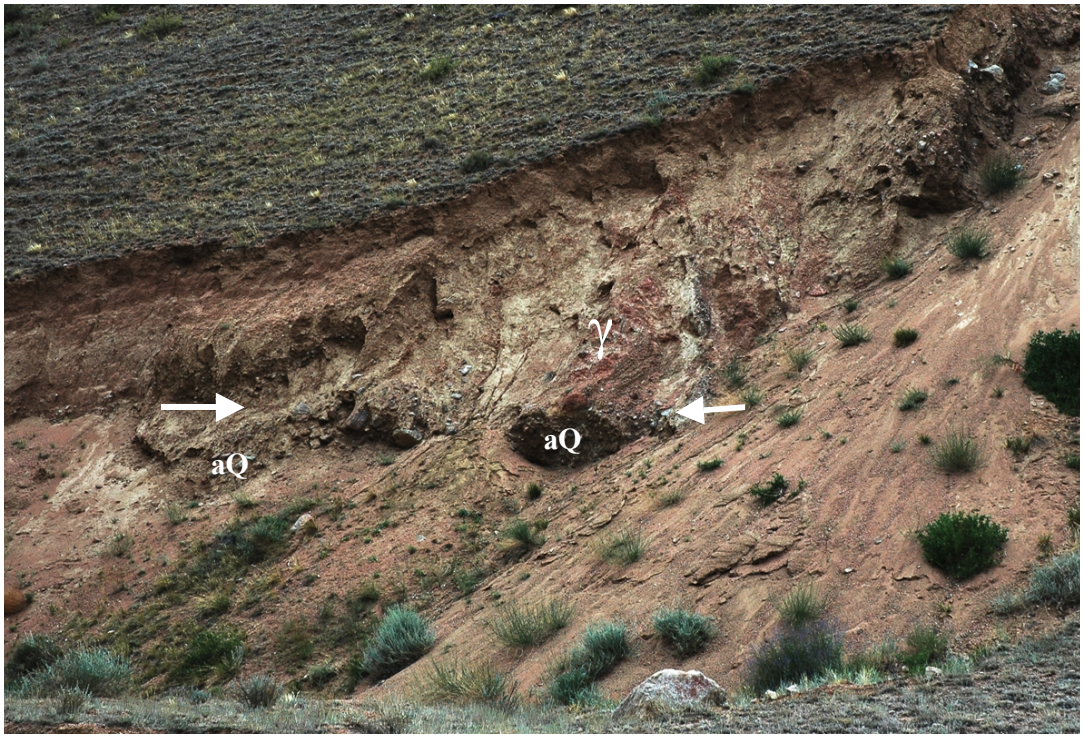

Figure 147. Crushed granite (**γ**) overthusting the alluvium (**aQ**)
Right bank of the Kokomeren River. Fault plane is marked by white arrows

3.1.4 Evidence of inundation and subsequent breach

The at least 200-m high Kokomeren rockslide dam caused inundation of a large part of the Kokomeren River valley and formed a lake that stretched for more than 15 km upstream. The lake's volume can be roughly estimated as 10^9 m^3. The powerful Kokomeren River, with a present-day mean annual discharge of 2.5×10^9 m^3/year [State Water Inventory 1987] should have formed a lake in less than one year. Even though it was likely overtopped, the rockslide dam existed for a rather long time. Due to a combination of geological and geomorphic features at the blockage site the new gorge was cut through bedrock (see Figure 128) that should have slowed down the process of dam breach significantly [Hartvich, et al. 2008]. This resulted in the accumulation of a large quantity of lacustrine sediments, represented mainly as thin-bedded silt sediments that can be observed in the numerous outcrops upstream (Figure 148 – Figure 152).

Practically all of these lacustrine units are not higher than 100 m above the present-day riverbed level. This indicates that the dammed lake was not filled by sediments completely, unlike, for example, the lake in the middle part of the Naryn River basin dammed by the gigantic (~10 km^3) Beshkiol landslide [Korup, et al. 2006].

The total volume of lacustrine sediments accumulated in the dammed Kokomeren River valley can be roughly estimated as 10^8 m^3 (~1/10 of the lake volume). This allows the determination of the longevity of river damming [Korup, et. al., 2006]. According to the State Water Inventory [1987], present-day mean sediment yield of the Kokomeren is 140,000 tons/year, which roughly corresponds to 7×10^4 m^3/year. Assuming the same rate of sedimentation at the end of the Pleistocene when river damming took place, we obtain the time necessary to accumulate the above-mentioned amount of sediments, which is about 1500 years. Palinological analysis of two samples collected from sandy and clayey layers at the outcrop shown on Figure 12 indicate that dam formation most likely took place in the Late Pleistocene, during a warm and rather wet epoch. This, in turn, allows the assumption that both river discharge and sedimentary yield in the period of river damming were larger than at present and, thus, the longevity of the Kokomeren Lake should be shorter, likely not more than few centuries.

Assuming that fine grading of lacustrine sediments (see Figure 11, Figure 149, inset in Figure 152) corresponds to the seasonal variations of washout, thus allowing us to count years when these strata had accumulated, this estimate seems to be reasonable.

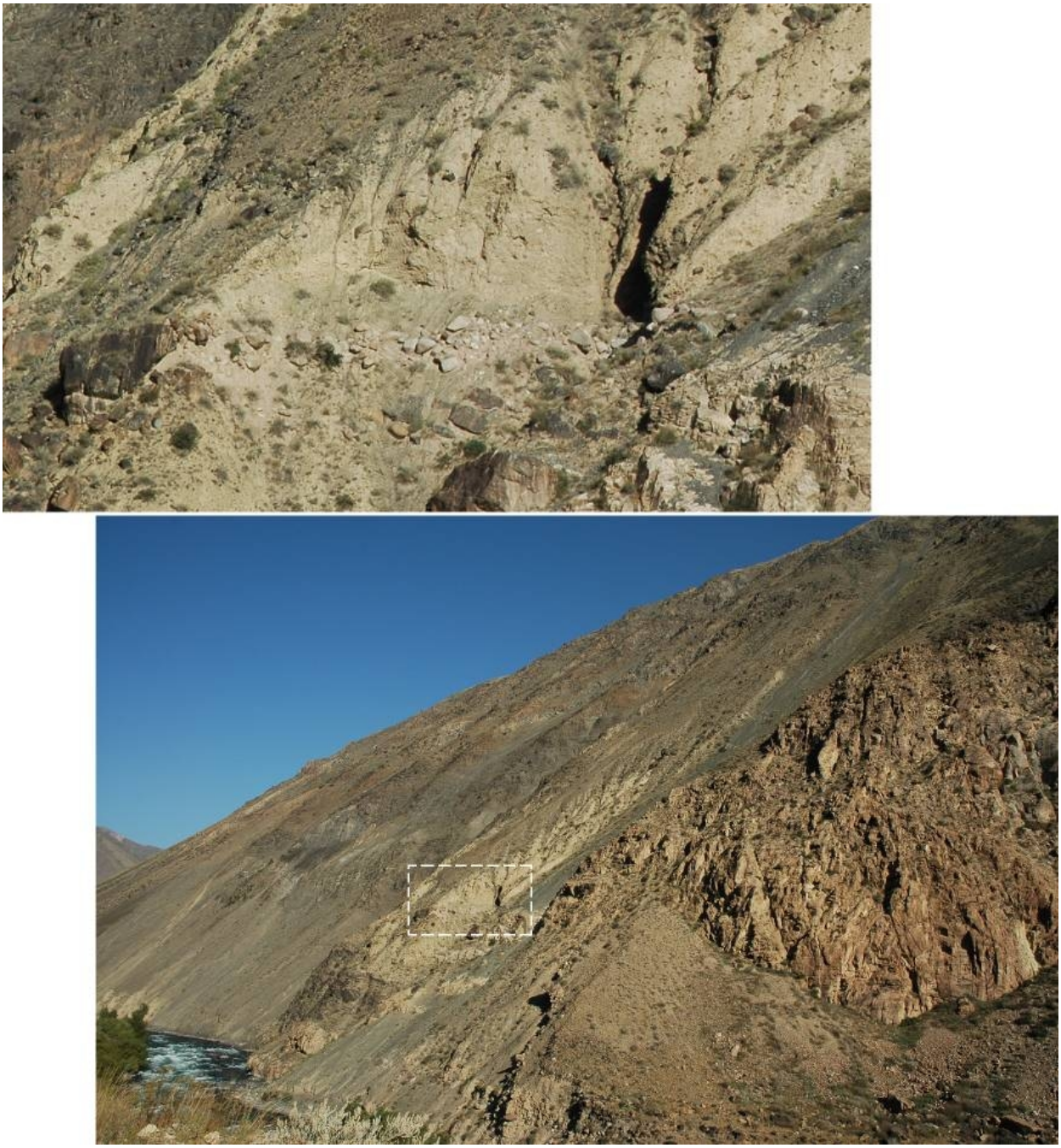

Figure 148. Assumed lacustrine sediments overly bouldery alluvial deposits
Deposition of thick unit of fines at such a deep and narrow valley is possible in lake conditions only

This allows the estimation of the incision rate of the stream that eroded the ~100 m deep bypass gorge through the left-bank bedrock (see Figure 128).

The first outcrop of lake sediments (moving upstream from the dam) can be seen on the left bank of the valley just upstream of the Kashkasu River mouth (41.929º N, 74.18º E) where thin-bedded silt overlays thin bouldery alluvium representing stream facies (see Figure 148). It is obvious that such a thick stratum of fines could not accumulate in the deep narrow gorge with rapids. The abrupt change in the lithology (silt overlaying large boulders) also indicates a sharp change in sedimentation conditions. However, this outcrop is located close to the dam, and likely represents the final stage of lake infilling, since initial sedimentation occurred at the upstream part of the natural reservoir as occurred in the Toktogul Reservoir, for example (Figure 153).

The widest distribution of the sediments accumulated in the dammed lake can be observed in the Kyzyl-Oi depression, on the right bank of the Kokomeren River between the Chongsu and Kobiuksu

River mouths (see Figure 11, Figure 12) and on its left bank opposite the Kyzyl-Oi village (41.96º N, 74.17º E) (see Figure 150) where almost one half of the 100-m high terrace-like surface is composed of bedded silt mixed with talus that was transported from the adjacent slope (see Figure 149).

Figure 149. Fine bedded lacustrine sediments overlying alluvium
Detail of the outcrop shown on Figure 150

Figure 150. Overview of the left bank of Kokomeren River opposite the Kyzyl-Oi village
Outcrop is composed of laminated debris flow deposits resting over the "normal" alluvial sediments

The lithology of the basal units of lacustrine sediments visible at the outcrops along the road cut south of Kyzyl-Oi village allows reconstruction of the Kokomeren Lake's early history. Typical alluvium (pebbles with sandy fill) is overlain by a ~1.5 m thick unit composed of angular macadam-size clasts of metasediments that could only have been transported here from the left bank of the Kokomeren River, with a red silty matrix that originated from the Neogene red beds of the Kyzyl-Oi depression. This unit, in turn, is overlain by 'classical' lake sediments – well-bedded silt layers with sandy interbeds and rare pebbles (see Figure 151). Boundaries between these units are sharp, indicating abrupt changes in the sedimentation conditions. It can be assumed that black debris with a silty matrix with relatively thick and alternating layers was accumulated when rising water disturbed talus of the right bank and silt of the left bank, which mixed and was deposited over the floodplain (?) alluvium. It is possible that large amounts of debris could have collapsed from adjacent slopes due to strong seismic shaking [Strom, Stepanchikova, 2008]. If so, this unit corresponds to unit 2 shown on Figure 11. Later on, when water level rose rapidly, sedimentation conditions changed and lacustrine thin-bedded silt started accumulating. Generally, sedimentation in mountainous lakes and reservoirs takes place where tributaries enter these water bodies. This can be seen at Toktogul reservoir (Figure 153).

Figure 151. Basal units of the lacustrine succession
Right bank of the Kokomeren River south of the Kyzyl-Oi village

Near the outcrop shown on Figure 11 one can see inclusions of coarse bouldery material in the lower part of the lacustrine deposits. We interpret them as deposits of debris flows that entered the dammed lake, likely due to the breach of temporary blockages that could be caused by local slope failures in the western part of the Kyzyl-Oi depression.

The outermost site where fine lacustrine sediments can be observed is in the road cut opposite the Burundu River Mouth about 13 km from the Kokomeren blockage (see Figure 152). Here, at 42º N, 74.16º E, thin-bedded silt is overlain by slope scree. Further upstream, in the narrow gorge with slopes completely covered by talus, no similar sediments have been found.

Figure 152. Lacustrine deposits with bouldery inclusions opposite the Burundu River mouth, overlain by talus

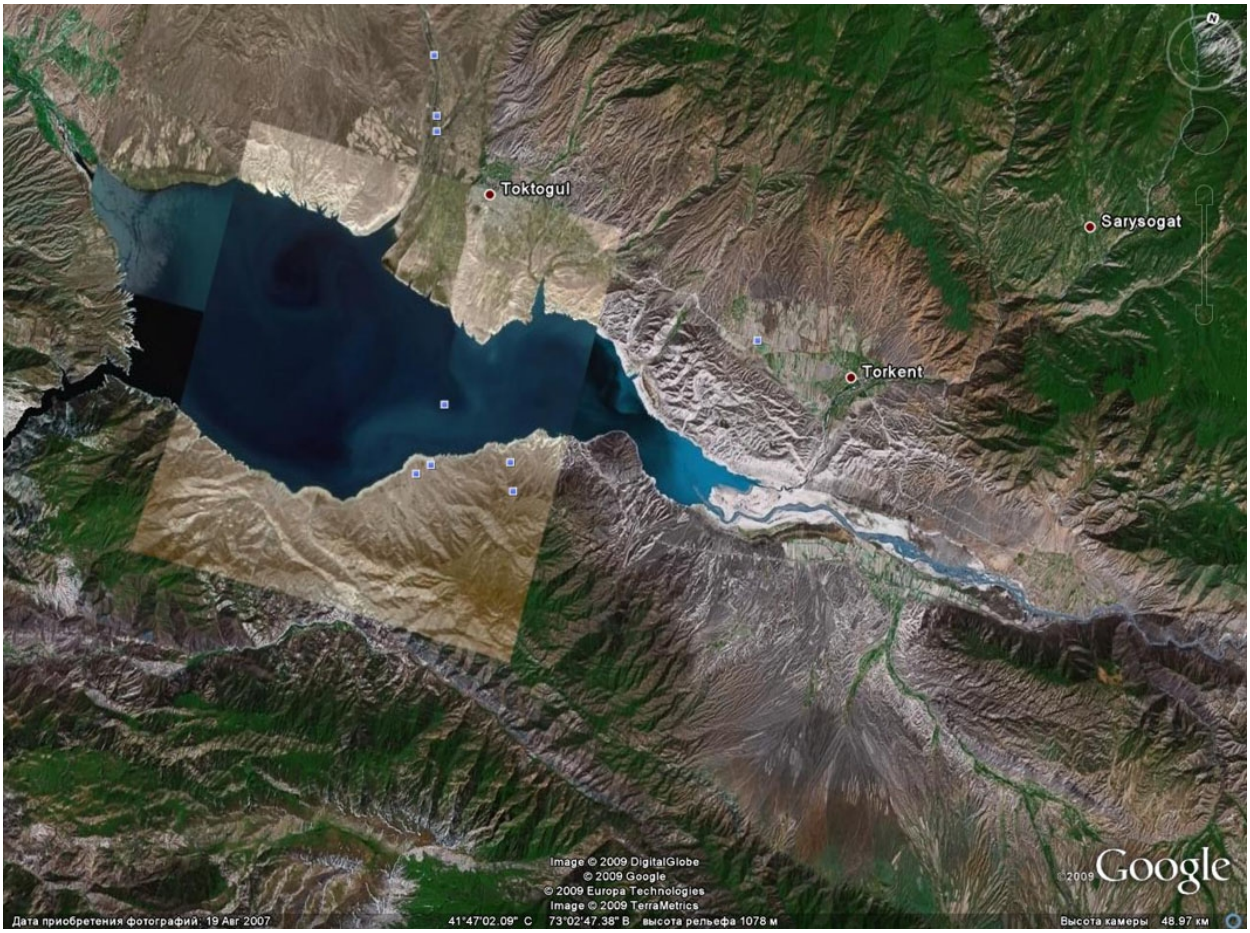

Figure 153. Lake-head deltas of rivers flowing into the Toktogul reservoir

Unlike the expressive evidence of upstream inundation caused by the Kokomeren rockslide, data on the mechanism and rate of this dam breach are limited. Presence of coarse bouldery sediments all over the river valley complicates outburst flood deposit identification. It can be hypothesized, nevertheless, that huge bouldery deposits that are widely developed at the western termination of the Djumgal depression, where Kokomeren River enters it, could have been deposited by a powerful outburst flood. However, the presence of younger blockages in the gorge downstream of the Kokomeren Dam site does not allow for the conclusive identification of which dam breach could be responsible for their deposition.

3.2 The Displaced Peneplain rockslide

The Kokomeren rockslide is not the only large-scale Pleistocene rock slope failure in the upper part of the Kokomeren River basin. One more Pre-Holocene event occurred at its right bank at 41.90º N, 74.25º E (No 15 on Figure 2). This rockslide was significantly reworked by subsequent erosion (Figure 154), so that it could hardly be identified on space and aerial images (Figure 155, DP on Figure 73) and DEMs. Nevertheless, geomorphic and structural analyses indicate that a huge mass of gneiss descended from the right slope of the valley and blocked the Kokomeren River valley completely.

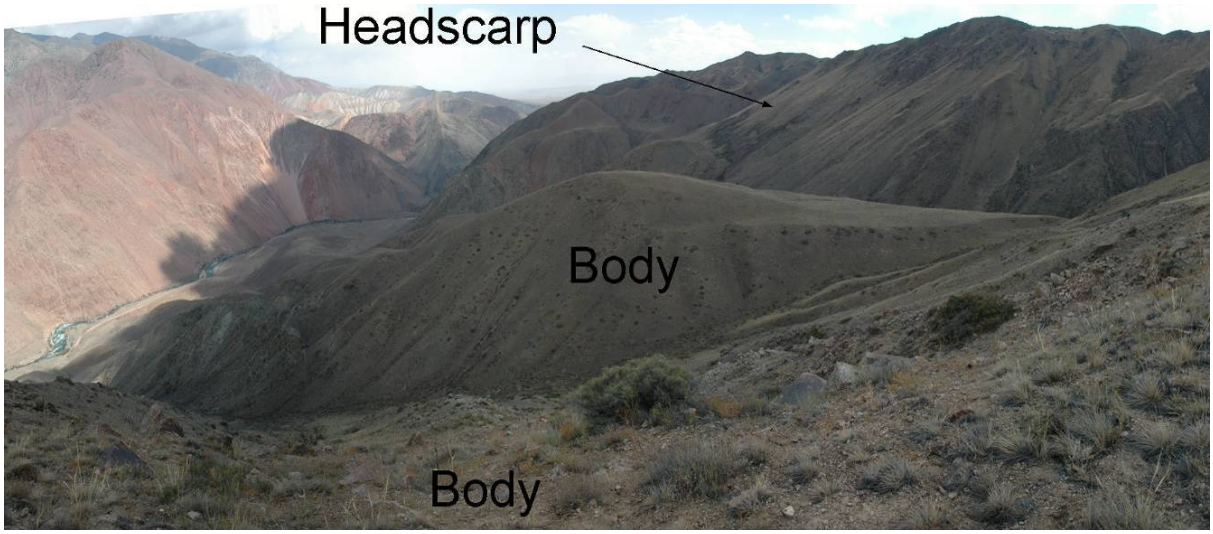

Figure 154. Deeply eroded body of the Displaced Peneplain rockslide
View from the uppermost part of the deposits (*brandung*?)

Remnants of its proximal part marked by fragments of the displaced Pre-Neogene planation surface still remain on the right bank of an unnamed gully (Figure 156). That is why we called this feature the "Displaced Peneplain" rockslide.The 300-m high slope covered by scree further upstream represents its sliding surface.

The "Displaced Peneplain" rockslide formed a body about 2 km^2 in plan view and up to 300 m thick. Its volume is estimated to be 400-500×10^6 m^3. Its distal part rests on the slope of the right bank of the Kokomeren River valley much above the proximal deposit forming something like a *brandung* (Figure 157).

Unlike the above-mentioned Kokomeren rockslide, the internal structure of which could be studied and reconstructed in detail, the "Displaced Peneplain" rockslide body, though being strongly reworked by erosion, does not have so many good outcrops where one can observe its composition. Locally, there are angular gneiss boulders on top of the body (see Figure 157, Figure 158). Some outcrops at the north-eastern part of the body are composed of heavily shattered "stratified" debris (Figure 159). However, since the rockslide source zone is composed of more or less uniform lithology – mainly gneiss – and is largely masked by scree, we could not reconstruct the original position of units that can be identified within the rockslide body. This case study is an excellent example of an old rockslide that could be identified on the basis of its debris analysis rather than morphologically.

As noted above, the "Displaced Peneplain" rockslide blocked the Kokomeren River valley. The newly formed gorge bypassed the blockage at its distal boundary through bedrock of the River's left bank. The smooth hill composed of red, heavily weathered granite that stretches along the right bank of the present-day Kokomeren River (Figure 160) represents the remnant of the original left bank of the valley. The river incised a new channel; the abandoned river channel can be seen beside the road 10-15 m above the present-day river level (Figure 161). Large boulders resting just above the road represent the stream facies of the alluvium that was buried by much finer material, likely washed out from the adjacent slopes and distal part of the rockslide body.

Figure 155. High resolution space image of the "Displaced Peneplain" rockslide.
White dashed line marks deposit boundary; red arrows – the headscarp

As compared to the Kokomeren rockslide, the frontal part of which filled the stream that was about 40 m above the present level (see Figure 128 and Figure 135), this channel should be younger and, thus, the "Displaced Peneplain" rockslide must be also younger than the Kokomeren event. Since both of them occurred quite close to the active fault described in section 3.1.3, it is proposed that both failures were triggered by the recurrent movements along this fault and, thus that the "Displaced Peneplain" rockslide is a seismically triggered phenomenon, similar to the Kokomeren rockslide [Strom, Stepanchikova, 2008].

At least two river damming episodes can be identified at this part of the Kokomeren River valley after the breach of the dam formed by the Kokomeren rockslide. The older one corresponds to a lacustrine silt layer overlain by stream alluvium that outcrops in the road cut at 41.918º N, 74.216º E (Figure 162). The younger episode led to formation of the second silt-rich succession that overlays the above mentioned stream alluvium. It can be seen on the same bank about 50 m higher at 41.921º N, 74.211º E (Figure 163). The lacustrine sediments are divided by typical mountain river alluvium transported and accumulated by the unconfined stream.

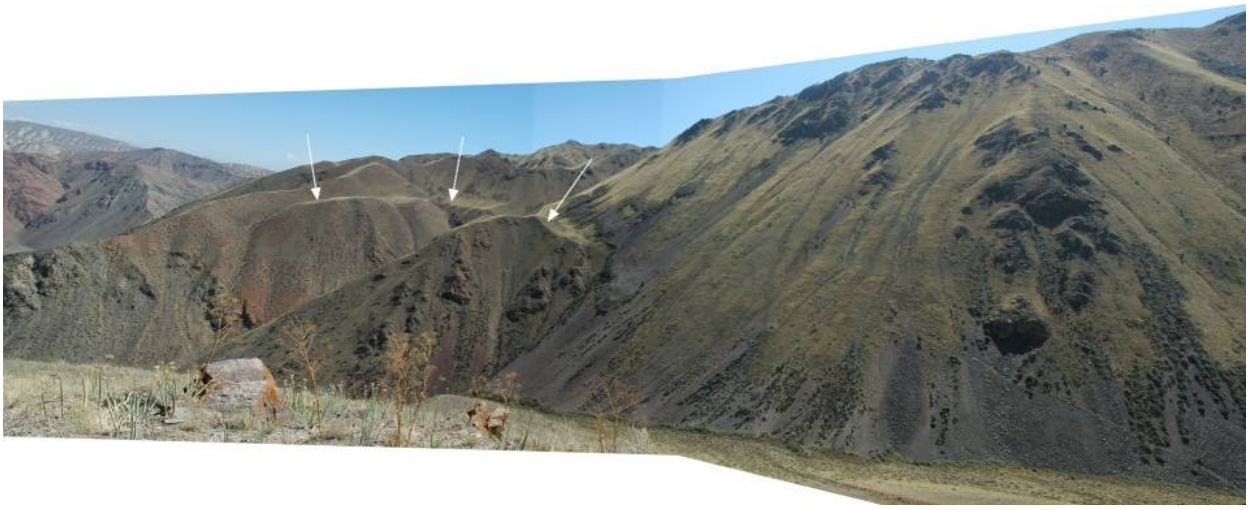

Figure 156. Headscarp of the Displaced Peneplain rockslide
Remnants of displaced Pre-Neogene peneplain are marked by arrows

Figure 157. The Displaced Peneplain rockslide body.
Gully that dissects it was eroded after rockslide emplacement. Black arrow marks the uppermost part of the rockslide deposits (*brandung*?)

Figure 158. Crushed gneiss of the Displaced Peneplain rockslide body upper part resting over red granite (lower right corner of the photograph)

Figure 159. Outcrop where the "stratified" internal structure of the rockslide body is visible

Figure 160. Fragment of the left bank of the abandoned stream of the Kokomeren River
Arrow marks the outcrop shown on Figure 161

It is evident that accumulation of thick stratum of fine well-bedded sediments in the narrow gorge without a well-developed floodplain is not possible in "normal" stream conditions. Thus they are good indications of lacustrine conditions, which are possible due to river damming only. Besides the "Displaced Peneplain" event, which, likely, caused the formation of a lacustrine unit, river damming

could be associated either with the Mini-Köfels rockslide described in section 2.1.2 of the Guidebook or by catastrophic debris flows that formed a huge fan at the Tuurakaing Creek mouth (see Figure 190).

Figure 161. The upstream part of the abandoned pre-Kokomeren valley filled by alluvium


Figure 162. Lacustrine silt sediments overlain by stream alluvium
Road cut at the Kokomeren River right bank at 41.918 N, 74.216 E

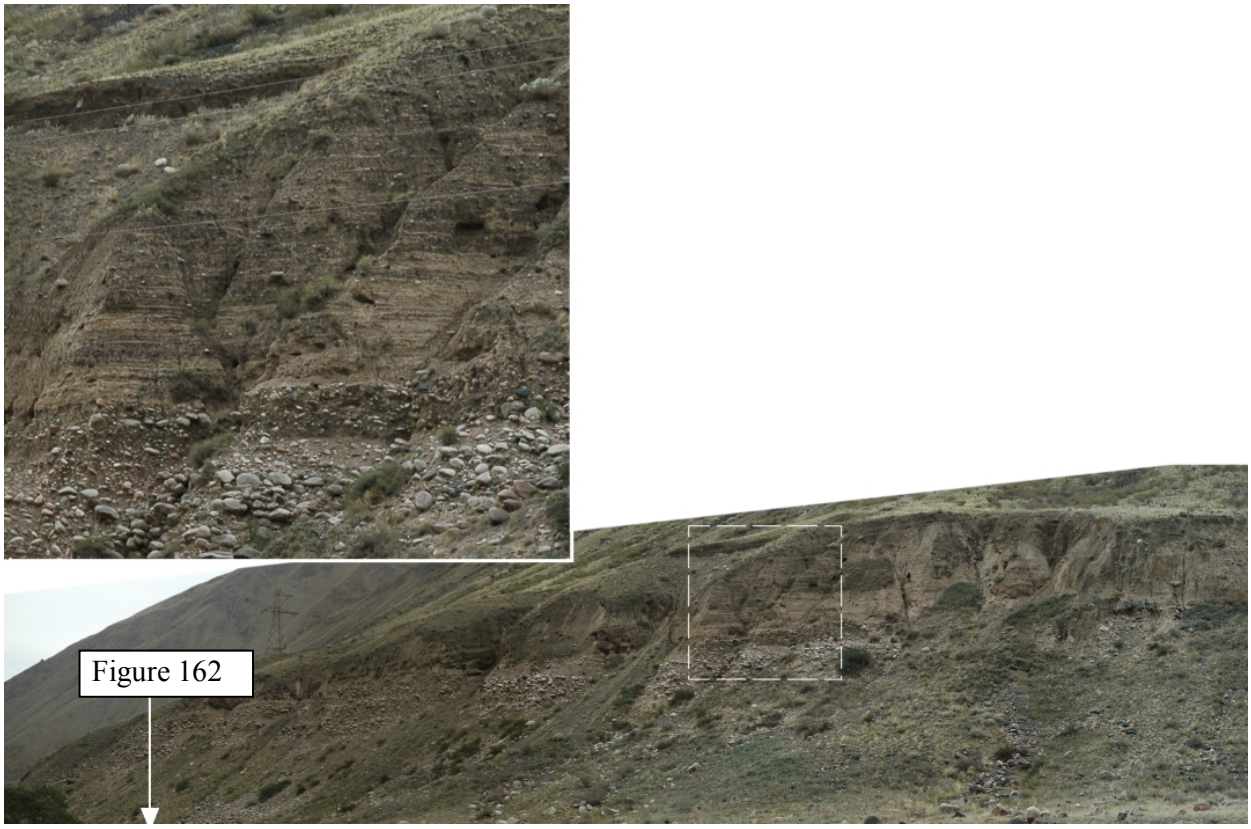

Figure 163. Fine thin-layered sediments overlaying stream alluvium at 41.921 N, 74.211 E

3.3 The Ornok rock avalanche

May be the most impressive 'stratification' of rockslide/rock avalanche deposits can be observed at the Ornok rockslide (No 14 on Figure 2) on the left bank of the Kokomeren River valley downstream of the Minkush River mouth (41º43' N, 74º13.5' E). Slope failure occurred on the slope, which base is composed of Neogene red beds (sandstone and conglomerate mainly) and dark gray Carboniferous sedimentary rocks thrusted over the Neogene strata (Figure 164).

The rockslide initiated from a 500-600 meter high slope and converted into a rock avalanche that travelled at least 2.3 km (actually more, but its frontal part was eroded); its frontal part forms a well-stratified body about 100 m thick, resting on alluvial gravel (Figure 165). Its lower part is composed of "layers" of crushed Neogene red beds and the upper part of a "layer" of crushed Carboniferous rocks. In situ Neogene strata dipping ~40º are shown in the zoomed fragment of Figure 165. The entire horizontally bedded succession represents a 'stratified' rockslide body resting on alluvium (aQ). It should be noted that the uppermost gray 'layer' originated from Paleozoic rocks that form the topmost part of the headscarp (same as at Kokomeren rockslide shown on the sketch in Figure 130).

A fault zone composed of mylonitized Paleozoic claystone rocks, along which the claystone is thrusted over compacted scree (Figure 166), can be seen at the base of the rock avalanche body (see Figure 164, Figure 165). The fault zone is very similar (Figure 167) to one seen in situ more than 1 km southward, where it stretches along the foot of the main headscarp (see Figure 164). Since it is unlikely that this part of the rockslide could "jump over" a rather wide Neogene belt, it can be assumed that the tectonic contact shown on Figure 166 is the displaced part of the original fault zone passing within the zone, composed of Neogene conglomerates. Some evidence of the tectonic contact can be observed on the left bank of the Kokomeren valley west of the Ornok rockslide (Figure 168).

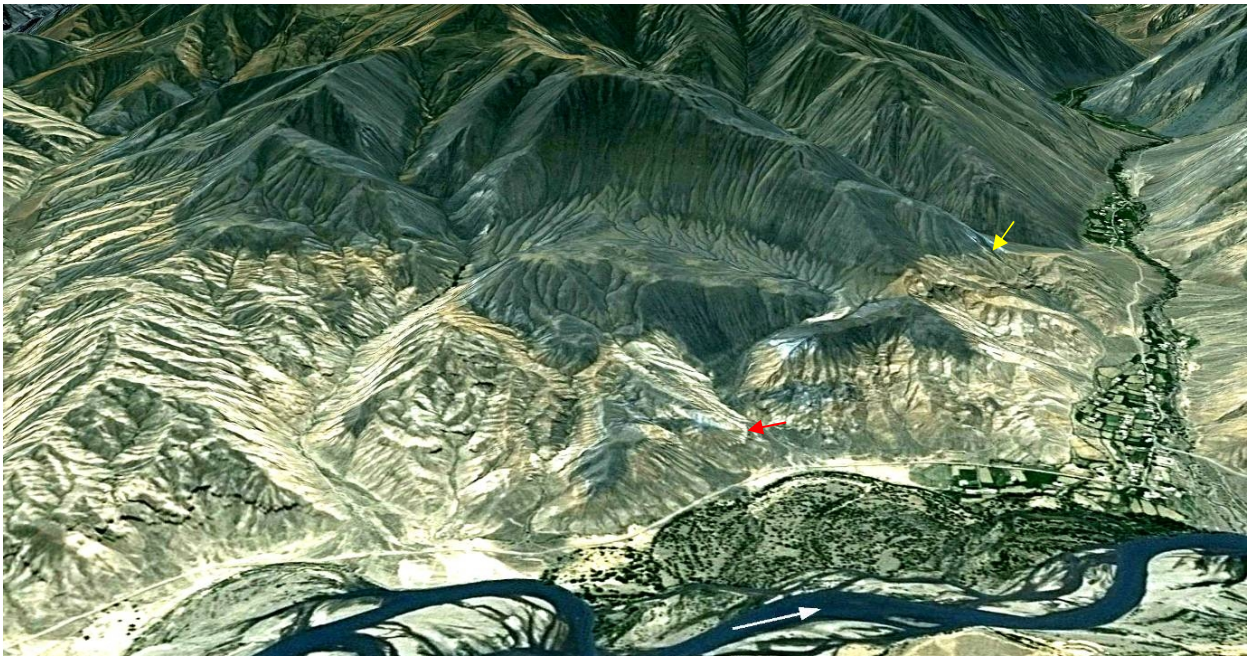

Figure 164. 3-D Google earth image of the Ornok rock avalanche.
The base of the headscarp is ~1.5 km wide. Yellow and whitish areas are Neogene red beds and rockslide debris originated from them; dark-grey – Carboniferous sediment and corresponding rockslide debris. Red arrow marks fault zone within rockslide body shown on Figure 166 and yellow arrow – very similar zone in its original position (Figure 167)

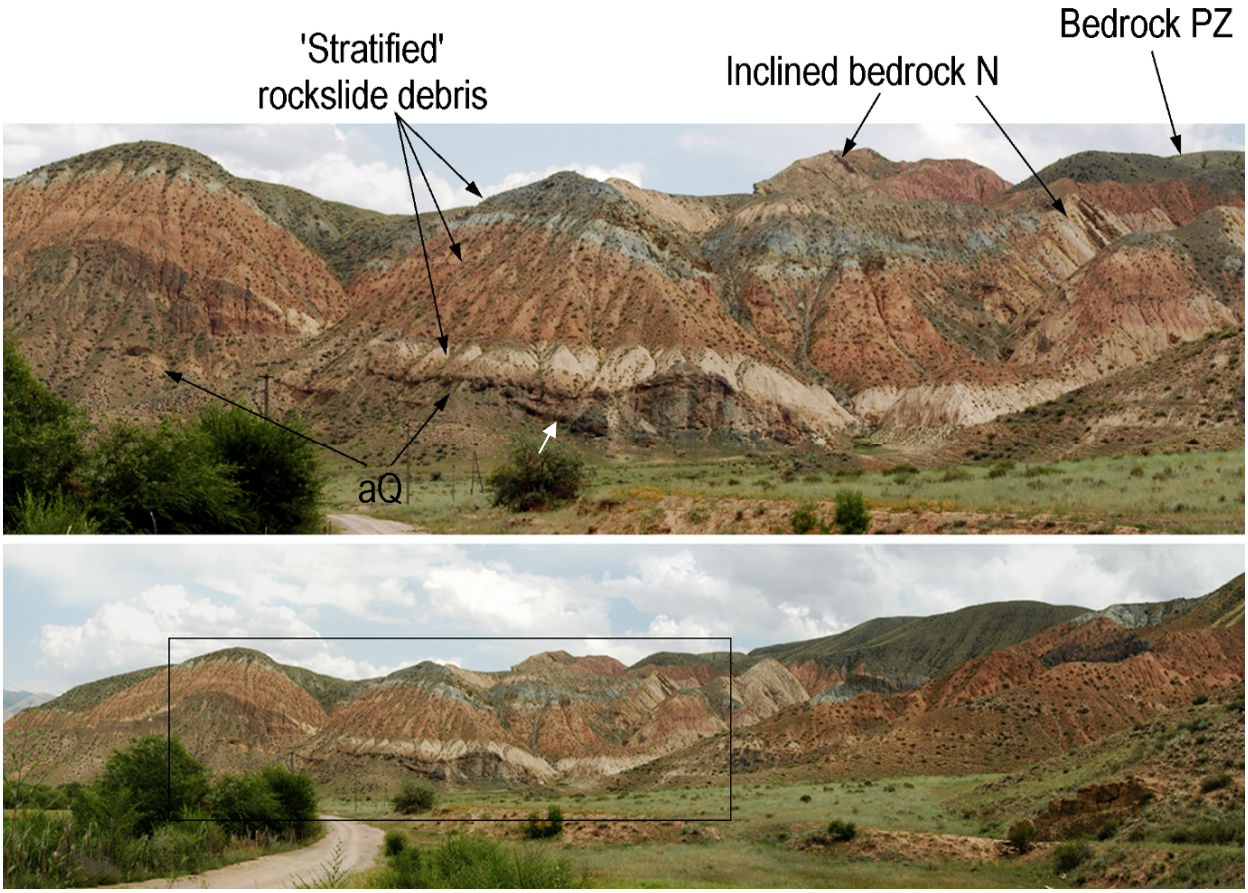

Figure 165. Debris 'stratification' of the Ornok rockslide
Zoomed photo above corresponds to the outlined area below. White arrow marks outcrop shown on Figure 166.

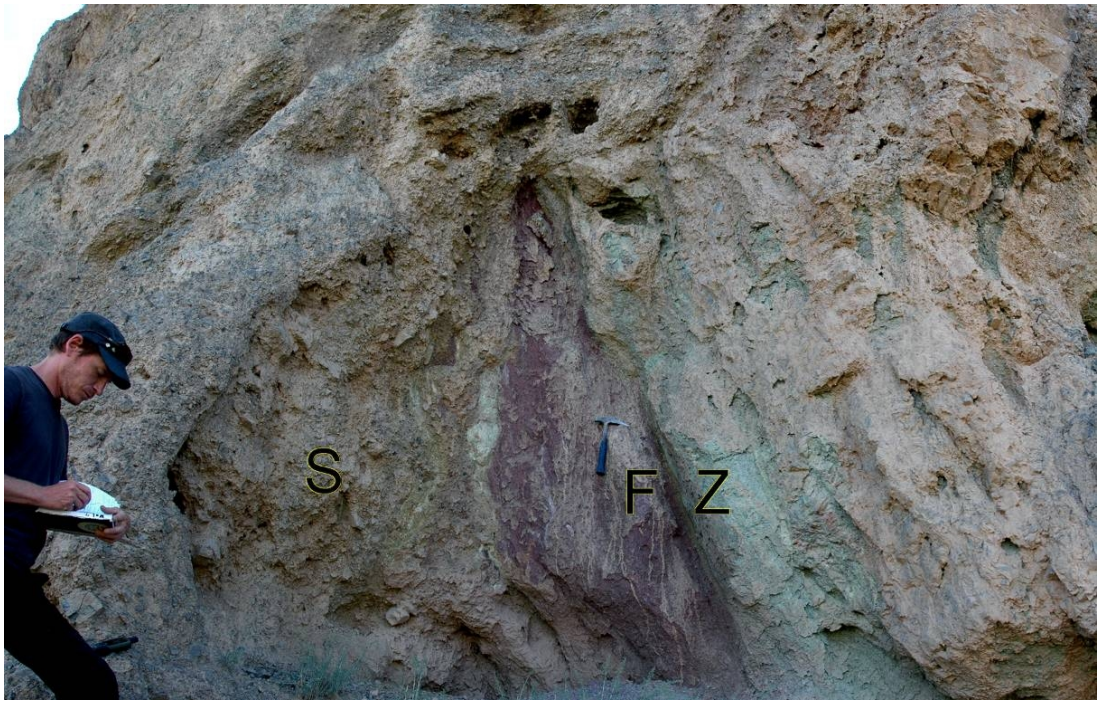

Figure 166. Fault zone (FZ) of dual structure composed of violet and green mylonite overthrusted on rubbly scree (S).

This succession is within the basal zone of the rock avalanche body more than 1 km from the original position of the fault zone

Figure 167. Tectonic contact between grey Paleozoic metasediments (right) and Neogene red beds (left)

Figure 168. Two south-dipping fault zones (red arrows) along the southern boundary of the Minkush-Kokomeren neotectonic depression west of the Ornok rockslide

The composition of the Ornok rockslide body is rather complex. There is more than one succession of the multi-coloured rock debris (Figure 169), and deciphering the relative position of debris units that originated from various parts of the headscarp area requires detailed mapping. The presence of lake sediments in the proximal depression at the foot of the main headscarp (Figure 170) allows the possibility to date this unique feature.

Figure 169. Internal structure of the western part of the Ornok rockslide body

Figure 170. Lake sediments in the proximal depression of the main rockslide body (arrow)

3.4 The Karachauli and Lower Kokomeren rockslides

Downstream of the Ornok rockslide and up to the Kokomeren River mouth one can find several rockslides; most of them collapsed from the left side of the valley, undercut by an active fault. The largest one is the Karachauli rockslide about 1 km^3 in volume that blocked the Kokomeren valley ~12 km downstream of Ornok (No 17 on Figure 2, Figure 171). Though the main remaining part of its body up to 350 m thick rests at the foot of the gigantic headscarp on the left bank of the river, its frontal part that filled the lowering on the right bank can be observed as well.

The rockslide originated on the 1300 m high left bank of the Kokomeren River valley and is composed of Paleozoic terrigenous rocks. The foot of this slope, however, is composed of the Neogene red beds (conglomerate, sandstone, and siltstone) that were also affected by the landslide. Corresponding deposits can be seen in the road cut on the opposite, right bank of the river, where they can be distinguished from the overlying scree and slope outwash accumulations of similar lithology (Figure 172).

Figure 171. The Karachauli rockslide

View upstream. The proximal part of this ancient rockslide body resting at the foot of the headscarp is about 350 m high

Figure 172. Frontal part of the Karachauli rockslide

Rockslide body composed of crushed Neogene (clasts in matrix) is overlain by stratified slope outwash and colluvium of the same lithology (Neogene red beds). Above – original photograph, below – same image in false color

On the right bank of the valley where the bedrock is represented by the Neogene red beds only one can find remnants of crushed Paleozoic metasediments that had been brought here by the Karachauli rockslide. They are represented by angular clasts and boulders, overlaying much more intensively crushed debris (Figure 173) or filling local depressions in the pre-slide relief (Figure 174). These patches are the remnants of the frontal part of the Karachauli rockslide. Material brought by debris flows from the Suusamyr Range has totally different lithology (granites) and boulder shape (rounded or semi-rounded).

Figure 173. Coarse Paleozoic debris (outlined) on top of finer material on the right bank of the Kokomeren Valley opposite the Karachauli rockslide

Figure 174. Coarse angular boulders on the right bank of the Kokomeren River valley about 200 m above the river bed

About 4 km downstream of the Karachauli rockslide the Kokomeren River was blocked again by an impressive rock avalanche that failed from its left bank (about 800 m high) and is composed of Paleozoic sedimentary rocks with low-grade metamorphism. Here, a fault zone dividing Paleozoic rocks from the Neogene red beds passes just along the stream. About 40 Mm^3 of debris had crossed the river and 'climbed' almost 150 m on the opposite bank where it dammed the dry tributary valley (Figure 175). This so-called Lower Kokomeren rockslide (No 18 on Figure 2) can be classified as a Primary rock avalanche in frontally confined conditions.

Both rockslides dammed the valley, demonstrating what was called by K. Hewitt "a disturbance regime" (Hewitt, 2006). It should be noted that while the upper part of the Kokomeren River valley is characterized by well-defined erosional or strath terraces (see Figure 144 for example), in its lower

part, downstream of the Minkush River mouth, the stream passes mainly through Quaternary alluvial fan deposits (Figure 176). At some pre-rockslide stage the river valley was eroded at least as deep as at present and, likely, even deeper. After that, most likely due to rockslide damming, the valley was filled by deposits transported both by the main stream (alluvium) and by the tributary valleys (debris flows). Generally the latter develop up to the present erosional level.

Figure 175. Dry valley dammed by rockslide that collapsed from the opposite bank of the Kokomeren River valley

Thus, accumulation of very thick alluvial fans with a rather uniform, slightly bedded silty-sandy matrix, without evidence of internal erosion indicate deposition in a lacustrine environment. More detailed description of the dammed lake sedimentation and of the subsequent outburst floods is presented in the next chapter.

Figure 176. Thick alluvial fan composed of more or less uniform debris flow deposits between the Ornok and Karachauli rockslides

4 EVIDENCE OF RIVER DAMMING AND CATASTROPHIC OUTBURST FLOODS

The most disastrous effect of landslide river damming is outburst flooding caused by dam breach. Numerous case studies from the Alps, Karakorum, Himalayas, Central American and Argentinean Andes, Tibet and Longmanshan mountains are described, for example, in various chapters of the book "Natural and Artificial Rockslide dams" [Evans et al., 2011].

Evidence of such prehistoric catastrophes has been found in the Kokomeren River basin. One case study represents formation and failure of a rockslide dam in the main stream of Kokomeren River and another in a small tributary valley.

4.1 Formation and failure of the Lower-Aral rockslide dam

Most of the landslide dams described above do not demonstrate evidence that allows assumption of their catastrophic breach. Some of them, like the Kashkasu or Karakungey blockages, remain almost intact. The gigantic Kokomeren and Displaced Peneplain rockslide dams caused formation of bypass gorges through the bedrock that should last for a long time, likely without catastrophic effects. Breach of the Mini-Köfels rockslide dam could have been rapid and catastrophic but we could not distinguish their outburst flood deposits from huge coarse bouldery accumulations in the western part of the Djumgal depression. The Lower Kokomeren rockslide appears to have evolved similarly; it seems to have breached soon after lake impoundment.

Nevertheless, formation and subsequent failure of the large rockslide dam that had blocked the main stream of Kokomeren River can be found downstream of Aral village at 41º47.9' N, 74º17.3' E

(No 12 on Figure 2). Failure occurred on top of the ridge composed of Paleozoic granite where the Kokomeren enters the Minkush-Kokomeren neotectonic depression. Since it was not associated with slope undercutting, the mass movement was likely triggered by a strong prehistoric earthquake. The collapsing debris divided on its way downslope into two parts that, finally, formed two separate bodies about 800 m from each other (Figure 177). The upper one, composed of heavily comminuted granite with a coarse carapace, formed a dam about 80 m high (A on Figure 177, Figure 178), whereas the lower one presumably caused just partial blockage of the river. Up to 250 Mm^3 of water (maybe even more) accumulated in the dammed lake that extended more than 8 km upstream, judging from the presence of laminated silt in the outcrops in the road cut at the junction of the Kokomeren and Djumgal rivers (Figure 179).

An interesting peculiarity of the latter outcrop is the presence of liquefaction-induced features – the lowermost layers of laminated silt sank into the underlying basal coarser unit, while younger laminae are not subjected to such deformations. This means that both units – the massive poorly sorted basal layer and overlying laminae – were in a liquefiable state and, thus, liquefaction occurred soon after deposition of these units.

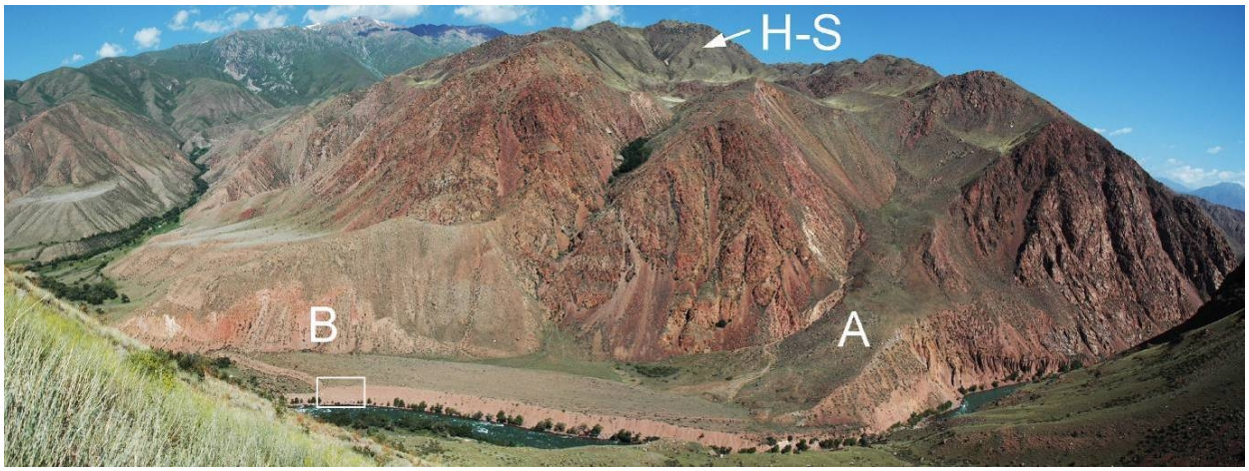

Figure 177. Bodies of the Lower Aral Rockslide and "terrace" left by the outburst flood caused by its breach.

River damming was caused by the upper body (A). H-S –the headscarp area. Outlined part of the terrace-like surface is shown on Figure 182

Figure 178. Upstream body of the Lower-Aral rock avalanche.

Coarse carapace is shown on the inset

Quite limited extent of the outcrops (part shown on Figure 179 was significantly reworked in 2015 during road construction) do not allow such sound conclusions regarding seismic origin of the features described as, for example, in the Issyk-Kul basin, where liquefaction-induced features were observed in the numerous kilometers-long exposures of Quaternary lacustrine sediments (Korjenkov 2000). Nevertheless, this case study demonstrates features distant from the master event in space but

closely linked with it in time, which allows assumption of seismic origin of both. Our attempt to date these sediments using OSL method gave Late Pleistocene age but with inconsistent numerical values. Despite the rather "fresh" topographic expression of the rock avalanche body such age seems to be realistic, considering that lacustrine laminated silt was eroded by a likely Pre-Holocene or Early Holocene debris flow that overlaid it (Figure 180).

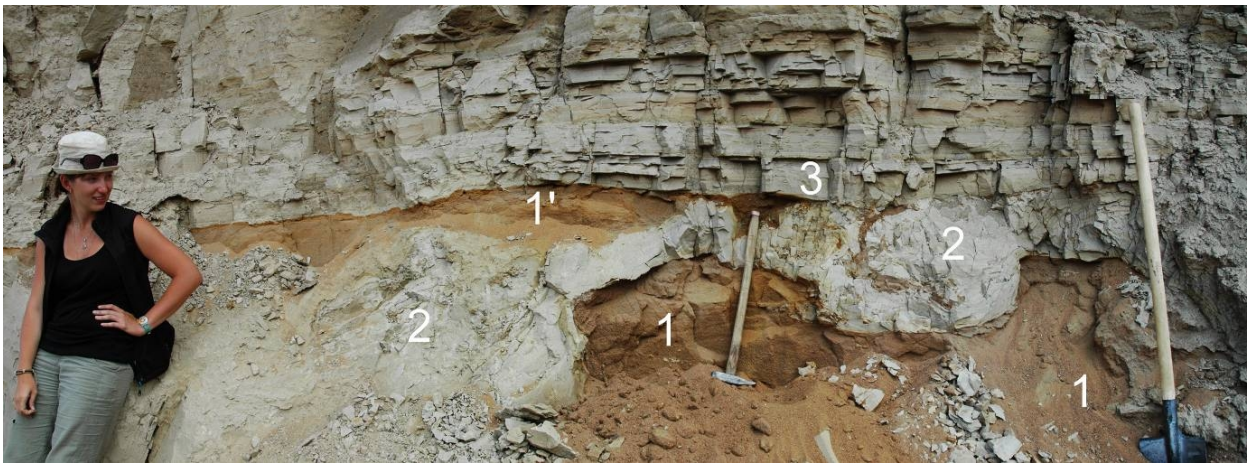

Figure 179. Lacustrine sediment accumulated at the tail-end of the past lake dammed by the Lower-Aral rockslide.

Outcrop located just downstream from the bridge in the Aral village across the Kokomeren River. 1 – basal massive coarse arkose sand liquefied and ejected (1') ; 2 – lower part of silt unit affected by liquefaction, whose portions sank in the basal sand; 3 – upper part of silt unit represented by nearly horizontal laminated layers

Figure 180. Lacustrine sediments (whitish laminated silt) eroded and overlain by thick debris flow deposits

Outcrop in the road cut opposite the base camp

Direct evidence of catastrophic outburst flooding can be seen ~2 km downstream of the dam where large angular boulders were left on top of a small 37-m high cliff (Figure 181). Large angular blocks of granite up to 1 m in size carried by the first, most powerful 'wave' of the outburst flood have been left immediately downstream from the cliff in its 'shadow' (left inset on Figure 181). This material was likely eroded from the dams' upper part (see inset on Figure 178). The following portion of the outburst debris flow left smaller fragments on top of the cliff (right inset on Figure 181). The orientations of flattened fragments clearly indicate the direction of debris flow motion. Note that the debris flow was thick enough to leave about 2-m thick debris nearly 40 m above the river level.

Calculations performed by A. Zhirkevich (Hydroproject Institute, Moscow) returned a debris flow peak discharge of about 28,000-30,000 m^3/sec – about 45 times more than the maximum value ever recorded here (~600 m^3/sec).

Deposits left by the final stages of this catastrophic event could be seen on the right bank of the Kokomeren River, in the 14-m high terrace-like surface eroded by the stream visible on Figure 177. While morphologically it looks similar to the alluvial river terrace, its cross-section is completely different (Figure 182). This body is composed of layers of angular clasts. Much of the debris is fines typical of the internal part of the blockage, but a layer of larger clasts appears in the middle part of the section, indicating a more powerful episode of flow.

This case study demonstrates that careful analysis even of small local outcrops allows reliable reconstruction of the evolution of a large section of the River valley.

Figure 181. Debris left by outburst flood after breach of the Lower Aral Landslide dam on the isolated ~10 m high cliff

about 2 km downstream from the breached dam. Dark blue arrow shows river flow direction. Brown arrows – direction of debris flow

Figure 182. Typical section of the outburst flood deposits forming terrace-like surface downstream of the Lower-Aral breached dam

4.2 Failure of the Lower Ak-Kiol dam in the Unkursai River valley

Evidence of one more outburst flood could be found at 41º42.10' N, 74º16.53' E in the Unkursay River valley – the left tributary of the Kokomeren River. This valley had been blocked by two landslide dams (No 10 on Figure 2). The upper one that originated on the left bank of the valley composed of Paleozoic conglomerate, sand- and siltstone still retains the Ak-Kiol Lake (Section 2.1.3) that poses a threat to the communities in the lower Kokomeren being dammed by a deeply eroded rockslide that could be breached in case of extreme flooding or due to retrogressive erosion (see Figure 51).

About 2 km downstream, the valley was blocked by a Lower Ak-Kiol rockslide that originated on the right bank of the valley in gently dipping Neogene conglomerates. The sliding surface coincided with bedding (Figure 183) and the rockslide body, with a distinct proximal depression, is composed, at least at the surface, of huge blocks of conglomerates (Figure 184). A rockslide body more than 100×10^6 m^3 in volume has distinct evidence of a Secondary rock avalanche (Figure 185). A swampy area several hectares in size upstream of the dam represents the remnant of the partially filled lake (Figure 186).

Figure 183. Headscarp (on the right) and body of the Ak-Kiol-Lower rockslide

Figure 184. Proximal depression of the Lower Ak-Kiol rockslide
view from the edge of the main body

Figure 185. Aerial photo of Lower Ak-Kiol rockslide

Figure 186. Swampy area remaining after outburst of the Lower Ak-Kiol Lake
View from the breached rockslide dam

Breach of this dam likely occurred rather recently. Banks of this depression at a level of about 15 m above the present day valley bottom are covered by a crust of fossilized lake algae (Figure 187). Similar algae can be found underwater in the Ak-Kiol Lake. It can be hypothesized that the presence of such a crust of dry algae could be formed if the lake was emptied very fast (catastrophically), releasing 2–3 million cubic meters of water. Otherwise algae that would appear gradually above water level would die and would have been replaced by ground vegetation. In our case it looks as if well-developed underwater vegetation appeared on land immediately and was petrified due to the presence of carbonates.

Figure 187. Crust of fossilized lake algae at the bank of the former Lower Ak-Kiol lake

No deposits that could be attributed to this outburst flood were distinguished downstream in the Unkursay River valley. However, about 80 km downstream, in the Naryn River valley close to the Kambarata-1 dam site we found evidence of an abnormal flood with estimated peak discharge of about

10 000 m^3/sec—almost 3 times more than the maximum value ever recorded at this part of the Naryn River.

Here, on a low right-bank terrace of the Naryn River that rises about 5 m above the mean stream level one can see dry tree trunks up to 40–50 cm thick elongated along the smooth curve [Strom, 2012] that could be brought here by an abnormal water flow only. Discharge estimates were calculated considering that water carrying such trees should flow about one meter above the terrace. It was assumed that such an excessive flood could be caused by breach of the Lower Ak-Kiol dam.

5 OTHER LANDSLIDES IN THE KOKOMEREN RIVER BASIN

5.1 Rock avalanches

Several rock slope failures occurred in the deep valleys of the Kokomeren left tributaries – the Oigaing and the Burunsu Rivers. A rockslide about 30×10^6 m^3 in volume descended from the right bank of the Oigaing River valley about 10 km upstream of its mouth (42.12º N, 74.24º E). The slope is composed of Paleozoic granites and metasediments. The 50–70 m thick rockslide body has been significantly eroded by the river and only its proximal part remains at the scar's foot. Its internal structure, along with a well-expressed rockslide scar 750 m high and up to 1000 m wide, can be observed from the opposite bank of the Oigaing River (Figure 188).

A much smaller bedrock landslide about 10^6 m^3 in volume dammed the Burundu creek – the small left tributary of the Kokomeren River that meets it 4 kilometers upstream of Kyzyl-Oi village. It blocked the river at 41.99º N, 74.19º E, two kilometers upstream of the creek mouth, with a compact dam up to 100 m high with convex slopes. The dam's surface is composed of angular granite boulders. The angle of repose of its upstream slope is about 35º. Most of rockslide debris accumulated at the scar's foot and Burundu River incised its new path with a 15-20-m high waterfall through the right bank bedrock that indicates that the pre-rockslide level has not been reached yet.

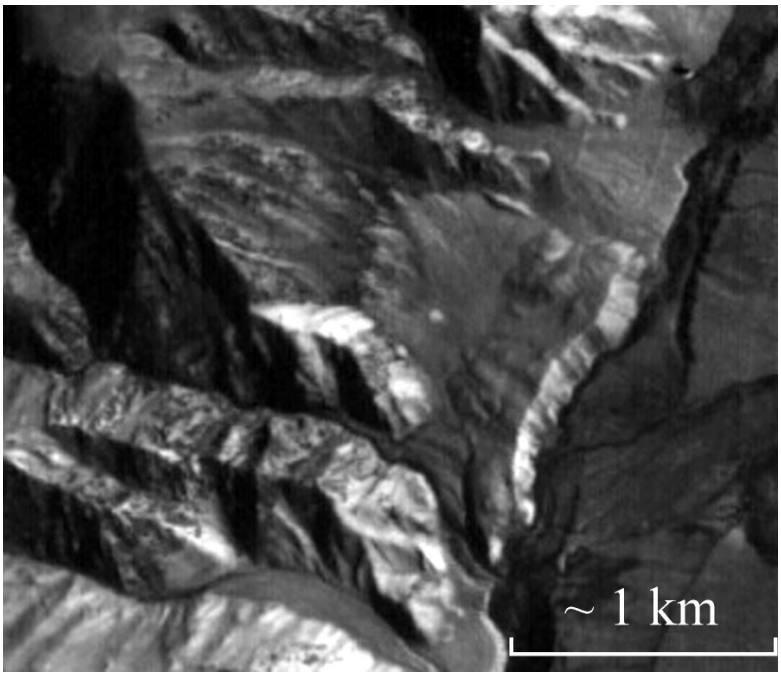

Figure 188. The Oigaing rockslide
Zoomed fragment of high resolution KFA-3000 space photograph

At least two more rock avalanches can be found in the central part of the Tuurakaing River basin (Figure 189) at 41.88º N, 72.21º E and 41.89º N, 74.19º E. This small river that meets Kokomeren opposite the Kokomeren rockslide has an enormous fan composed of huge, subangular granite and

gneiss boulders (Figure 190) that differs significantly from much smaller fans of other tributaries of the Kokomeren River that have the same-order catchment areas.

Glaciers, which have existed at the upper reaches of this river in the past, never extended towards its mouth, at least in the Holocene, while freshness and expressiveness of the alluvial fan indicates that it was formed rather recently, at least after formation and breach of the Kokomeren rockslide. It can be assumed that huge blocks resting on top of this fan (Figure 191) could be brought by an outburst flood, though the exact location of a possible damming event is not known yet.

An interesting feature can be observed east of the Southern Karakungey rock avalanche, about 4.5 km from the foot of the rocky slope at 41.86º N, 74.3º E (see Figure 73). Here the low plateau that forms the left bank of South Karakungey Creek valley has an unusual dual structure. Its base as well as the entire plateau farther to the east is composed of rounded or semi-rounded granite boulders with sandy-gravel fill. These are typical debris flow (maybe glacial-fluvial) deposits that constitute most Quaternary sediments at the western termination of the Djumgal depression. They could have accumulated during the retreat of Pleistocene glaciers. In contrast, the upper part of the plateau in question is composed of angular clasts and boulders (Figure 192), quite atypical of deposits that were transported by water for a long distance from its source zone – the upper reaches of the South Karakungey Creek dissecting the adjacent range. The same succession is observed at adjacent outcrops at a distance of about 1.5 km. We assume that this unit represents the remnant of old rock avalanche deposits that descended from somewhere in the upper reaches of Southern Karakungey Creek, thus being much bigger than the South Karakungey rock avalanche described above. Though it is difficult to locate its source zone, the runout distance of this Pleistocene Pre-Karakungey rock avalanche should be about 7 km if not longer.

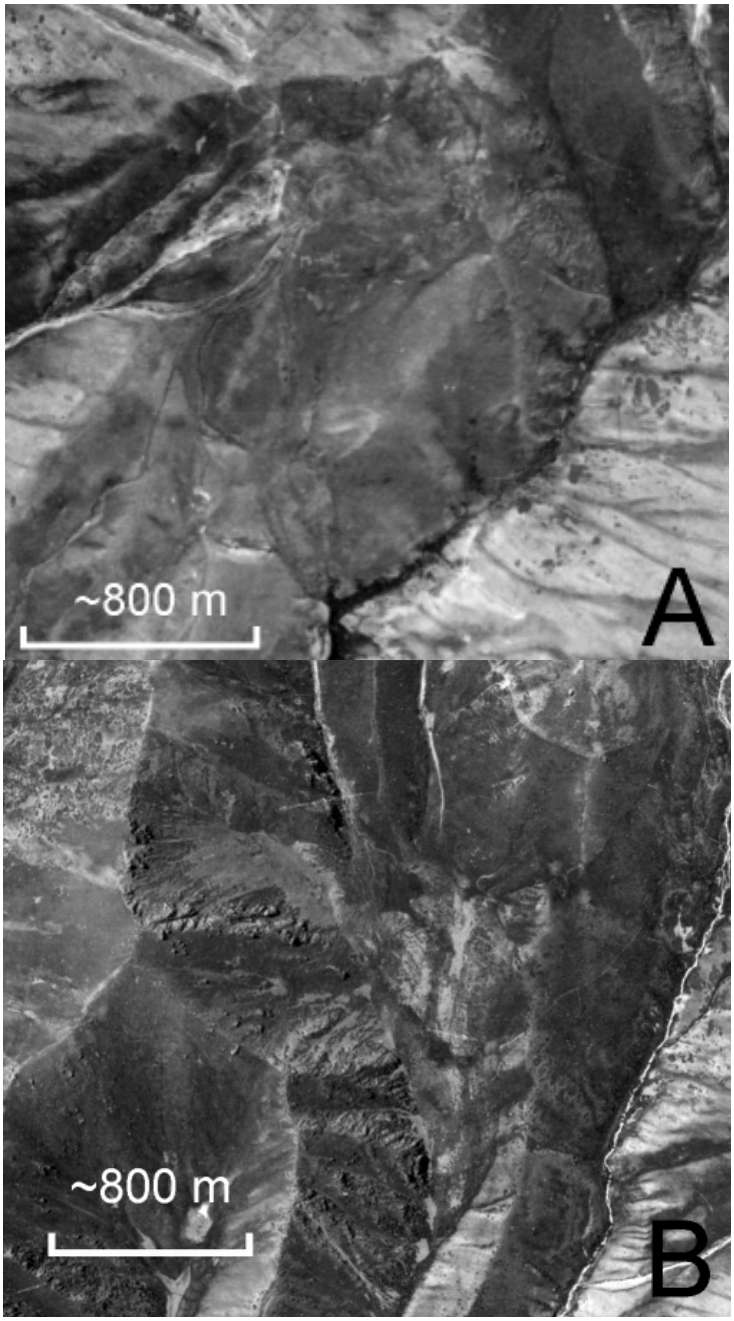

Figure 189. Left (A) and Right (B) Tuurakaing rock avalanche
Zoomed fragments of aerial photographs

It is unlikely that the emplacement of such a voluminous body composed of angular boulders could be due to any other process. The deposition area is too low in elevation and too far from the mountain range to be interpreted as an end moraine. Thus, the proposed origin of this unit seems to be the most logical. The fact that large-scale bedrock slope failures have occurred repeatedly at the same place proves the assumption of spatial clustering of such events [Strom, Abdrakhmatov 2004], which was mentioned before when we described the Snake-head rock avalanche.

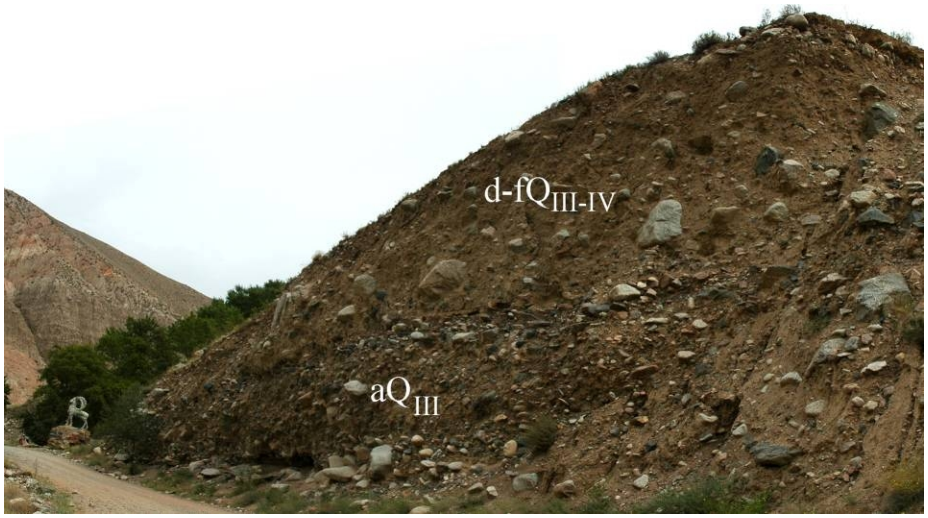

Figure 190. Debris flow deposits of the Upper Pleistocene – Holocene (?) age overlying Upper Pleistocene alluvium at the upstream part of the Tuurakaing River fan

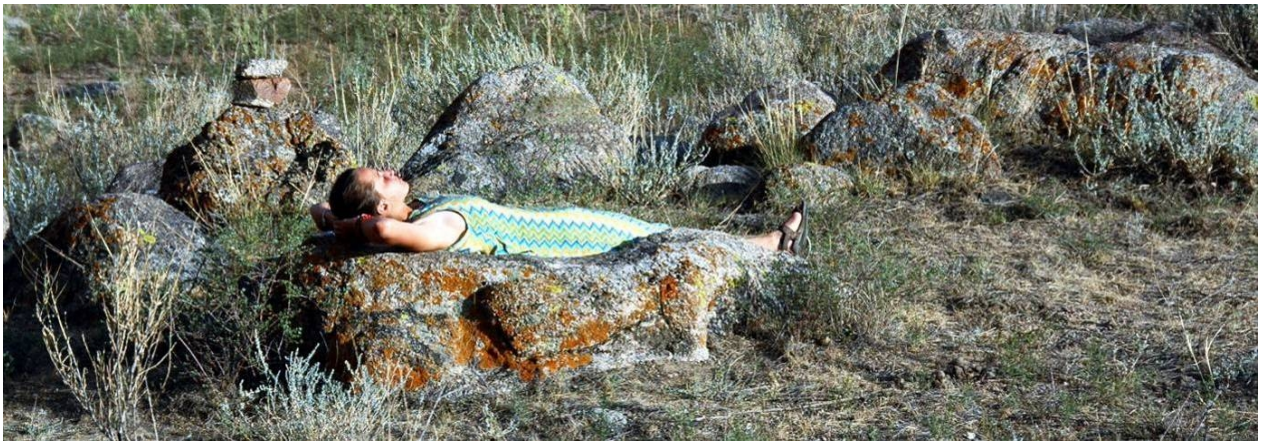
Figure 191. Granite semi-rounded boulders on top of the alluvial (debris flow) Tuurakaing River fan

Several interesting slope failures not described in detail could be observed in the lower part of the Kokomeren River basin. Among them is a quite unusual erosional gully dissecting the left side of the valley between the Ornok and the Karachauli rockslides. Debris flows originating in this gully form a huge alluvial fan overlapping an older alluvial fan that comes from a much larger tributary valley (Figure 193).

Figure 192. Angular boulders of the assumed Pleistocene Pre-Karakungey rock avalanche
The Holocene Southern Karakungey rock avalanche in the background

Figure 193. Very large erosional gulley on the left bank of the Kokomeren River valley

5.2 Large landslides in the Neogene-Quaternary sediments

Besides the above rockslides and rock avalanches there are several large landslides within the study area that affect non-lithified Neogene and Quaternary deposits in the intermontane neotectonic depressions. Some of them are described hereafter briefly.

Huge rotational landslides in Neogene and Quaternary deposits that affected areas about 3×2 km each are visible in the central part of the Djumgal depression opposite the Chaek village and south of it (Figure 194). The first one forms a tremendous amphitheater at 41.93° N, 74.57° E (see Figure 16). Blocks inside the amphitheater are tilted due to rotation along the circular sliding surface (Figure 195).

Another landslide at 41.89º N, 74.52º E is significantly eroded and looks much older than the first one (Figure 196). These features are situated south of the recent anticline following the axis of the Djumgal intermontane depression (see section 1.2).

Another large landslide in the Djumgal depression is located at its western centroclinal termination (41.87º N, 74.32º E). This Western-Djumgal landslide (WDL on Figure 73) affected about 10 km^2 – almost the entire western termination of the depression on the right bank of the Kokomeren River valley composed of Neogene and Quaternary sediments. It is bounded by a horseshoe-like headscarp up to 50-70 m high. The depth of the sliding surface of this landslide is unknown. It can be assumed, however, that it comes out below the present-day Kokomeren riverbed.

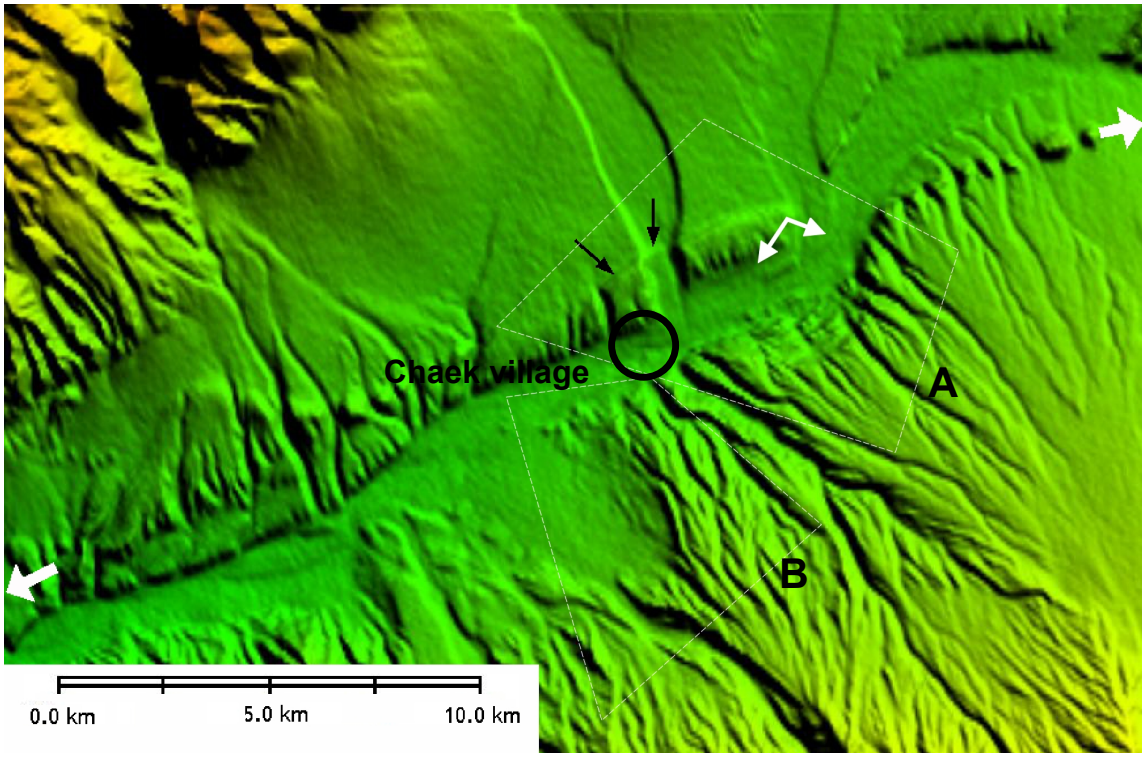

Figure 194. Huge rotational landslides in the N-Q deposits of the Djumgal intermontane depression (3" SRTM DEM). Outlined areas are shown on Figure 16 (A) and Figure 196 (B). Large white arrows - recent anticline axis; small double-head white arrow - point of the panorama (Figure 195); black arrows mark recent offsets along the northern limb of the anticline; the offset value at the higher elevation exceeds that at the more recent terrace indicating recurrent displacements

Figure 195. Panoramic view of the Chaek landslide

Most of its sliding surface, except the headscarp, should dip quite gently (Figure 197). At its south-eastern part the uppermost layers have been completely removed, most likely by the intensive erosion of the area affected by superficial landslides. The entire landslide complex seems to be inactive at present. Unlike the Chaek rotational landslides, whose bodies formed several tilted steps, the Western-Djumgal landslide moved as a single block and can be classified as a landslide of the translational type.

One more complex landslide in the Neogene and Quaternary sediments is located in the southern part of the Suusamyr valley at 42.04º N, 73.88º E, at a small depression separated from the main part of the intermontane depression by a several hundred meter high ridge.

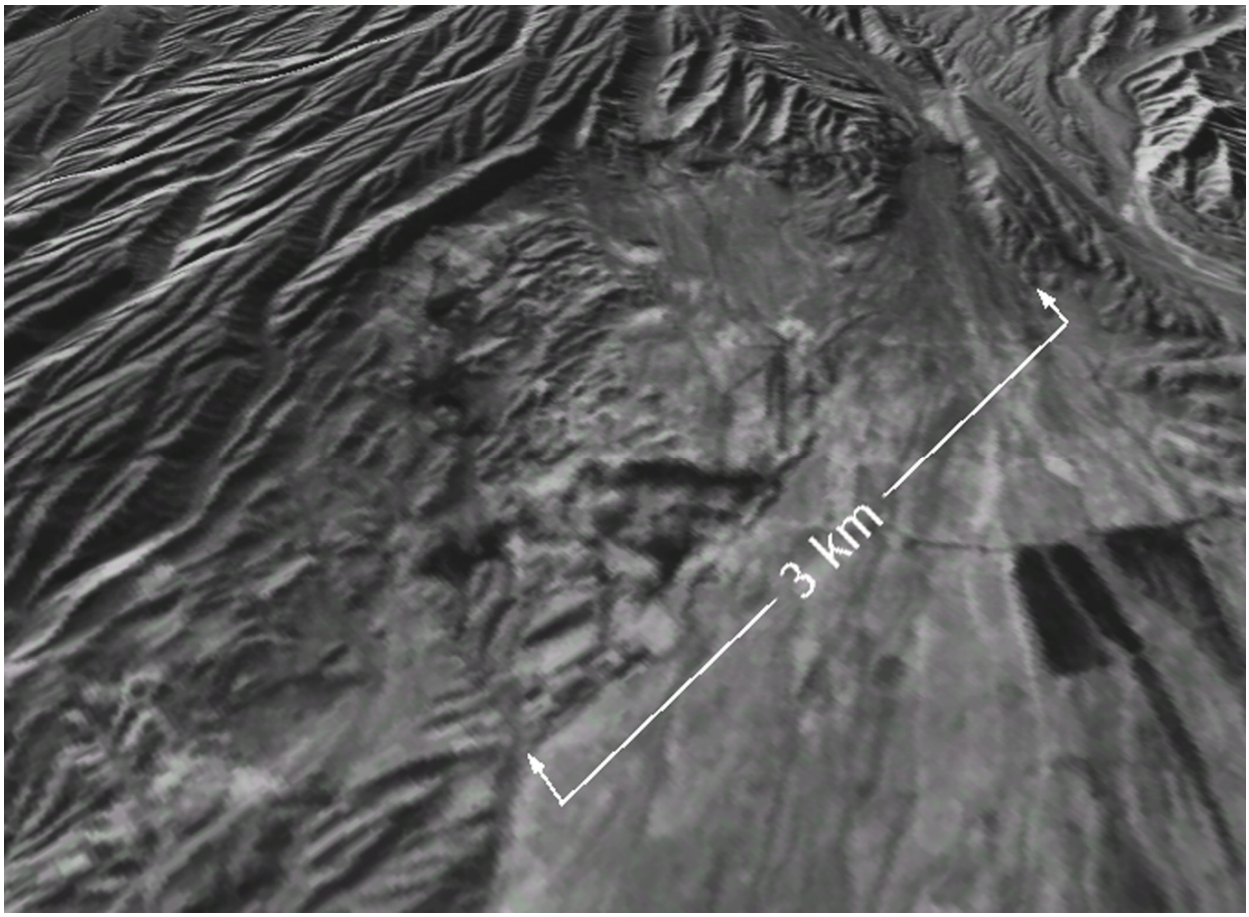

Figure 196. 3-D view of the area B, shown on Figure 194

Significantly reworked rotational landslide South of the Chaek village. Large extent of erosion allows assumption that this feature is much older than the Chaek landslide

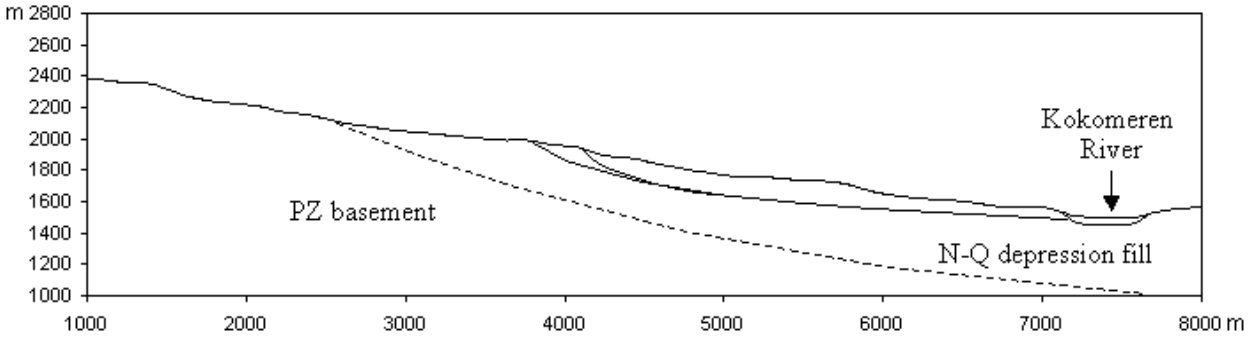

Figure 197. Hypothetical cross-section of the Western Djumgal landslide

The landslide represents lowering by about 3×4 km in size bounded by the horseshoe-shaped headscarp up to 50 m high (Figure 198). Its relief has been significantly reworked by erosion, but most likely it could be classified as some combination of a rotational landslide and lateral spread.

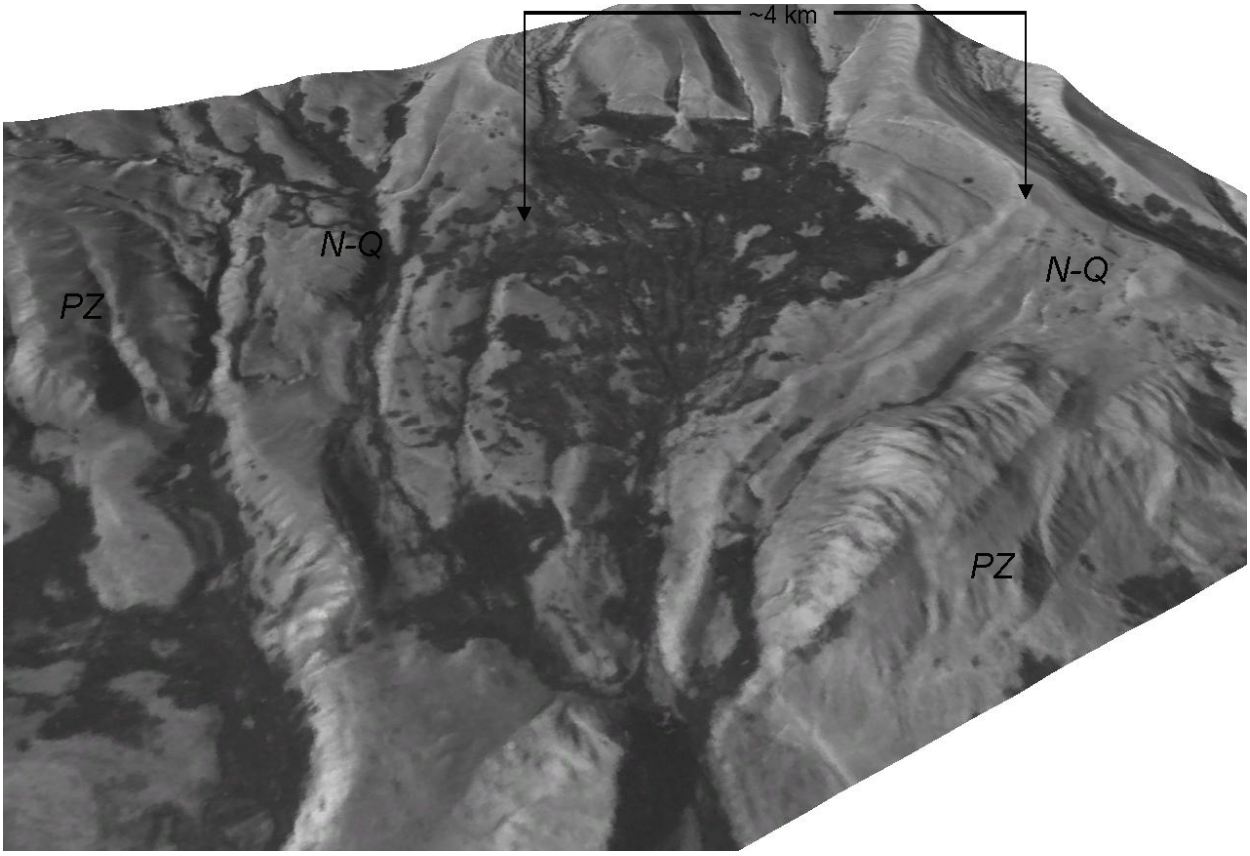

Figure 198. Combined 3D DEM and KFA-1000 space image of the landslide in the southern part of the Suusamyr valley

5.3 Toppling site

A phenomenon directly related to rockslide formation can be observed at the southern boundary of the Kyzyl-Oi depression at 41.94º N, 74.095º E. Here the northern slope of a 500-600 m high ridge (Figure 199) composed of Paleozoic metasediments with distinct bedding planes steeply dipping south (inside the slope) (Figure 200) is crossed by numerous upslope-facing scarps up to several meters high (Figure 201, Figure 202). According to the first impression the entire rock massif is sliding southward.

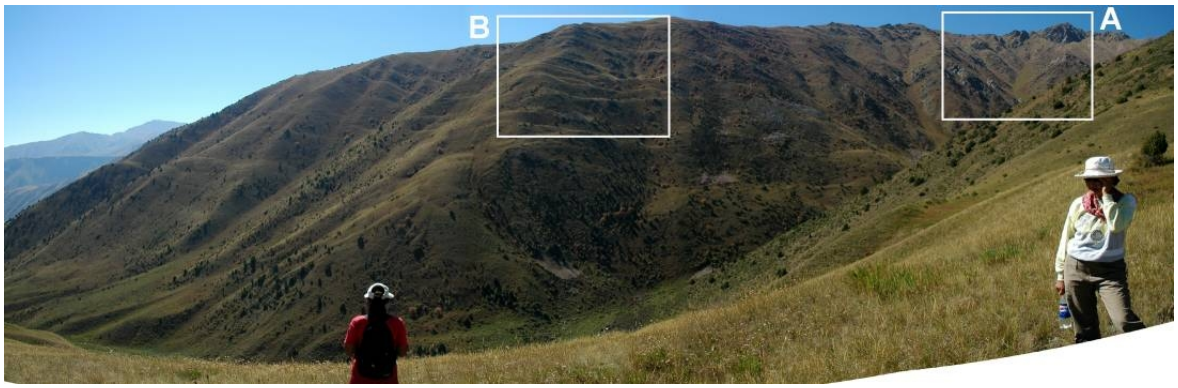

Figure 199 . Upslope-facing scarps at the upper part of the slope
Ridge bounding the Kyzyl-Oi depression from the south. Rectangles mark areas shown on Figure 200 (A) and Figure 201 (B)

However, this impression is false. In fact these upslope-facing scarps indicate that almost the entire northern slope of this ridge undergoes gradual creep deformation (Figure 203) associated with downslope bending of bed heads (Figure 204). This process is known as toppling [Varnes 1978].

Figure 200. Structure of rock massif shown on Figure 199
Bedding planes steeply dip in the massif

Figure 201. Upslope-facing scarps at the most affected part of the slope, shown on Figure 199

According to Nichol et al. "*Slow, ductile toppling of rock masses commonly creates large-scale mountain slope deformations. In some cases, toppling can initiate a brittle catastrophic rockslide. A theoretical and field-based study has been aimed at distinguishing these two alternative modes of toppling. The results indicated two distinct types of behavior: ductile, self-stabilizing flexural toppling in weak rock with a single dominant joint set; and brittle, catastrophic block toppling in strong rock containing persistent, down-slope oriented or horizontal cross-joints. The two mechanisms exhibit very different patterns of pre-failure stress*" [Nichol, et al. 2002]. However, intensive seismic shaking can cause rapid slope failure even at sites featuring the first of the above two mechanisms. This could happen, in particular, at the site shown on Figure 204, which collapsed during the 1992 Suusamyr earthquake. Similar processes at the Chet-Korumdu Ridge composed of Neogene semi-lithified sediments still continue as can be seen on Figure 27.

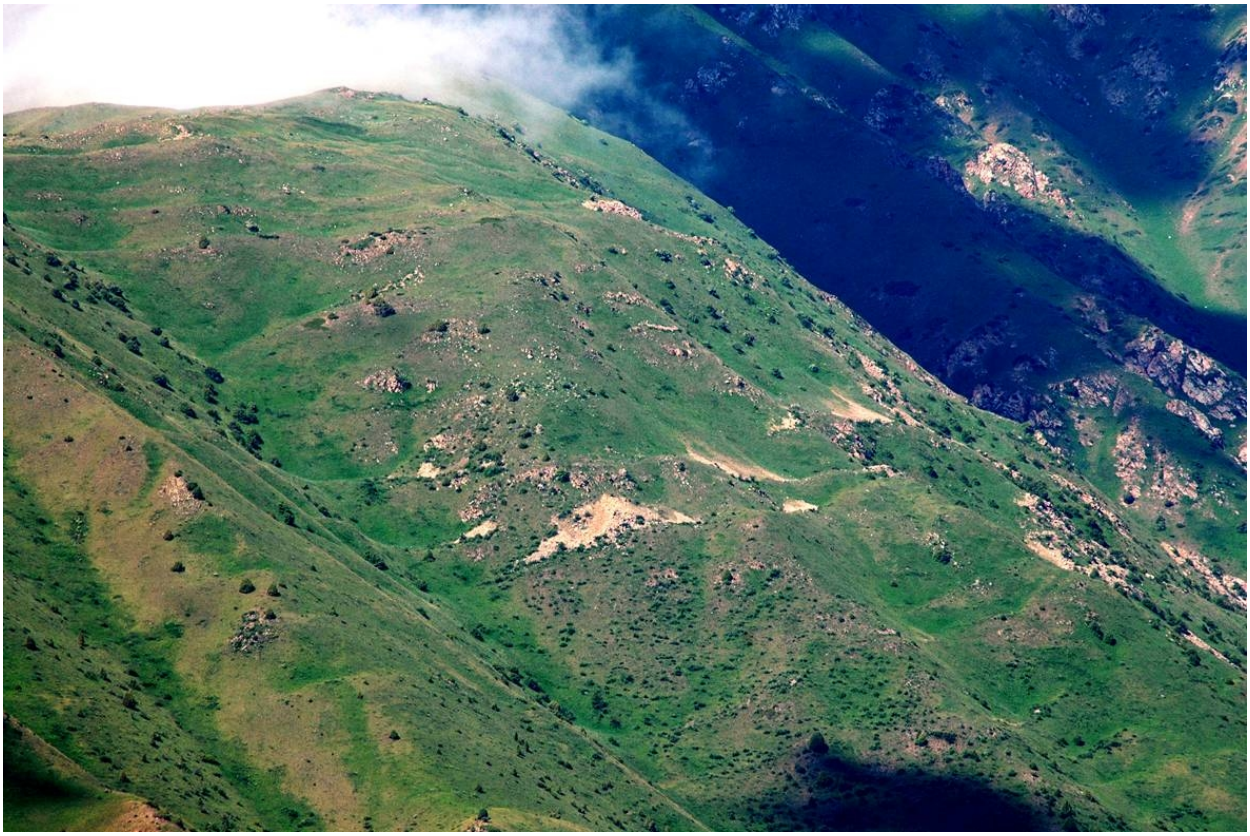

Figure 202. Side view on the toppling site
Note interception of the talus

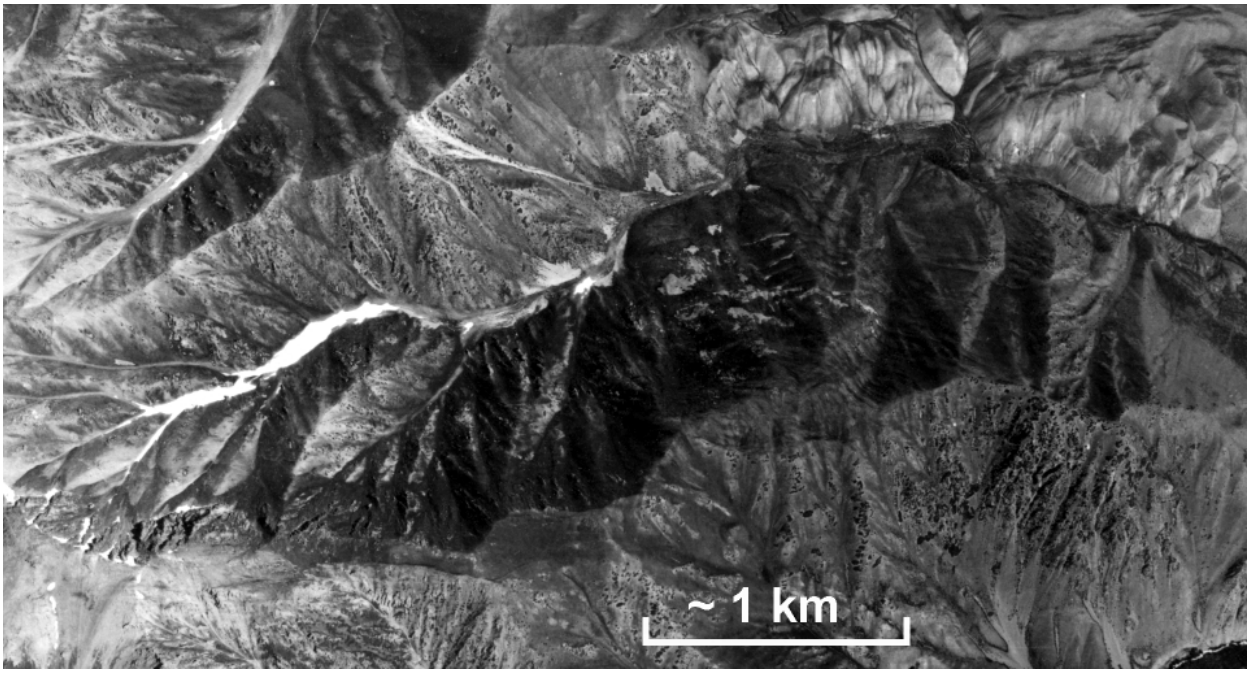

Figure 203. Aerial photograph of the ridge undergoing toppling deformations
Deposits of several minor rockslides can be seen in the gully at the foot of the most affected part of the slope

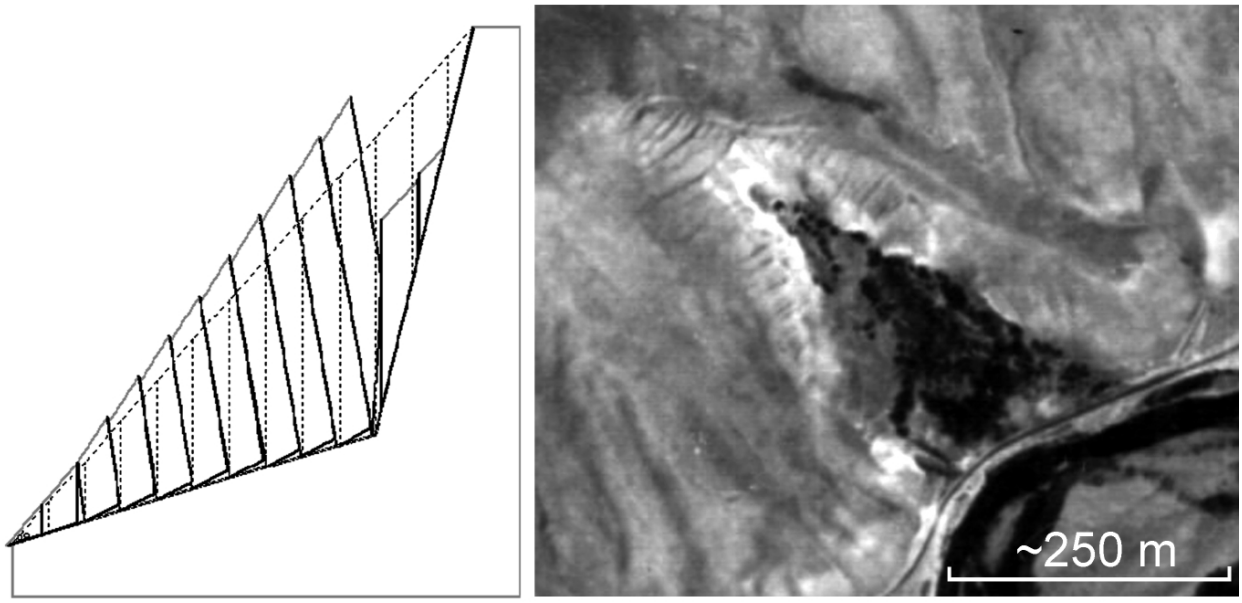

Figure 204. General scheme of toppling and example of such phenomenon that occurred on the southern slope of the Chet-Korumdu Ridge composed of Neogene sediments. Part of the slope affected by toppling failed in 1992 during the Suusamyr earthquake along with other landslides shown on Figure 26. This image was obtained several years prior to the earthquake

6 KUZYLKIOL DEPRESSION – THE CALDERA-LIKE COLLAPSE ON THE ANTICLINE ARCH

The rockslides and landslides described above do not exhaust all examples of these natural phenomena that can be found in the Kokomeren River basin and in the adjacent part of the Naryn River basin.

Numerous large rockslides were found in the Kokomeren River valley downstream of the village of Aral, especially where the river enters the Minkush-Kokomeren intermontane depression – one of the most active neotectonic structures of the Central Tien Shan [Sadybakasov 1972, Chedia 1986]. This zone extends for more than 125 km along the Naryn, Lower Kokomeren and Minkush River valleys from the Ketmen-Tiube intermontane depression in the west up to the Sonkul intermontane depression in the east [Strom, 1982, Belousov, et al., 1994].

Besides landslides, rockslides, sackungen and surface ruptures there are two unique geomorphic features – caldera-like cavities at the right bank watersheds of the Naryn River valley where hundred millions and billions of cubic meters of rocks "disappear" in the range interiors [Strom 2000, Strom, Groshev, 2009]. One of them is located in the central part of the Santash Ridge that forms the right bank of the Naryn river valley in the upper reaches of the Kyzylkiol creek (41.81º N, 73.74º E, No 16 on Figure 2) [Orlov, 1980; Strom, 1982]. It is a roughly rhomboid cavity (Figure 205) about 3×2 km in size with 250 to 700 m high, steep slopes and a relatively flat southward inclined bottom. Its south-eastern edge is dissected by the Kyzylkiol creek gorge, the upper reaches of which have eroded the cavity's bottom at a depth of about 300 m (Figure 206).

The Santash ridge comprises the igneous and metamorphic Proterozoic and Palaeozoic rocks overlain by Carbon red beds developed at its northern slope only (Figure 207). Though these red beds contain some gypsum layers, it seems that no rocks are subjected to karst in the ridge's interior. In the Kyzylkiol gorge, where it cuts the south-eastern cavity's edge (point "A" on Figure 205), only the lowermost 20-25 m of slopes are "painted" by red mud left by debris flows that originated from the cavity. Slopes above this level are covered by the gray-colored scree of local igneous and metamorphic rocks. This indicates that the collapse of the southern edge of the cavity caused by stream erosion, took place recently, maybe hundreds of years ago. Earlier the depression about 3 km^3 in volume was closed. It should be noted that in Kyrgyz language "Kyzylkiol" means "Red Lake" (maybe there was really a lake in the past?). After the Kyzylkiol stream erosion dissected it, the southern part of the cavity's

bottom was eroded (see Figure 206). Torn topographic features at the northern part of the cavity wall indicate its catastrophic origin (Figure 208).

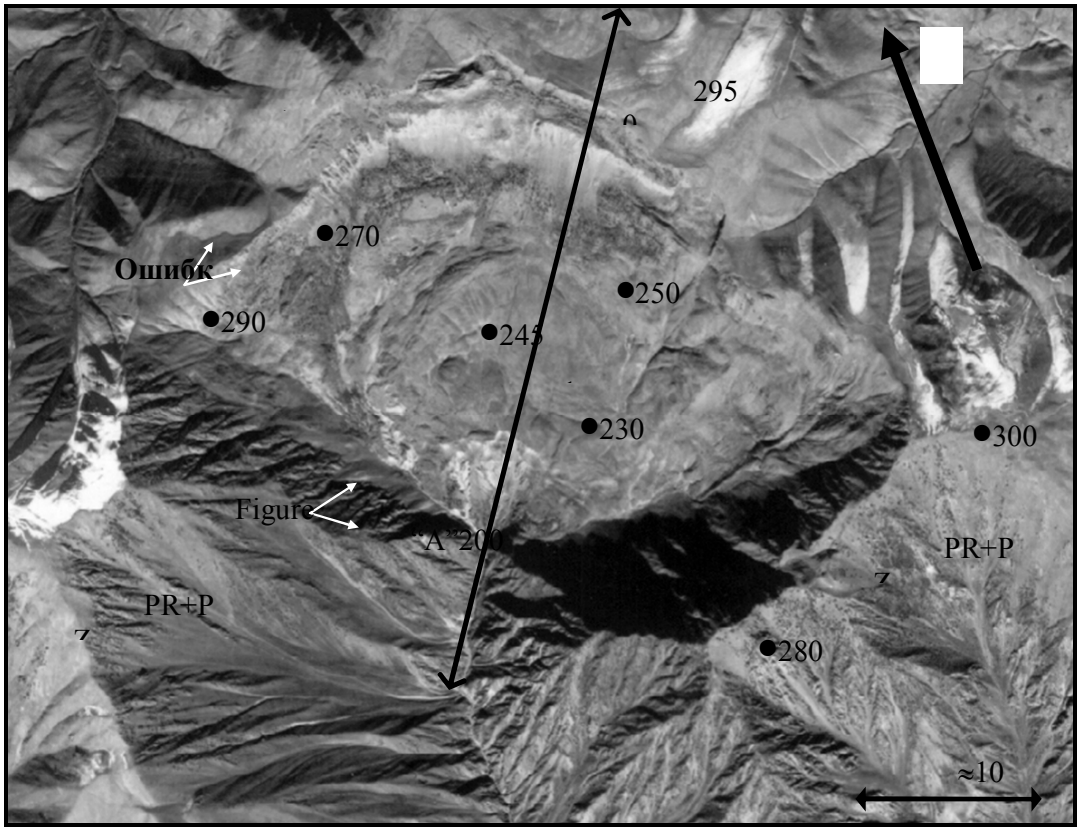

Figure 205. The Kysylkiol caldera-like collapse

Fragment of high resolution KFA-3000 space photograph. Numbers – height of the specified points (•) above sea level; ⟷ cross-section (Figure 207) ⌐ – sites from which photographs were made.

It could be hypothesized that this caldera-like cavity originated due to a strong earthquake. The only known analogue – the so called "Bitut" structure was formed during the 1957 catastrophic (M>8) Gobi Altai earthquake in Mongolia [Gobi Altai ..., 1963]. However, to explain the nature and mechanism of such dislocations we should, at first, understand where the tremendous amount of rocks that initially occupied the cavities "disappeared" to (Figure 209) since erosion has only removed a small portion of material, incomparable with the total volume of the cavity.

The geology of the mountain ranges where the cavity is located excludes its karst origin. The morphology of its bottoms and of the upper reaches of the gorge that cut its southern edge don't allow the explanation of the cavity's genesis as the result of glacial or erosion processes. It is really a caldera-like collapse, though its volcanic origin should be excluded as well.

One more caldera-like collapse, much smaller in size and, likely, much older, is located 30 km west of the Kyzylkiol one at 41.81º N, 73.38º E, outside the area shown on Figure 2 [Strom, 2000].

It is hypothesized that such tremendous subsurface cavities – hundreds of millions and billions of cubic meters in volume – could appear in the course of the detachment basement folding in the tectonically stratified rigid upper crust (Figure 210) that could last for dozens of millennia, preceding rapid, likely single-event collapse [Strom, Groshev, 2009]. Such a model, though being quite exotic, seems to be the only one that could explain the sudden 'disappearance' of hundreds of millions and billions of cubic meters of rocks in the mountain ridge interior in this specific tectonic environment.

Figure 206. Upper reaches of the Kyzylkiol creek, eroding the cavity bottom
Note none-erosive flat relief of the cavity bottom outside the eroded part

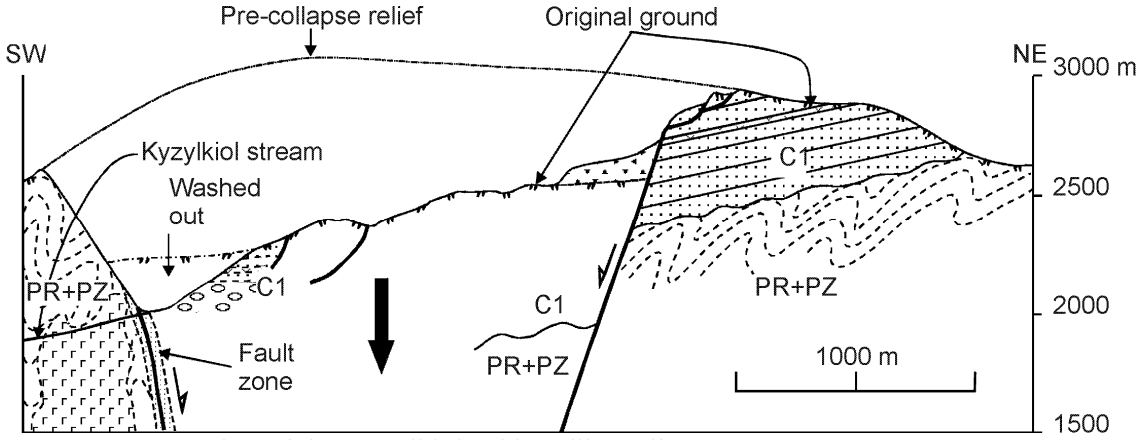

Figure 207. Cross-section of the Kyzylkiol caldera-like collapse
C_1 - Carbon sandstone and conglomerate with gypsum interbeds; PR+PZ - Proterozoic and Palaeozoic metamorphic and igneous rocks

Anyhow further detail mapping and geophysical investigations are necessary to reveal real mechanism of these unique features' origin.

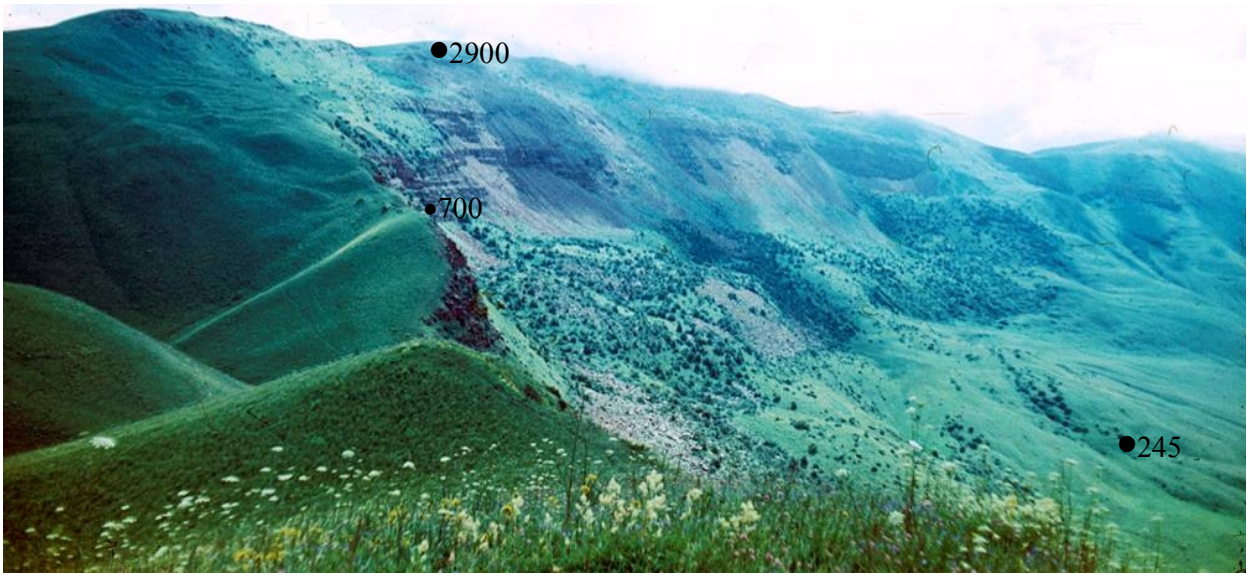

Figure 208. Torn topographic features at the northern edge of the Kyzylkiol cavity

Figure 209. View of the Santash Ridge at the Kyzylkiol section from the north

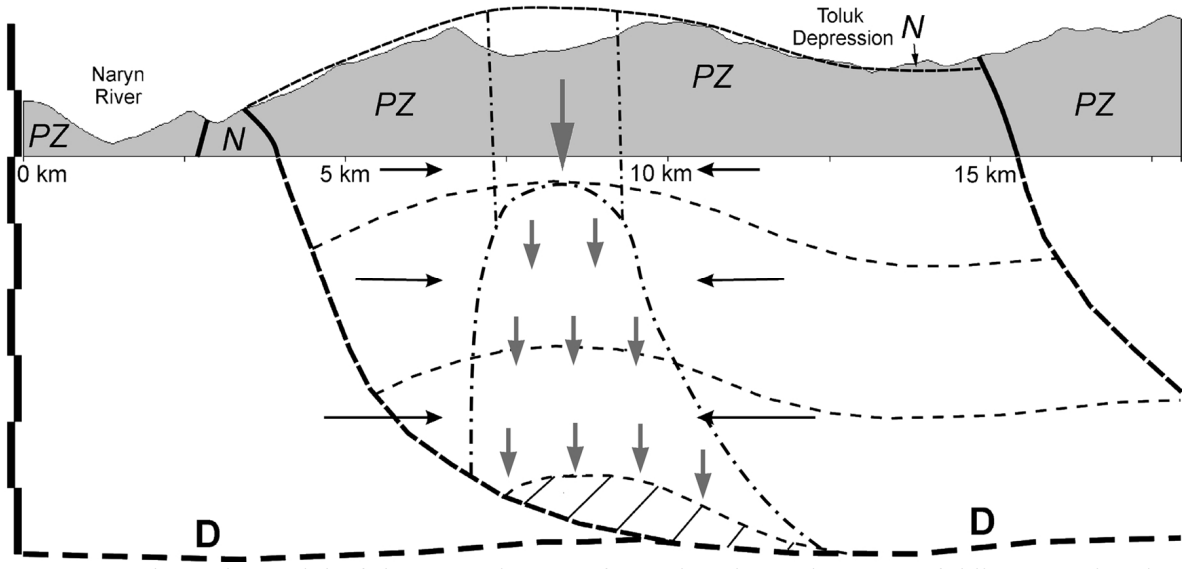

Figure 210. Schematic model of the 'tectonic cave' formation due to basement folding associated with the deep-seated detachment.

The upper part is the cross-section of the Santash ridge with reconstructed deformed pre-orogen planation surface indicating well-pronounced basement folding. Shaded area – the assumed 'initial free space' in the core of an anticline above the detachment zone (D); black arrows show qualitative distribution of the horizontal

stress; small gray arrows below the dashed-dotted line – gradual failure and formation of the cavity roof arch; large gray arrow – final catastrophic collapse

7 CONCLUSIONS

The case studies described above represent various types of rockslides and landslides, which differ in volume, age, runout, morphology, style and extent of river damming, etc. They can be classified according to various classification systems proposed by Zolotariov, et al. [1969], Emelianova [1972], Varnes [1978], Costa & Schuster [1988], Nicoletti & Sorriso-Valvo [1991], Hermanns, et al. [2004], Dunning et al. [2005], and Strom [2006].

Most features described in this Guidebook are large-scale bedrock landslides (rockslides), and many of them converted into highly mobile rock avalanches; they were classified into three main types, according to Strom [2006]: i) "Primary" rock avalanches in unconfined (the Seit rock avalanche – see section 2.1.1) and confined (the Mini-Köfels rockslide – see section 2.1.2, the Ak-Kiol rockslide – see section 2.1.3) conditions; ii) "Jumping" rock avalanches exemplified by the Kashkasu (see section 2.2.1) and the Northern Karakungey (see section 2.3.1) case studies; and iii) widely developed "Secondary" rock avalanches. The latter belong to two subtypes: secondary rock avalanches with a prominent "secondary" scar above the avalanche-like part (the best examples are the Chongsu – see section 2.3.2 and the Southern Karakungey – see section 2.3.1 rock avalanches) and those, which originated, likely, due to the "bottle-neck effect" (the Snake-head rock avalanche – see section 2.3.5). It is evident that extensive further studies, including physical and numerical modeling are necessary to understand the real mechanisms of rock avalanches' formation and their high mobility.

It is likely that most of the studied features originated due to strong past earthquakes. In some cases, such as the Snake-head rock avalanche, the giant Kokomeren rockslide, and the Lower Aral rock avalanche, this assumption has reasonable grounds (see sections 2.3.5, 3.1, 4.1), while in many other cases additional studies should be performed to prove (or disprove) this assumption.

No one land/rockslide, except those formed by the 1992 Suusamyr earthquake, has been dated precisely up to now. Age estimates are based on morphological “freshness” and on the relationships with other geomorphic elements such as river terraces. The upper age limits of the Seit and Karakungey rock avalanches were estimated by tree-ring dating. Along with geomorphic data, it allows assumption of their origin in the Late Holocene time. Several large-scale rock slope failures, namely the Kokomeren rockslide, the Displaced Peneplain rockslide, the Kara-Kungey-Old and the Pre-Karakungey rock avalanches, and, presumably, the Sarysu rock avalanche, are Late Pleistocene features.

Lack of rockslide ages is a critical gap in our knowledge preventing reliable rockslide risk assessment of the upper part of the Kokomeren River basin. Thus, dating is one of the main fields of further rockslide investigations in this region.

8 ACKNOWLEDGEMENTS

We want to express out gratitude to Prof. Kyoji Sassa for his kind attention to our activities in the Tien Shan Region. Preparation of Summer School Guidebook was strongly supported by the UNESCO IPL grants provided by ICL in 2004-2012. In 2008-2009 this work was also supported by the Scientific Program of the Presidium of Russian Academy of Sciences No 16 (Catastrophic Processes) and we want to thank the Director of IDG RAS Julius Zetzer and IDG Programme leader Sergey Turuntaev for their help in organization of field trips. In 2009, the Summer School was also supported by the NATO SFP Project 983289 (LADATSHA – Prevention of Landslide Dam Disasters in the Tien Shan, Kyrgyz Republic) led by Prof. Hans-Balder Havenith (Liege University) and Dr. Isakbek Torgoev (Scientific Engineering Centre GEOPRIBOR).

We had useful discussions with Mikhail Akhmetiev, Stuart Dunning, Stephen Evans, Reginald Hermanns, Hans-Balder Havenith, Oldrich Hungr, Oliver Korup, Mauri McSaveney, Tim Davies, Gabriele Scarascia Mugnozza, Isakbek Torgoev, Andrea Wolter, Anatoliy Zhirkevich and Oleg Zerkal.

We express our special gratitude to Andrea Wolter for careful check of the text of this Guidebook and correction of English.

We were glad to host participants of the 2006-2015 Summer Schools from Argentina, Austria, Belgium, China (including Hong Kong), Czech Republic, France, Germany, Great Britain, Italy, Japan, Kyrgyzstan, New Zealand, Russia, Switzerland, Spain, Taiwan, Tajikistan, and USA and hope to see them in the Tien Shan in future.

Field investigations that provide data described in the Guidebook could not have been performed without the hard work and overall assistance of Atyr Djumabaeva, Zhyldyz Dyikanalieva, Cholponbek Ormukov, Kazbek Abdrakhmatov, Seit Duishenaliev, Kyzylgul Beishekova, Sagyn Mukambetov, and Mukhtar Isaev.

9 REFERENCES

.bdrakhmatov, K., Lemsin, I., Strom, A. 1994. Neotectonics of the Ketmen-Tiube depression. In: The Tien Shan in the Recent Orogeny Period. Bishkek, Ilim, 86-96 (in Russian).

.bdrakhmatov, K., Strom, A., 2006. Dissected rockslide and rock avalanche deposits; Tien Shan Kyrgyzstan. In Evans, S.G.; Scarascia Mugnozza, G.; Strom, A.; Hermanns, R.L. (Eds.) Landslides from Massive Rock Slope Failure. NATO Science Series: IV: Earth and Environmental Sciences, Springer, Vol. 49, 551-572.

.lford, D. and Schuster R. (Eds.) 2000. Usoi Landslide Dam and Lake Sarez. An assessment of Hazard and Risk in the Pamir Mountains, Tajikistan.. UN Publication. Sales No. E.00.III.M.1.

elousov T.P., Skobelev S.F., and Strom A.L. 1994. On estimation of the recurrence period of strong earthquakes of the central Tien Shan (according to the data of absolute geochronology). Journal of Earthquake Prediction Research, 3, 226-236.

ogachkin, B.M., Korjenkov, A.M., Mamyrov, E., Nechaev, Yu.V., Omuraliev, M., Petrosian, A.E., Pletniov, K.G., Rogozhin, E.A., Charimov, T.A. 1997. Structure of the 1992 Suusamyr earthquake source on the basis of its geological and seismological effects analysis. Physics of the Earth, No 11, 3-18 (in Russian, English translation).

ogdanovich, M.C., Kark, J. Korolkov, B. and Muchketov D. 1914. Earthquake of the 4th January 1911 in the northern districts of the Tien Shan, Transactions Geol. Com., New Series 89: 270 p. (in Russian).

ull, W.B. 1996. Prehistorical earthquakes on the Alpine fault, New Zealand. Journal of Geophysical Research, 101 No B3, 6037-6050.

assie, J.W., Van Gassen, W., Cruden, D.M. 1988. Laboratory analogue of the formation of mollards, cones on rock-avalanche debris. Geology, 16, 735-738.

hedia, O.K. 1986. Morphostructures and Neotectonic of the Tien Shan. Frunze, Ilim Publishing House, 314 p. (in Russian).

osta, J.E., and Schuster, R.L. 1988. The formation and failure of natural dams, Geol. Soc. Am. Bull. 100, 1054-1068.

rosta, G.B., Frattini, P, Valbuzzi, E., and Hermanns, R.L. (2015) The Cerro Caquilluco–Cerrillos Negros Giant Rock Avalanches (Tacna, Peru). In: G. Lollino et al. (eds.), Engineering Geology for Society and Territory – Volume 2, DOI: 10.1007/978-3-319-09057-3_159, © Springer International Publishing Switzerland, 921-924.

ui, P., Chen, X., Chen, Z. 2009. The Barrier Lakes created during the Wenchuan Earthquake and its disaster mitigation works. Rock Characterisation, Modelling and Engineering Design Methods. Proc. of the ISRM-Sponsored International Symposium on Rock Mechanics, Hong Kong, 19-22 May 2009, CD-ROM.

avies TR, McSaveney MJ (2011) Rock-avalanche size and runout—implications for landslide dams. In: Evans SG, Hermanns R, Strom AL, Scarascia-Mugnozza G (eds) Natural and artificial rockslide dams. Lecture Notes in Earth Sciences vol 133. Springer, Heidelberg, 441–462.

elvaux, D., Abdrakhmatov, K.E., Lemzin, I.N. and Strom A.L. 2001. Landslides and surface breaks of the 1911, Ms 8.2 Kemin earthquake, Kyrgyzstan, Russian Geology and Geophysics 42(10): 1167-1177.

ubovskoi, A.N., Pernik, L.M., Strom A.L. 2008. Experimental simulation of rockslide fragmentation. Journal of Mining Science, Volume 44, Issue 2, 123-130.

Dunning, S.A., Petley, D.N., Rosser N.J., Strom, A.L. 2005. The morphology and sedimentology of valley confined rock-avalanche deposits and their effect on potential dam hazard. In: Hungr, O, Fell, R., Couture, R., and Eberhardt, E. Landslide Risk Management, A.T. Balkema, Amsterdam, 691-704.

Emelianova, E.P. 1972. Main regularities of landslide processes. Moscow, Nedra Publishing House, 310 p. (in Russian).

Erismann, T.H. 1979. Mechanisms of large landslides, Rock Mechanics 12, 15-46.

Evans, S.G., Clague, J.J., Woodsworth, G.J, and Hungr, O. 1989. The Pandemonium Creek rock avalanche, British Columbia. Can. Geotechnical Journal 26, 427-446.

Evans, S.G., Hungr, O., & Enegren, E.G. 1994. The Avalanche Lake rock avalanche, Mackenzie Mountains, Northwest Territories, Canada: description, dating and dynamics. Can. Geotechnical Journal 31, 749-768.

Evans, S.G., Roberts, N.J., Ischuck, A., Delaney, K.B., Morozova, G.S., Tutubalina, O. 2009. Landslides triggered by the 1949 Khait earthquake, Tajikistan, and associated loss of life. Engineering Geology 109 (3-4), 195-212.

Evan, S.G., Delaney, K.B., Hermanns, R.L., Strom, A., Scarascia-Mugnozza, G. 2011. The Formation and Behaviour of Natural and Artificial Rockslide Dams; Implications for Engineering Performance and Hazard Management. In: Evans SG, Hermanns R, Scarascia-Mugnozza G, Strom AL (eds.), Natural and Artificial Rockslide Dams. Lecture Notes in Earth Sciences 133, 1-75.

Gaziev, E., 1984. Study of the Usoi Landslide in Pamir. Proc. 4th Int. Symp. on Landslides, Toronto, 1, 511-514.

Ghose, S., Mellors, R.J., Korjenkov, A.M., Hamburger, M.W., Pavlis, T.L., Pavlis, G.L., Mamyrov, E. and Muraliev, A.R., 1997. The Ms = 7.3 1992 Suusamyr, Kyrgyzstan earthquake: 2. Aftershock Focal Mechanisms and Surface Deformation. Bulletin of the Seismological Society of America, 87: 23-38.

Gobi Altai earthquake, 1963. N.A. Florensov, V.P. Solonenko (eds.) Publishing House of the Academy of Sciences of the USSR, Moscow, 391 p. (in Russian, English edition is available).

Hartvich, F., Mugnai, F., Proietti, C., Smolkova, V., Strom, A. 2008. A reconstruction of a former rockslide-dammed lake: the case of the Kokomeren River valley (Tien Shan, Kyrgyzstan). Poster presentation at the EGU conference, Vien.

Havenith, H.-B., Strom, A. Jongmans, D., Abdrakhmatov, K., Delvaux, D., Tréfois P. 2003. Seismic triggering of landslides, Part A: Field evidence from the Northern Tien Shan. Natural Hazards and Earth System Sciences, 3 135–149.

Havenith, H.-B., Strom, A., Caceres, F., Pirard, E., 2006. Analysis of landslide susceptibility in the Suusamyr region, Tien Shan: statistical and geotechnical approach. Landslides, 3, 39-50.

Heim, A. 1882. Der Bergsturz von Elm. Deutsch. Geol. Gesell. Zeitschr. 34, 74-115.

Heim, A. 1932, Bergsturz und Menschenleben. Fretz and Wasmuth, Zürich.

Hermanns, R.L., Niedermann, S., Gonzales Diaz, F.E., Faugue, L., Folguera, A., Ivy-Ochs, S., Kupic, P. 2004. Landslide dams in the Argentine Andes. In: Security a Natural and Artificial Rockslide Dams. NATO ARW Extended Abstracts, 79-85.

Hewitt K., 2002. Styles of rock avalanche depositional complex in very rugged terrain, Karakoram Himalaya, Pakistan. In Evans S.G. (ed.) Catastrophic Landslides: effects, occurrence and mechanisms, Reviews in Engineering Geology. Geological Society of America, Boulder, Colorado, 345-378.

Hewitt, K., 2006. Disturbance regime landscapes: mountain drainage systems interrupted by large rockslides. Progress in Physical Geography, 30, No 3, 365-393.

Hsü, K.J. 1975. Catastrophic debris streams (sturzstroms) generated by rock falls. Geological Society of America, Bulletin 86, 129-140

Ignatiev, I.V. 1886. The earthquake in the Tokmak district in the 1885. Proceedings of the Russian Imperial Geographic Society, 22, Issue 2. (in Russian).

Korjenkov, A.M. 2000. Seismogenic convolutionsin soft lacustrine sediments of the Issyk-Kul Lake, Tien Shan, Kyrgyzstan – initial report. Journal of Earthquake Prediction Research 8, 514- 519.

Korup, O., Strom, A.L., and Weidinger, J.T. 2006. Fluvial response to large rock-slope failures – examples from the Himalayas, the Tien Shan and the New Zealand Southern Alps. Geomorphology, 78, 3-21.

Kuchai, V.K., 1969. The results of repeated inspection of residual deformations in the pleistoseismal area of the Kebin earthquake. Geology and Geophysics, 1969, N°8 (116), 101-108. (in Russian).

uchai, V.K. 1971. Use of paleoseismic dislocations for studying seismic regime (exemplified by the pleistoseismal zone of the 1946 Chatkal earthquake). Geology and Geophysics, No 4, 124-129 (in Russian).
ee C.F. and Dai F.C. 2011. The1786 Dadu River Landslide Dam, Sichuan, China. In: Evans SG, Hermanns R, Scarascia-Mugnozza G, Strom AL (eds.), Natural and Artificial Rockslide Dams. Lecture Notes in Earth Sciences 133, 369-388.
eonov, N.N., 1960. The Khait 1949 earthquake and geological conditions of its origin. Proceedings of Academy of Sciences of the USSR Geophysical Series 3, 409-424 (in Russian).
eonov, N.N. 1970. The 1946 Chatkal earthquake. Problems of the engineering seismology, Issue 13, Moscow, Nauka, 64 - 77. (in Russian).
itovchenko, A.F. 1964. Catastrophic debris flow along the Issyk River. Meteorology and Hydrology. No 4, 39-42 (in Russian).
Iakarov, V.I. 1977. Newest Tectonic Structure of Central Tien Shan. Transactions of Geological Institute of RAS, Vol. 307 (in Russian).
IcSaveney MJ, Davies TRH (2006) Rapid rock-mass flow with dynamic fragmentation: inferences from the morphology and internal structure of rockslides and rock avalanches. In: Evans SG, Scarascia Mugnozza G, Strom A, Hermanns RL (eds) Landslides from massive rock slope failure. NATO science series: IV: earth and environmental sciences, vol 49. Springer, Heidelberg, pp 285–304.
Iushketov, I.V., Orlov, A.P. 1893. Catalogue of Earthquakes of Russian Empire. Proceedings of Russian Geographic Society, 26. (in Russian).
ichol, S., Hungr, O., Evans, S.G. 2002. Large-scale brittle and ductile toppling of rock slopes. Canadian Geotechical Jounal, Vol. 39, 773-780.
icoletti, P.G. and Sorriso-Valvo M. 1991. Geomorphic controls of the shape and mobility of rock avalanches, Geol. Soc. Am. Bull. 103, 1365-1373.
ikitin, M., Huggel, C., Schwarz, M., Goncharenko, O., and Galushkin, I.V. 2006. The analysis of the remotely sensed materials for the reconstruction of the Kolka Glacier collapse. In: Proc. Of the International Conference on High Mountain Hazard Prevention, Vladikavkaz – Moscow, June 23-26, 2004, 160-171.
rlov, L.N. 1980. On the kinematics and dynamics of the overthrusts at the boundary of the Northern and Middle Tien Shan. Seismotectonics and seismicity of Tien Shan. Ilim Publishing House, Frunze, 50-59. (in Russian).
ahman, Md. A., Konagai K. (in press) Substantiation of debris flow velocity from super-elevation: A numerical approach. Paper submitted to Landslides.
adybakasov, I. 1972. Neotectonics of the Central part of the Tien Shan. Frunze, Ilim, 116 p.
adybakasov, I. 1990. Neotectonics of High Asia. Moscow, Nauka, 180 p.
hultz, S.S. 1948. Analysis of Newest Tectonics and Relief of the Tien Shan. Proceedings of the All-Union Geographic Society. New Series, Vol. 3, 222 p.
tate Water Inventory. Perennial data on the mainland superficial water regime and resources. Volume IX, Kyrgyz SSR. 1987. Leningrad, Gidrometeoizdat Publishing House, 450 p. (In Russian).
trom, A.L. 1982. About new zone of paleoseismodislocations in the Northern part of the Central Tien Shan. Main problems of seismotectonics. Moscow, 4-13, deposited in VINITI, No 3290-83. (in Russian).
trom, A.L. 1996. Some morphological types of long-runout rockslides: effect of the relief on their mechanism and on the rockslide deposits distribution, in K. Senneset (Ed.) Landslides. Proc. of the Seventh International Symposium on Landslides, 1996, Trondheim, Norway, Rotterdam, Balkema, 1977-1982.
trom, A.L. 2000. Caldera-like collapses at the watersheds in the Central Tien Shan, in Landslides in Research, Theory and Practice. Balkema.
trom, A.L. 2006. Morphology and internal structure of rockslides and rock avalanches: grounds and constraints for their modelling. In Evans, S.G.; Scarascia Mugnozza, G.; Strom, A.; Hermanns, R.L. (Eds.) Landslides from Massive Rock Slope Failure. NATO Science Series: IV: Earth and Environmental Sciences, Vol. 49, 305-328.
trom, A.L. 2010a. Evidence of momentum transfer during large-scale rockslides' motion. In: Williams AL, Pinches GM, Chin CY, McMorran TG, Massei CI (eds.) Geologically Active.Proc. of the 11th IAEG Congress, Auckland, New Zealand, 5-10 September 2010, Tailor & Frensis Group, London, 73-86.

Strom, A.L. 2010b. Landslide dams in Central Asia region. Landslides – Journal of the Japan Landslide Society 47(6), 1-16.

Strom, A.L. 2012. Effects of rockslides and rock avalanches on hydropower schemes in the Naryn River valley. In Eberhardt et al. (eds) Landslides and Engineered Slopes: Protecting Society through Improved Understanding. Proc. of the 11th ISL and 2nd NASL. Taylor & Francis Group, 1867-1872.

Strom, A. (2013a) Geological Prerequisites for Landslide Dams' Disaster Assessment and Mitigation in Central Asia. In: Wang F, Miyajima M, Li T, Fathani TF (eds). Progress of Geo-Disaster Mitigation Technology in Asia, Springer-Verlag Berlin Heidelberg. (ISBN 978-3-642-29106-7), 17-53.

Strom, A. (2013b) Use of indirect evidence for the prehistoric earthquake-induced landslide identifi-cation. In: Ugai K, Yagi H, Wakai A (eds). Earthquake-induced landslides. Springer Heidelberg New York Dordrecht, London (ISBN 978-3-642-32237-2), 21-30.

Strom, A.L., Abdrakhmatov, K.E. 2004. Clustering of large rockslides: the phenomenon and its possible causes. In: Lacerda,W.A., Ehrlich, M., Fontoura, A.B., Sayao, A. (Eds.), Landslides: Evaluation and Stabilization. Taylor and Francis Group, London, 317–320.

Strom, A.L., Groshev, M.E. 2009. Mysteries of Rock Massifs Destruction. In: M. Abbie and J.S. Bedford (Eds.) Rock Mechanics: New Research. Nova Science Publishers.

Strom, A.L., Korup, O. 2006. Extremely Large Rockslides and Rock Avalanches in the Tien Shan, Kyrgyzstan. Landslides, Vol. 3, 125-136.

Strom, A., Pernik, L. 2013. Modeling of debris crushing during rock avalanche motion. Geophysical Research Abstracts, Vol. 15, EGU2013-1373.

Strom, A.L., Stepanchikova P. 2008. Seismic triggering of large prehistoric rockslides: Pro and Con case studies. Proceedings of the International Conference on Management of Landslide Hazard in the Asia-Pacific Region (Satellite symposium of the First World Landslide Forum, Tokyo), Sendai, 11th – 12th November 2008, 202-211.

Varnes, D.J., 1978, Slope Movement types and processes, in Schuster, R.L. and R.J. Krizek (ed.), Landslides – Analysis and Control: National Academy of Sciences Transportation Research Board Special Report No. 176, p. 12-33.

Wang, F., Cheng, Q., Highland, L., Miyajima M., Wanmg, H., Yan, C. 2009. Preliminary investigation of some large landslides triggered by the 2008 Wenchuan earthquake, Sichuan Province, China. Landslides, 6, 47-54.

Yin, Y., Wang F., Sun, P. 2008. Landslide hazards triggered by the 12 May 2008 Wenchuan earthquake, Sichuan, China. Proc. of the First World Landslide Forum, 18021 November 2008, UNU, Tokyo, Japan. Parallel Session Volume, 1-17.

Zolotariev, V.S., Kalinin, E.V., Fedorenko, V.S., Sheshenia, N.L. 1969. Engineering-geological study of rockfalls and other gravitational phenomena on mountainous slopes. Moscow State University, 188 p.